LIBRARY Michigan State University

PLACE IN RETURN BOX to remove this checkout from your record. TO AVOID FINES return on or before date due.

DATE DUE	DATE DUE	DATE DUE

MSU is An Affirmative Action/Equal Opportunity Institution
c:\circletedus.pm3-p.1

FLOW MODEL FOR A ROTATING DIE PRE-PREGGER

by

Nancy Stoneking Losure

A THESIS

Submitted to
Michigan State University
in partial fulfillment of the requirements
for the degree of

MASTER OF SCIENCE

Department of Chemical Engineering

1991

ABSTRACT

A FLOW MODEL FOR A ROTATING DIE PRE-PREGGER

by

Nancy Stoneking Losure

In this research, a rotating die impregnation device, which pre-shears a thermoplastic melt prior to the fiber/melt contact zone, is evaluated with a shear thinning viscoelastic fluid (polyacrylamide solution) and a constant viscosity viscoelastic fluid (polyisobutylene solution).

The operating conditions necessary to attain impregnation were explored experimentally. In the absence of a fiber tow, a mathematical model for the rotating die pre-pregger assisted in the identification of design conditions for maximum flow rates. The theory, which employs the CEF model for viscoelastic behavior, predicts the existence of an optimum flow rate for certain designs and fluid characteristics. Although only qualitative agreement between the model calculations and the flow capacity data in the prototype impregnation die was obtained, the theory nevertheless suggests that practical impregnation rates of 20 cm/sec for a 3,000 fiber tow may be attained using this approach.

To my husband, Ronald J. Losure, who took on extra chores, rearranged his schedule, and hugged me when I was grouchy.

ACKNOWLEDGMENTS

I wish to thank the State of Michigan for supporting this work through the Research Excellence Funding (REF). I am grateful for support through the Dow Chemical Company Foundation Fellowship Fund, and for support through the Amoco Doctoral Fellowship.

I also want to thank the Composite Materials and Structures center at Michigan State University for the use of their space and equipment, and the people at Hycar for generously supplying resins.

Most of all, I wish to thank my advisors, Dr. Charles Petty and Dr. K. Jayaraman for their guidance and patience.

TABLE OF CONTENTS

List of	Tab.	les	v
List of	Figu	ıres	vi
List of	Nome	enclature	viii
Chapter	1	Introduction	1
Chapter	2	Objectives	8
Chapter	3	Background	10
	3.1	The Rotating Die Pre-pregger	10
	3.2	The Centripetal Pump	15
	3.3	Viscoelastic Fluids	19
	3.4	Selection Criteria for Experimental Fluids	23
Chapter	4	Mathematical Model	26
	4.1	Introduction	26
	4.2	Pre-pregger Flow Geometry	27
	4.3	Kinematics	28
	4.4	The Rheological Model	31
	4.5	The Macroscopic Mechanical Energy Balance	34
	4.6	Dimensional Analysis	41
		Flow Capacity for a Boger Fluid	46
	4.8		49
Chapter	5	<u>-</u>	60
-		Introduction	60
		Rheological Parameters	63
		Experimental Apparatus and Procedure	74
		Experimental Results	81
	5.5	Experimental Discussion	87
Chapter	6	Conclusions	99
Chapter	7	Recommendations	104
Appendi	x A	Kinematic Tensors	106
Appendi	K B		118
Appendi	x C	The Mechanical Energy Balance	120
Appendi	x D	Computer Program Listing	128
Appendi	x E	Rheological Data	134
Appendi	ĸ F	Pre-pregger Data	142
List of	Ref	erences	159

LIST OF TABLES

Table 5.1	Experimental Fluids; Constituents	61
	and Suppliers	
Table 5.2	Rheological Constants for Experimental	71
	Fluids	

LIST OF FIGURES

Figure	1.1	A Device for Impregnating Continuous Fibers with a Viscoelastic Fluid	5
Figure	3.1	Schematic of the Centripetal Pump	14
Figure		Rod-climbing Behavior in Viscoelastic	24
		Fluids	
Figure		Flow Structure in Disk Region	32
Figure	4.2	The Effect of the Viscosity Exponent on the Velocity Ratio.	50
Figure	4.3	The Effect of Elasticity on the Velocity Ratio.	53
Figure	4.4	The Effect of Land Length on the Velocity Ratio.	54
Figure	4.5	The Effect of the Disk Radius on the Velocity Ratio.	55
Figure	4.6	The Effect of the Viscosity Exponent on the Velocity Ratio.	57
Figure	4.7	The Effect of the Normal Stress	59
_		Coefficient Exponent on the Velocity Ratio.	
Figure	5.1	The Cone and Plate Rheometer	64
Figure	5.2	Shear Stress Data from RMS-800 for Low Viscosity Fluids.	67
Figure	5.3	Shear Stress Data from RMS-800 for High Viscosity Fluids.	69
Figure	5.4	Normal Stress Data from RMS-800.	70
Figure	5.5	Relationship between b and n for Various Fluids.	75
Figure	5.6	The Rotating Die Pre-Pregger.	77
Figure	5.7	Schematic of the Rotating Die Pre-pregger.	78
Figure	5.8	Typical Pre-pregger Data.	82
Figure	5.9	Flow rate data for 0.3 wt% PIB.	85
Figure	5.10	Flow rate data for Fresh Separan AP-30.	86
Figure	5.11	Flow rate data for Aged Separan AP-30.	88
_		Model compared with experiment for 0.3	90
-		wt% PIB.	
Figure	5.13	Value of H _c for experimental fluids, from model calculations.	92
Figure	5.14	Model compared with experiment for Fresh Separan AP-30.	93
Figure	5.15	Model compared with experiment for Aged Separan AP-30.	95

Figure	5.16	Model compared with data from Good et al.	97
		(Fig. 6, 1974).	
Figure	A.1	The Cone and Plate Rheometer Coordinates	115
Figure	F.1	Spreadsheet Diagram	142

LIST OF NOMENCLATURE

a fluid elasticity coefficient	[dyne sec ^b / cm ²]
b fluid elasticity exponent	[dimensionless]
c_1 , c_2 , c_3 coefficients of the	[dimensionless]
flow equation	
\hat{c}_1 , \hat{c}_2 , \hat{c}_3 , coefficients of the	[dimensional]
flow equation	-
c,', c,', ratios of coefficients	
D, viscous dissipation in the disk	[dyne cm/sec]
D ₁₁ viscous dissipation in the	[dyne cm/sec]
••	[dyne cm/sec]
transition region	[dam = /]
D _{rrr} viscous dissipation in the	[dyne cm/sec]
die tube	
E work arising from elastic response of	[dyne cm/sec]
fluid	
G ratio of elastic to viscous effects	-
H gap width	[cm]
H _c critical gap width	[cm]
k fluid viscosity coefficient	[dyne sec ⁿ / cm ²]
l fluid parameter	
L length of the exit die	[cm]
n fluid viscosity exponent	[dimensionless]
N, first normal stress difference	[dyne/cm²]
-	= '
Q volumetric flow rate	[cm³/sec]
R radius of the disk	[cm]
R _a radius of the exit die	[cm]
s strain rate tensor	
u _r tow speed through pre-pregger	[cm/sec]
u_{θ} , u_{r} , u_{r} components of velocity field in	[cm/sec]
cylindrical coordinates	
u, u, components of velocity field in	n [cm/sec]
spherical coordinates	
W, work on the disk region by shearing	[dyne cm/sec]
action of the rotor	[,
W, work on the disk region by the	[dyne cm/sec]
entering fluid	[4] 4
We Weissenberg number	[dimensionless]
X ratio of dissipation to storage	[dimensionless]
of energy in disk region	[~]
or elietal til grav region	

α B _m	velocity ratio gap width	[dimensionless] [dimensionless]
₽ B	exit die length	[dimensionless]
B	disk radius	[dimensionless]
ÿ	strain rate	[1/sec]
,	characteristic strain rate	[1/sec]
λ	characteristic time of the fluid	[sec]
η	fluid viscosity	[dyne/cm²]
ψ	angle characteristic of flow between	disks [deg]
ρ	fluid density	$[g/cm^3]$
7	stress tensor	
Ψ ,	first normal stress coefficient	[dyne/cm²]
ω	rotation rate	[rad/sec]

Chapter 1 Introduction

Processing thermoplastic polymers in order to manufacture useful articles is a much-studied art, and the enormous diversity of polymers available has allowed manufacturers to replace metal, glass, and wood in many applications.

Plastic replacement parts are cheaper, lighter, stronger, or more chemically resistant than traditional materials, and designing articles entirely in plastic can save material and production steps through part consolidation. This has been the driving force behind much of the ongoing plastics processing and design research.

Thermoplastics can be used neat or as plastic alloys, and are often mixed with short fiber reinforcements. However, despite widespread interest in long-fiber composite materials with thermoplastic matrices, the combination of long or continuous fibers with polymers has, in the past, been done almost exclusively with thermosetting resins. The reason for this is that thermosetting resins are mixed with the fibers when the resin is still a liquid, of relatively low (10 Poise) viscosity (Lee, 1988). This liquid can be impregnated into bundles of delicate carbon fibers by a

variety of processes, designed to intimately mix the resin with the individual fibers of the the tow while causing them little damage. The thermosetting resin is then cured, or set, and the finished article is a block of polymer with typically 60% by volume continuous fibers embedded in it (Hull, 1981).

In contrast, thermoplastic melts are ordinarily very viscous (1,000 to 10,000 Poise). The task of impregnating a bundle of small diameter fibers with a thermoplastic melt has been likened to the task of spreading a lump of chewing gum evenly over the surface of a desk (Cattanach, 1986), a job which seems theoretically possible, but is practically daunting. Fortunately the viscosity of a thermoplastic melt can be reduced during processing to make the production of continuous fiber composites feasible. These methods include increasing the operating temperatures and using additives and solvents. Another approach to making thermoplastic prepreg has been to impregnate fiber tows with powdered polymer, so that the polymer is in intimate contact with the fibers before it becomes a viscous melt. The co-mingling of fibers with fine strands of thermoplastic is another version of this idea.

The practice of reducing the melt viscosity of a thermoplastic resin by raising the processing temperature is limited by the temperature at which significant degradation of the polymer takes place. For some common polymers, a

100°C temperature rise will decrease the viscosity by 10 fold (Middleman p. 291. 1977). Polymer melts can also be plasticized by the addition of mineral oils to lower the viscosity, but the added ease of processing is often offset by a loss in strength, creep resistance, or chemical resistance (Rodriguez, p. 39-41, 1982). Another method for processing a highly viscous polymer is to deal with a solution of the polymer, rather than a melt. A polymer solution can easily approach the viscosities typical of thermoset resins, and pre-pregging operations suitable for thermosets are usually suitable for thermoplastic solutions as well. However, most thermoplastics are soluble only to a limited extent, in solvents that are expensive or hazardous or both. In addition, processes using solutions of thermoplastic polymers must be designed to compensate for low polymer deposition from the solution, for long drying cycles that require high temperatures, and for a high voids content caused by the evaporation of residual solvent during consolidation. The high voids content is also a problem in depositing thermoplastic powders in a tow, and in the comingling operation (Cattanach, 1986).

Another possibility, to be investigated here, is to make use of the shear-thinning characteristic of most polymer melts by using a device that delivers shear-thinned polymer to the fiber tow for impregnation. The polyethylene used in the study by Good et al. (1974) has a viscosity of 87,000

Poise at a shear rate of 1 sec⁻¹ and a temperature of 150 °C. However, as the shear rate increases to 100 sec⁻¹, the viscosity decreases to 5,500 Poise. At shear rates of 1,000 sec⁻¹, the viscosity of polyethylene at 150 °C is only 1,400 Poise, a reduction of almost two orders of magnitude. Thus shear thinning, perhaps combined with an increase in temperature, or the use of a plasticizing additive, could bring the viscosity of polymer resins into the range where impregnation of fiber bundles can take place on a relatively short time scale.

The centripetal pump is a device which uses shearing action to pump viscoelastic fluids. It makes use of the elastic nature evident in polymer melts (and other fluids) to create a pressure difference in the pump through the normal stress response in the fluid generated by the shearing action of the pump rotor. The polymer is fed into a gap between two disks, a rotor and a stator (see Figure 1.1). The polymer adheres to both disks, and so is sheared by the action of the rotor. Since the polymer is elastic, it tends to seek a low-shear environment. The shear field in the pump decreases toward the center of rotation, so the polymer travels in that direction. The die at the center of the stator provides an exit, so a continuous flow occurs, with polymer moving from the periphery of the disks to the center. The flow of the polymer through the pump is due to a balance between the elastic response of the fluid, which

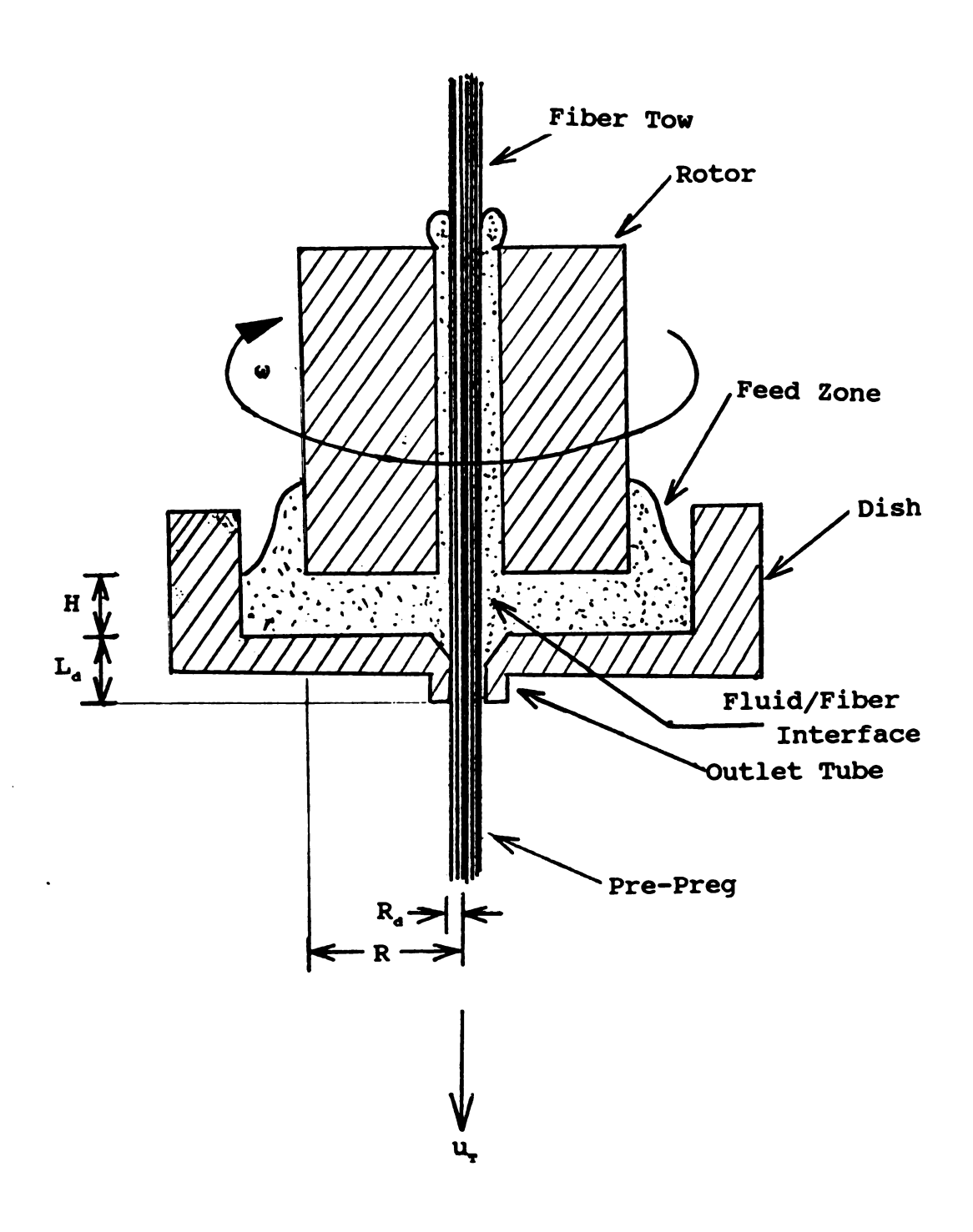


Figure 1.1 A Device for Impregnating Continuous Fibers with a Viscoelastic Fluid.

drives the flow, and the viscous response, which tends to retard the flow. If the polymer is shear-thinning, then the shear environment within the centripetal pump could lower its viscosity by as much as two orders of magnitude.

However, because the normal stress effect will also decrease as the viscosity of the fluid decreases, it is unclear if the centripetal effect will remain large enough to deliver resin to the fiber tow without an imposed pressure. If the thinned polymer could be combined with a fiber tow inside the pre-pregger, then perhaps pre-preg could be made in a continuous process where tow is drawn through the center of the flow field in the pre-pregger, as illustrated by Figure 1.1.

To test this idea, exploratory work involved the construction of a rotating die pre-pregger, as shown in Figure 1.1. Maxwell (1962) developed a similar device for manufacture of reinforced tubing. With the rotating die pre-pregger, a tow of twelve thousand (12K) carbon fibers was successfully impregnated with an aqueous solution of a polyacrylamide with a viscosity of 1,800 Poise at a shear rate of 1 sec⁻¹.

In the pre-pregging experiments, it was observed that the tow dragged more polymer fluid out of the pre-pregger than could be pumped out when there was no tow. On the other hand, drawing the tow through the pre-pregger when it was not rotating soon resulted in the output tow becoming bare

of polymer fluid. It was obvious that two flow regimes were operating in the pre-pregger, and that to understand the pre-pregging operation, one would need to understand both the shear-induced flow and the drag-induced flow in the pre-pregger. Thus, this work is intended to explore the operation of the pre-pregger without the tow in order to determine what fluid characteristics are likely to produce good flow rates. The theoretical model developed and the preliminary model experiments represent a first step towards evaluating the rotating die pre-pregger as a practical means to impregnate fiber tows with viscoelastic resins.

Chapter 2 Objectives

The objective of this study is to evaluate the potential of a rotating die for use in impregnating a continuous fiber tow with a thermoplastic melt. Toward this end, an experimental and theoretical evaluation of the pre-pregger concept is developed. The approach is to use a high shear environment, such as two parallel rotating disks (see Figure 1.1), to reduce the viscosity of a shear-thinning polymer melt and to simultaneously deliver the melt to an impregnation zone by exploiting the elastic pumping properties of viscoelastic materials. The purpose of the theory, therefore, is to provide some insights into selecting specific fluid characteristics and design parameters for optimal pumping in the absence of a fiber tow. Complementary experiments with model fluids are designed to explore the limitations of the theory and to demonstrate that a rotating die device can generate practical flow rates to impregnate fiber tows at tow speeds as large as 20 cm/sec.

A specific goal of this exploratory development is to relate the intrinsic meclogical properties of the fluid to

this goal, a modified version of the empirical CEF-equation for viscoelastic fluids is used to relate the stress and strain rate fields in the complex environment of a rotating die. A power balance (or mechanical energy balance) over the entire flow domain is used to estimate the volumetric flow rate in terms of a specified structure for the velocity field within the pre-pregger. This type of analysis should yield some understanding of how energy is dissipated by the flow. This knowledge, albeit approximate, should assist in the design of the feed zone, the outlet tube, and the fiber contacting zone.

Chapter 3 Background

3.1 The Rotating Die Pre-pregger

A schematic of the rotating die pre-pregger is shown in Figure 1.1. It consists of two disk-shaped surfaces facing each other. H denotes the spacing between the two disks. The bottom disk is mounted on a stand of adjustable height, and has an outlet die on the axis. The rotating top disk is the bottom of a cylinder driven at an angular velocity of ω . An axial cylindrical channel is provided so that a fiber tow can be drawn through the rotor into the center of the velocity field and out through the stationary die tube. The die tube has radius R_a at the constriction and length L_a .

When the pre-pregger is running, the fluid in the gap travels from the periphery of the disks to the center because the elastic nature of the fluid gives rise to a non-zero first normal stress difference. For an arbitrary fluid at steady state, the radial component of the equation of motion within the gap shows that the radial pressure gradient is balanced by an inertial term, a normal stress difference term, and a shear stress term:

$$\frac{\partial}{\partial r}(p-\tau_{rr}) = \rho \frac{v_{\theta}^2 + v_{r}^2}{r} - \frac{\tau_{\theta\theta} - \tau_{rr}}{r} + \frac{\partial \tau_{rz}}{\partial z}$$
 (3.1)

Eq. (3.1) assumes axisymmetry and that the axial component of the velocity field within the gap is zero so the continuity equation has been used to rewrite $\partial v_r/\partial r$ as $-v_r/r$. When the inertial term dominates, as it does for a Newtonian fluid, then the gradient of the net pressure in the disks is positive, and the fluid is thrown outward by centrifugal force. When the first normal stress term, $\tau_{\theta\theta}$ - $\tau_{\rm rr}$, dominates and is greater than zero, then the net pressure rises toward the center of the disks thereby forcing the fluid into the fiber tow and through the die opening. Because of continuity, the fluid flows from the periphery to the center. Thus, it can be seen that the pre-pregger operates on a balance between the inward action of the normal stress difference, and the outward action of the inertial forces. The viscous stress term retards the motion of the fluid in either direction. For viscoelastic fluids, the normal stress difference provides a means to deliver fluid to a fiber tow located on the axis of the pre-pregger.

At the center of the pre-pregger, the fluid contacts the tow and is pulled through the die opening. The rate at which finished pre-preg can be produced depends upon the ability of the pre-pregger to deliver fluid to the impregnation zone. The finished pre-preg will have the same

diameter as the die constriction in the absence of die swell. Die swell may be significant in the extrusion of elastic fluids (see Middleman, p. 464, 1977), but the presence of fibers in the pre-preg will suppress this phenomenon. The volumetric fluid flow rate, Q, that must be provided by the pumping action of the pre-pregger can be estimated as follows

$$Q = \pi R_a^2 (1-V_e) u_r$$
 (3.2)

where:

u is the tow speed,

Q is the volumetric flow rate of the fluid,

R, is the radius of the pre-preg, and

V, is the volume fraction of fibers in the pre-preg.

For $V_f = 0.65$ and $R_d = 0.1$ cm, a tow speed of 20 cm/sec requires a volumetric flow rate of 0.22 cm³/sec.

The calculation of Q does not take into consideration the location of the fluid in the finished pre-preg. The standard for the production of thermoset pre-preg is to produce pre-preg whose fibers are individually coated with the resin. This pre-preg can then be used in lay-ups and in pultrusion with the assurance that voids within the pre-preg have been minimized. Because of the very high viscosities involved, attempts at production of pre-preg with thermoplastic resins have resulted in pre-preg which is incompletely impregnated, or is merely coated. Coated tows, however, are also useful, if an adequate consolidation step

follows the coating operation. Thus, the rotating die prepregger will be considered for further development provided tow speeds of 20 cm/sec or more can be achieved, with thermoplastic melts or viscoelastic model fluids.

As discussed in Chapter 1, preliminary work at Michigan State University concluded that both the shear-induced and the drag-induced flow within the pre-pregger contribute to the operation of the pre-pregger. The present work focuses on the shear-induced flow by eliminating the tow from consideration. The experimental and mathematical problem is then reduced to an analysis of a traditional centripetal pump (see Figure 3.1). The flow equation for the centripetal pump will provide an estimate of the design and operating conditions needed to deliver 0.22 cm³/sec of fluid to the exit die. Since the action of drawing the tow through the flow field will tend to add momentum to the fluid, the flow equation for the centripetal pump will serve as a lower limiting case in the study of the rotating die pre-pregger. The history of the centripetal pump is discussed in Section 3.2. Section 3.3 contains a discussion of the background for the rheological part of this study, and the criteria for the choice of the experimental fluids are discussed in Section 3.4.

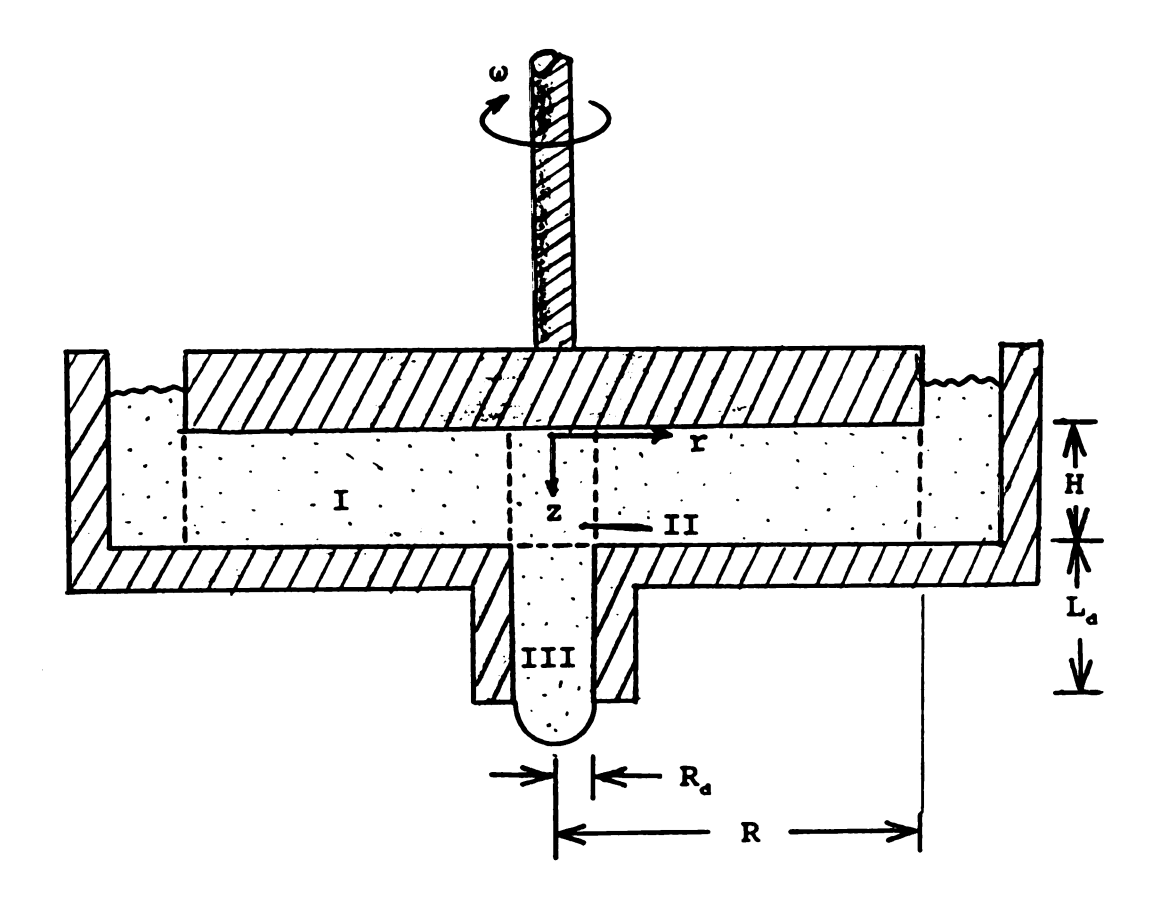


Figure 3.1: Schematic of the Centripetal Pump.

3.2 The Centripetal Pump

The centripetal pump was first described by Maxwell and Scalora in 1960, and a patent was issued to Bryce Maxwell in 1962. In its simplest form, a centripetal pump consists of two disks facing each other across a small separation gap. One disk is held motionless, and the other is rotated about their common axis (see Figure 3.1). Because of the elasticity of the fluid, a flow field is established wherein fluid entering at the periphery of the disks is transported as an inward spiral toward the center, whence it exits through the die tube.

Maxwell (1959, 1962, 1970, 1973) has published several papers on ways the pump may be used in processing polymers, and on the calculations necessary to scale up the centripetal pump from laboratory size to full production sizes. He has studied the effects of the radius, R, and rotation rate, ω, of the rotating disk and the width, H, of the gap on the rate of output, Q, of a polymer melt.

Maxwell noted that when the exit die is the major restriction to flow in the pump, then the flow rate is insensitive to the gap width and depends strongly on the rotation rate and the diameter of the disk. This was later confirmed by studies by D'Amato (1975). However, when the exit die is not restrictive to flow, then the flow rate is very sensitive to the gap width. Thus for each rotation rate, there is a gap width which would produce a maximum

volumetric flow rate. The existence of a critical gap width was also confirmed by Good, et al. (1974).

Maxwell (1970), Goppel (1969), and D'Amato (1975) claim that the centripetal pump is capable of mixing action superior to the screw extruder, with shorter residence times and with a large part of the heat necessary to melt the polymer being provided by mechanical work rather than thermal input. Also claimed is better versatility with regards to the form of the feed, the lack of pulsation in the output stream, and the ability of the pump to handle fiberous additives without damaging them. Maxwell (1970) also demonstrated that the centripetal pump can be scaled for output rates equivalent to the output rates of commercial screw extruders. However, Maxwell did not study the effect of fluid rheology on output rates, except to state that fluids with low viscosity and high elasticity were pumped at higher rates than fluids with high viscosity and low elasticity.

Starita (1972) blended two thermodynamically incompatible polymers in a centripetal pump and studied the microstructure of the resulting blends. He found that the rheological characteristics of the two polymers were factors in the mixing process, though he did not mention whether they significantly affected the flow rates achieved.

Kocherov and Lukach (1973) used a pump with a glass stator to photograph flow patterns in the pump as it was filled

with polymer and as dyed particles were mixed into the polymer. They found that secondary flows developed in the pump and that these contributed significantly to the mixing action. Kataoka, et al. (1976) also studied the mixing action of the pump.

Kocherov (1973) and D'Amato (1975) both found that an efficient feed mechanism is an important factor in the operation of the centripetal pump. They noted that inefficient delivery of the feed decreased the flow rate and caused "instabilities" in the operation. Both these authors were feeding solids to the pump, but Good et al. (1974) noted that their fluids tended to climb over the rotating plate of their pump when rotation rates were too high. They did not conclude that a more efficient feed mechanism was necessary, but they did limit their investigation to rotation rates where the fluid remained within the pump.

Other studies have focused on the velocity and pressure profiles of the flow fields in the pump. Blyler (1966) used a pump with a glass stator and developed a photographic technique to study the velocity profiles both in the radial and gapwise directions. He found that the tangential velocity of the fluid varies in a linear manner across the gap, except for regions very near the stator where the deviation from linearity can be attributed to the thickness of the boundary layer which adheres to the stator. It was also observed that the tangential velocity does not depend

upon the radial position of the fluid for a given position in the gap. Blyler also noted that the profile of the radial velocity was parabolic, but that the profile was unsymmetric about the center of the gap. Also, plug flow profiles of shear thinning fluids were observed near the center of the gap, as opposed to a strictly parabolic profile for a fluid which has constant viscosity. Blyler did not attempt to quantify the effect that variation in rheological properties of the fluid might have on the velocity profiles or on the output rate of the pump.

Remnev and Tyabin (1971) derived a linear profile for the tangential velocity and a parabolic profile for the radial velocity from the equation of motion for power law fluids. However, the predicted parabolic profile, unlike the experimental observations of Blyler, was symmetrical across the gap. Tomita and Kato (1967) derived pressure profiles in the radial direction of the pump, and then performed confirmatory experiments.

Good, et al. (1974) also solved the equation of motion for the velocity profiles in a centripetal pump and derived a flow equation which incorporates the fluid characteristics. The shear stress was modeled as a power law, and the first normal stress difference coefficient was modeled as a polynomial function of the strain rate. The results of the calculation show that there is a gap width for any given fluid and rotation rate that yields a maximum flow rate.

This is confirmed by their experiments, and confirms the previous work of Maxwell (1973) and D'Amato (1975). The rotating die pre-pregger of the present study was designed so that physical dimensions of the disk, gap, and die tube would be similar to the device employed by Good et al. (1974). Thus, the present work complements this earlier study.

3.3 Viscoelastic Fluids

The stress necessary to deform a Newtonian fluid is proportional to the strain rate. When the applied stress goes to zero, the deformation of the fluid will instantaneously cease. An elastic or Hookean solid is also deformed by stress, with the extent of deformation being proportional to the stress. The solid is called elastic because it recovers its original shape when the applied stress is removed.

A viscoelastic fluid has a combination of viscous (dissipation) and elastic (storage) behavior. The ratio of the amount of energy that is dissipated to that which is stored depends on the characteristics of the specific fluid, and on the time span over which the stress is applied and the flow behavior is observed. The matter of observation time is crucial. Glaciers will be perceived to flow if observations occur over a span of years, and the time scale of a "belly flop" dive is short enough that water may be

perceived as a solid. The ratio of a time scale characteristic to the fluid to a time scale characteristic of the flow is often called the Deborah number, De. Ordinary viscous flow occurs for De << 1, and solid behavior occurs for De >> 1. Viscoelastic behavior is characterized by De \cong 1.

Viscoelastic behavior is sometimes modeled as a superposition of viscous and elastic effects. However, in practice, it is very difficult to separate fluid behavior due to elasticity from that due to viscosity, except for a limited class of flows, and a select class of fluids. The following constitutive model will be employed in this study to relate the stresses in the fluid to the strain rate field:

$$\underline{\tau} = 2\eta \left[\underline{S} - \lambda \frac{\delta \underline{S}}{\delta t} \right] \tag{3.3}$$

$$\underline{S} = \frac{1}{2} \left[\nabla \underline{u} + (\nabla \underline{u})^{T} \right]$$
 (3.4)

$$\frac{\delta S}{\delta t} = \frac{\partial S}{\partial t} + \underline{u} \cdot \nabla S - (\nabla \underline{u})^{T} \cdot \underline{S} - \underline{S} \cdot \nabla \underline{u}$$
 (3.5)

In Eq. (3.3), the parameters η and λ represent the shear viscosity and a characteristic time associated with the

fluid. η and λ will be positive functions of the invariants of the strain rate dyadic S. Eq. (3.3) is a special case of the Criminale-Erickson-Fibley (CEF) equation for which the second order term is zero (Bird et al., p. 503, 1987). Appendix A shows that Eq. (3.3) gives a zero second normal stress coefficient for simple shear flows and that $2\eta\lambda = \Psi_1$, the primary normal stress coefficient.

This equation was chosen to explore the behavior of a rotating impregnation die because it provides a good approximation for simple shear flows of viscoelastic fluids subjected to large deformations for which $\Psi_2 \cong 0$ (Tanner, see p. 126 and p. 222, 1988). Furthermore, Eq. (3.3) gives an explicit equation for the stress dyadic, 1, once the flow field has been specified.

The viscosity coefficient, η , and the primary normal stress coefficient, Ψ_1 , can be represented by the following empirical expressions over a limited range of flow conditions

$$\eta = k \left(2 \text{ S:S}\right)^{\frac{n-1}{2}}$$
 (3.6)

$$2\eta\lambda = \Psi_1 = a \left(2 \text{ S:S}\right)^{\frac{b-2}{2}}$$
 (3.7)

The parameters a, b, k, and n are intrinsic properties of the fluid and must be determined experimentally.

For a = 0 and $n \neq 1$, Eq. (3.3) reduces to a model for

a purely viscous fluid, whose viscosity is described by a power law expression such as Eq. (3.6). When n < 1, the fluid is shear-thinning; when n > 1 the fluid is shear-thickening. For the case of a = 0 and n = 1, Eq. (3.3) reduces to a Newtonian model.

The validity of the above model has been discussed by Tanner (p. 222, 1988) for viscometric flows. Its utility for this study is that it provides an unambiguous, albeit approximate, link between experimentally obtained fluid characteristics and process flow conditions. This will provide a means to interpret the complex flow behavior of viscoelastic fluids through the rotating die. When n=1 and b=2, the shear stress and the first normal stress difference are constants independent of the strain rate, and the fluid is a special case of a "Boger" fluid. "Boger" fluids are often employed to study the shear-thinning effects and elastic effects in non-viscometric flows (Choplin, 1983).

Tanner (1973) has observed that $b \cong 2n$ for a wide range of polymer solutions. According to Eqs. (3.6) and (3.7), for fluids with b=2n and n<1, the primary normal stress coefficient decreases significantly as the strain rate increases, inasmuch as $\psi_1 \sim \eta^2$. Paradoxically, the shear thinning nature of thermoplastic melts, which may provide a means to improve the intrinsic impregnation rates of fiber tows, may simultaneously hinder the transport of

fluid to the tow interface by centripetal pumping (see Figure 1.1).

One phenomenon associated with elastic fluids is rod climbing (see Figure 3.2). When a rod is rotated in a beaker of fluid with no elasticity, the momentum transfer from the rod to the fluid throws the fluid outward, and a vortex is formed around the rod. The elastic fluid, however, has a non-zero first normal stress difference, and the induced positive pressure gradient is expressed by a bulge of fluid forming about the shaft. The fluid may climb several shaft diameters above the surface, depending on the specific conditions. The material which climbs the rod necessarily lowers the level of the fluid surface in the beaker, unless the beaker is infinite in extent. Thus, rod climbing, or the Weissenberg effect (Beavers, 1975), may strongly interfere with other flows in the vicinity of the rotating rod by lowering the hydrostatic head or by altering the entrance effects. The fluid will not climb a rotating rod if the diameter of the rod is above a critical value, which depends on fluid characteristics (Beavers, 1975).

3.4 Selection Criteria for Experimental Fluids

Because the centripetal pumping phenomenon arises from the fluid characteristics of elasticity and viscosity, fluids representing four combinations of elasticity and viscosity were chosen for this study. All the fluids were

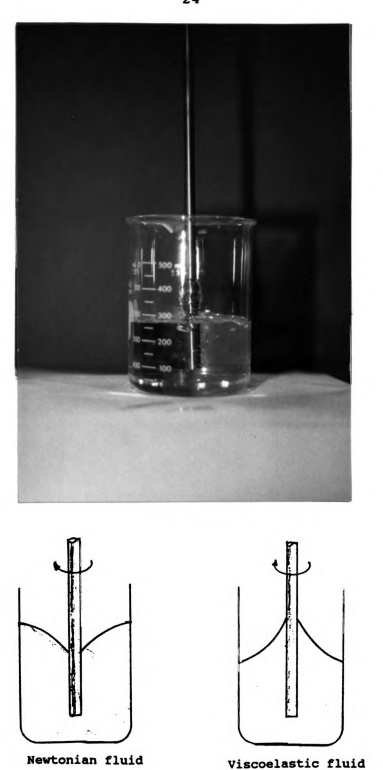


Figure 3.2 Rod-climbing Behavior in Viscoelastic Fluids.

above their melting points at room temperature, for ease of processing. Two of the fluids chosen were essentially Newtonian. They were chosen to serve as controls, and show how the pump operated with non-elastic fluids.

Two additional fluids were prepared by mixing a common epoxy resin with a high molecular weight rubber oligomer. The blends showed slight rod-climbing behavior on mixing, (see Figure 3.2), and they were tested to show how a slightly elastic fluid would behave in the centripetal pump. There has been recent interest in blends of epoxy with rubber oligomers, because the addition of rubber in the uncured system tends to toughen the cured product, thus allowing its use in applications for which neat epoxy resins are considered too brittle (Raghava, 1988).

A fifth fluid was chosen to be very elastic and to have a constant viscosity. It is a solution of polyisobutylene in polybutene and kerosene, and is a model fluid of the type known as a "Boger" fluid (Choplin, 1983). Another model fluid was formulated to be elastic and shear thinning, and was chosen to imitate one of the fluids studied by Good, et al. (1974). Formulations for these fluids appear in Table 5.1, and rheological constants appear in Table 5.2.

Chapter 4 Mathematical Model

4.1 Introduction

The rotating die is very similar to a centripetal pump when there is no tow being drawn through it. It is also identical to a plate and disk rheometer when the volumetric flow rate, Q, is zero. Therefore, the following theory parallels analyses which already exist for these flow situations. The geometry of the die is discussed in Section 4.2. The rheological model used to describe the response of the fluids to the stresses in the pre-pregger is presented in Section 3.3. Further simplifications of this theory for the rotating die pre-pregger are introduced in Section 4.3. The discussion of the velocity fields in Section 4.4 then leads to a macroscopic mechanical energy balance in Section The energy balance provides an equation for Q as a function of the geometric scales of the rotating die, the operating parameter of the die, and the characteristics of the fluids. This equation is discussed in Section 4.6, and the results of a parametric study are described in Section 4.7

4.2 Pre-Pregger Flow Geometry

The rotating die consists of two concentric disks of radius R separated by a gap of width H (see Figure 3.1). The upper disk rotates about its axis at an angular velocity ω , while the lower disk remains stationary. The stationary disk is provided with a die opening at the center, of radius R_d and length L_d . The working fluid is fed from the periphery of the rotating die and flows towards the axis with a spiralling motion. The origin of the cylindrical coordinate system is located at the center of the rotating upper disk as illustrated in Figure 3.1.

The steady state flow patterns within the rotating die can be separated into three distinct regions:

Region I Flow Between Two Disks: Fully-Developed,

Two-Dimensional, Axisymmetric Swirling Flow

$$R_{d} \leq r \leq R$$

$$0 \leq z \leq H$$

$$\underline{u}^{r} = u_{r}^{r}\underline{e}_{r} + u_{\theta}^{r}\underline{e}_{\theta}$$
(4.1)

Region II Transition Flow: Fully-Developed, Three-Dimensional, Axisymmetric Swirling Flow

$$0 \le z \le H$$

$$\underline{\mathbf{u}}^{\text{II}} = \mathbf{u}_{\mathbf{r}}^{\text{II}}\underline{\mathbf{e}}_{\mathbf{r}} + \mathbf{u}_{\mathbf{\theta}}^{\text{II}}\underline{\mathbf{e}}_{\mathbf{\theta}} + \mathbf{u}_{\mathbf{r}}^{\text{II}}\underline{\mathbf{e}}_{\mathbf{r}} \qquad (4.2)$$

Region III Flow in the Die Tube: Fully-Developed, One-Dimensional, Axisymmetric, Non-swirling Flow

$$0 \le r \le R_d$$

$$H \le z \le H + L_d$$

$$u^{\text{III}} = u_{s}^{\text{III}}e_{s}$$
(4.3)

4.3 Kinematics

The forced vortex flow induced by the relative motion of the two disks observed by Blyler (1974, see Chapter 3) is assumed to extend over both Regions I and II

$$u_{\theta}^{r} = u_{\theta}^{rr} = \omega r \left(1 - \frac{Z}{H}\right)$$
 (4.4)

For z=0, the tangential component of the velocity is ωr for $0 \le r \le R$. $u_{\theta}^{\ r}$ satisfies the no-slip condition on the lower stationary disk at z=H. $u_{\theta}^{\ r}$ is also zero at the entrance of the outlet tube.

The axial component of the velocity in Region III is given by (see Middleman, p. 88, 1977)

$$u_{z}^{III} = \frac{Q}{\pi R_{d}^{2}} \frac{3n+1}{n+1} \left[1 - \left(\frac{r}{R_{d}} \right)^{\frac{n+1}{n}} \right]$$
 (4.5)

where Q is the volumetric flow rate. For n = 1, Eq. (4.5) reduces to the Hagen-Poiseuelle law for fully developed laminar flow of a Newtonian fluid through a tube (see Middleman, p. 87, 1977).

The continuity equation and the no-slip boundary conditions in Region I at z=0 and z=H are satisfied by a radial velocity profile of the form

$$u_r^T = -\frac{3Q}{\pi H r} \frac{Z}{H} (1 - \frac{Z}{H}) ,$$
 (4.6)

where Q is the steady-state volumetric flow rate. The axial and radial components of the velocity within Region II are constructed to satisfy the continuity equation

$$\frac{1}{r} \frac{\partial}{\partial r} (r u_r^{ii}) + \frac{\partial u_r^{ii}}{\partial z} = 0$$
 (4.7)

as well as the condition that the three-dimensional flow field in Region II must provide a continuous transformation from the two-dimensional flow of Region I to the one-dimensional flow of Region III. This strategy, which was also employed by Good et al. (1974), yields the following expressions for the radial and axial components of the

velocity in Region II

$$u_{r}^{II} = -\frac{3Q}{\pi H R_{A}} \frac{3n+1}{n+1} \frac{r}{R_{A}} \left[1 - \frac{2n}{3n+1} \left(\frac{r}{R_{A}} \right)^{\frac{n+1}{n}} \right] \frac{z}{H} (1 - \frac{z}{H})$$
 (4.8)

$$u_{z}^{II} = + \frac{3Q}{\pi R_{d}^{2}} \frac{3n+1}{n+1} \left[1 - \left(\frac{r}{R_{d}} \right)^{\frac{n+1}{n}} \right] \left(\frac{z}{H} \right)^{2} \left(1 - \frac{2}{3} \frac{z}{H} \right) . \tag{4.9}$$

Note that Eq. (4.8) reduces to Eq. (4.6) for $r = R_d$ and that Eq. (4.9) reduces to Eq. (4.5) for z = H.

The local spiral structure of the two-dimensional flow in Region I can be characterized by the ratio of velocities evaluated at z = H/2:

$$\tan \psi = \alpha(r) = \frac{-u_r^{T}(r, \frac{H}{2})}{u_{\theta}^{T}(r, \frac{H}{2})} = \frac{3Q}{2\pi H \omega r^2}$$
 (4.10)

The angle ψ measures the transition from a purely tangential flow ($\alpha = 0$ or $\psi = 0^{\circ}$) to a purely radial flow ($\alpha = \infty$ or $\psi = 90^{\circ}$). Eq. (4.10) implies that

$$\frac{\tan \psi(R_d)}{\tan \psi(r)} = \frac{\alpha(R_d)}{\alpha(r)} = (\frac{r}{R_d})^2 . \qquad (4.11)$$

Thus, if $R_a = 2.5$ mm and r = 25 mm, the parameter α increases by two orders of magnitude from the periphery to the core of the flow field for all fluids and for all values of ω . This purely kinematical feature provides ample motivation to explore the utility of a rotating die as a continuous means to mix different resins prior to fiber tow impregnation. In pre-pregger applications, it may be important to specify α to control either the contact time of the viscoelastic fluid between the rotating disks or to orient the macromolecules prior to contact with the fiber tow.

In Section 4.5, α will be related to the operation and design of the pre-pregger by using a mechanical energy balance. However, it is beyond the scope of the present work to seek an optimal value of α based on impregnation results. Figure 4.1, however, shows that \(\psi \) decreases significantly as r/R_a increases. For $\alpha(R_a) \cong 1$, the transition from a two-dimensional flow to an approximate one-dimensional flow dominated by the tangential component of the velocity occurs for $1 \le r/R_A \le 5$ (see Figure 4.1); for $\alpha(R_a) = 10$, the transition occurs for $r/R_a \le 10$.

4.4 The Rheological Model

Eqs. (3.3), (3.6), and (3.7) define the class of fluids examined in this study. Appendix A gives the components of the strain rate dyadic S and its upper convected Oldroyd derivative for the three flow domains defined by Figure 3.1.

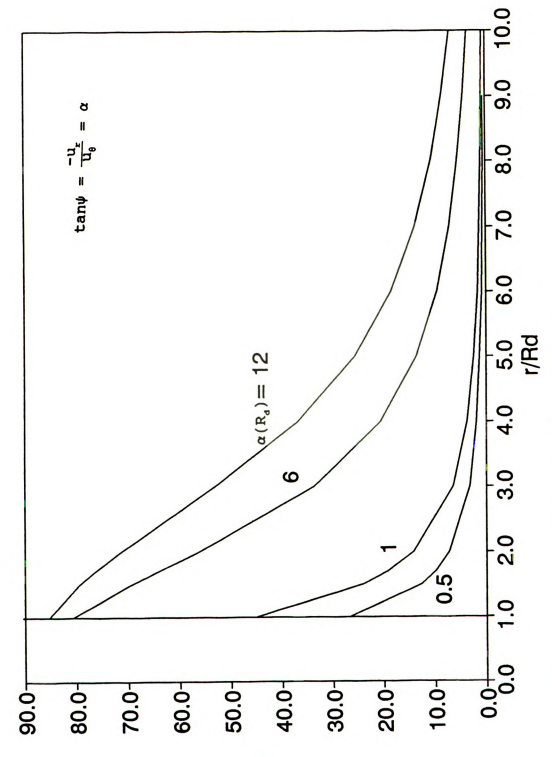


Figure 4.1 Flow Structure in Disk Region.

The second invariant of S (i.e., 2 S:S) is also listed in Appendix A for the three regions of the pre-pregger. Within Regions I and II, the major contribution to S arises from the axial gradient of the swirl component of the velocity. In Region III, however, the radial gradient of the axial velocity determines the local strain rate. Thus,

$$2 \cdot S : S \qquad \stackrel{:}{=} \qquad \left\{ \begin{array}{l} \left(\frac{\partial u_{\theta}^{\text{I}}}{\partial z}\right)^{2} & \text{Region I} & (4.12) \\ \\ \left(\frac{\partial u_{\theta}^{\text{II}}}{\partial z}\right)^{2} & \text{Region II} & (4.13) \\ \\ \left(\frac{\partial u_{z}^{\text{III}}}{\partial r}\right) & \text{Region III} & (4.14) \end{array} \right.$$

The elastic contribution to Eq. (3.3) will be neglected in Regions II and III (i.e., $\lambda = 0$). Eq. (3.3), however, will be used to estimate the components of $\underline{\tau}$ in Region I (see Figure 3.1). The stress in Region II will be estimated by using the following "effective" Newtonian model

$$\underline{\tau}^{\text{II}} = 2 \langle \eta \rangle S^{\text{II}} \qquad (4.15)$$

with a volume average viscosity defined by

$$\langle \eta \rangle \equiv \frac{\int_{v_{III}} \eta \ dV_{III}}{V_{III}}$$
 (4.16)

Eqs. (3.6) and (4.13) define η for Region II.

Eq. (3.3) with $\Psi_1 = 0$ is used to estimate the stress for Region III. Thus,

$$\underline{\tau}^{\text{III}} = 2 \eta \underline{S}^{\text{III}} . \tag{4.17}$$

The viscosity coefficient in Eq. (4.17) is defined by Eqs. (3.6) and (4.14). Appendix A gives the components of $\underline{\tau}$ for each of the flow regions.

It follows from Eqs. (4.12) through (4.14) and Eqs. (4.4) and (4.5) that

$$\dot{\gamma}_{c} = (2S:S)^{\frac{1}{2}} = \begin{cases} \frac{\omega r}{H} & \text{Regions I&II (4.18)} \\ \left(\frac{Q}{\pi R_{d}^{3}}\right) \left(\frac{3n+1}{n}\right) \left(\frac{r}{R_{d}}\right)^{\frac{1}{n}} \text{Region III . (4.19)} \end{cases}$$

Eq. (4.18) anticipates that the viscosity coefficient in Regions I and II, for n < 1 (see Eq. (3.6)) can be decreased either by increasing ω or by decreasing the gap width H. This action may either increase or decrease the viscosity within Region III, depending on the behavior of Q as ω and H change.

4.5 The Macroscopic Mechanical Energy Balance

The steady-state macroscopic mechanical energy balance

for the rotating die provides a means to estimate the volumetric flow rate Q. The equation can be written symbolically as

$$D = W_1 + W_2 (4.20)$$

where

$$D = \iiint_{v} \underline{\tau} : \nabla \underline{u} \, dV \qquad (4.21)$$

$$W_1 = -2\pi \int_0^R \left[\tau_{z\theta} u_{\theta} \right]_{z=0} r dr \qquad (4.22)$$

$$W_2 = 2\pi R \int_0^{\pi} \left[\tau_{r\theta} u_{\theta} \right]_{r=R} dz \qquad (4.23)$$

The dissipation function D represents the irreversible rate of conversion of mechanical energy into internal energy whereas W_1 and W_2 represent the rate of energy transfer to the fluid by shear stresses acting on the control surfaces at z=0 and r=R. Eq. (4.20) requires that the two work terms balance the dissipation terms. The following four assumptions have been made to bring the macroscopic energy equation to this form

- No slip at solid/fluid interfaces;
- 2. Gravitational work is neglected;
- 3. The changes in kinetic energy between the inlet and the outlet of the pre-pregger are neglected; and
- 4. The normal component of the stress at the inlet (i.e., $p \tau_{rr}^{I}$) equals the normal component of the stress at the outlet $(p \tau_{rr}^{III})$.

The two work contributions in Eq. (4.20) can be written in terms of the velocity components by using the stress models discussed in Section 4.4 (also see Appendix C).

Thus,

$$W_{1} = -2\pi \int_{0}^{R} \left. \left(\eta \frac{\partial u_{\theta}}{\partial z} u_{\theta} \right) \right|_{z=0} r dr \qquad (4.24)$$

$$W_{2} = +2\pi R \int_{0}^{R} \left(\Psi_{1} \frac{\partial u_{\theta}}{\partial z} \frac{\partial u_{r}}{\partial z} u_{\theta} \right) \Big|_{r=R} dz \qquad (4.25)$$

By inserting the models for u_{θ} , u_{r} , and Ψ_{1} defined previously, Eq. (4.25) can be written as

$$W_{2} = Q a \left(\frac{\omega R}{H}\right)^{b} . \qquad (4.26)$$

Because η does not depend on the axial coordinate z, W_1 will exactly balance a term contained in D, as will be shown presently.

The elastic nature of the fluid provides a means to redistribute the energy transferred across the two control surfaces at z=0 and r=R into the pressure field. As was previously mentioned, this induces an inward radial flow toward the outlet tube located on the axis. This viscoelastic process makes D smaller than the dissipation integral for a purely viscous fluid under the same kinematic

constraints. In order to analyze this feature explicitly, the total dissipation integral is decomposed into three contributions associated with the three volume Regions I, II, and III:

$$D = D_{r} + D_{rr} + D_{rrr} . {(4.27)}$$

The dissipation integral over Region III follows from the results summarized by Appendixes A and B and Eq. (4.5). The result can be written as (see Appendix C, Eq. (C.16))

$$D_{III} = \frac{2kL_d}{\pi^n R_d^{3n+1}} \left(\frac{3n+1}{n}\right)^n Q^{n+1} . \qquad (4.28)$$

For n = 1, Eq. (4.28) reduces to the dissipation integral for fully developed laminar flow of a Newtonian fluid (see Bird et al. p. 188, 1960.)

As the fluid passes through Region II, Eq. (4.28) assumes that the stress can be calculated as if the fluid were Newtonian with a viscosity coefficient defined by Eq. (4.16). Therefore, it follows from Eqs. (4.4) and (4.13) that

$$\langle \eta \rangle = \frac{2k}{1+n} \left(\frac{\omega R_d}{H} \right)^{n-1} . \qquad (4.29)$$

The dissipation integral over Region II can be written in

terms of the stress components summarized in Appendix B.

There are five distinct contributions to this integral as indicated below:

$$D_{rr} = 2\pi \int_{0}^{\pi} \int_{0}^{R_{d}} <\eta> \left[\left(\frac{\partial u_{\theta}^{rr}}{\partial z}\right)^{2} + 2\left(\frac{u_{r}^{rr}}{r}\right)^{2} + 2\left(\frac{\partial u_{r}^{rr}}{\partial r}\right)^{2} \right]$$

$$+ \left(\frac{\partial u_r^{II}}{\partial r} + \frac{\partial u_r^{II}}{\partial z}\right)^2 + 2\left(\frac{\partial u_r^{II}}{\partial z}\right)^2 \right] \quad r \quad dr \quad dz \quad .(4.30)$$

The dissipation integral over Region I can also be written in terms of the strain rates by using the stress components summarized in Appendix B. The result is

$$D_{r} = 2\pi \int_{0}^{\pi} \int_{R_{d}}^{R} \left[\eta \left[\left(\frac{\partial u_{\theta}^{r}}{\partial z} \right)^{2} + 4 \left(\frac{u_{r}^{r}}{r} \right)^{2} + \left(\frac{\partial u_{r}^{r}}{\partial z} \right)^{2} \right]$$

$$+ \Psi_{1} \frac{u_{r}^{T}}{T} \left[\left(\frac{\partial u_{\theta}}{\partial z} \right)^{2} + 4 \left(\frac{u_{r}^{T}}{T} \right)^{2} - \left(\frac{\partial u_{r}^{T}}{\partial z} \right)^{2} \right] \quad r \quad dr \quad dz \quad . \tag{4.31}$$

The first term of D_r and the first term of D_{rr} can be combined as

$$2\pi H \left[\int_{0}^{R_{d}} \langle \eta \rangle \left(\frac{\omega r}{H} \right)^{2} r dr + \int_{R_{d}}^{R} \eta \left(\frac{\omega r}{H} \right)^{2} r dr \right] . \quad (4.32)$$

Note that the above result equals W_1 defined by Eq. (4.24). Thus, Eq. (4.4) together with the approximations defined by Eqs. (4.12) and (4.13) cause the sum of the first terms in D_1 and D_{11} to balance W_1 exactly. Therefore, the remaining terms in D_1 and D_{11} combine with D_{111} to balance W_2 .

The term which arises from the primary normal stress difference in Eq. (4.31) reduces the magnitude of D_r because $u_r^{\ r} < 0$. This contribution to D_r will be denoted as

$$-E = 2\pi \int_{0}^{\pi} \int_{R_{A}}^{R} \Psi_{1} \frac{u_{r}^{T}}{T} \left(\frac{\partial u_{\theta}^{T}}{\partial z}\right)^{2} r dr dz . \qquad (4.33)$$

Because $\Psi_1 \geq 0$ and $u_r^T \leq 0$, the integral E is always positive. Eq. (4.33) neglects the strain rates related to the radial component of the velocity in comparison to the strain rate associated with the tangential velocity. This is consistent with the approximation given by Eq. (4.12). Thus, by inserting the models for u_θ , u_r , and Ψ_1 into Eq. (4.33), the following result obtains

$$E = \frac{W_2}{D} \left[1 - \left(\frac{R_d}{R} \right)^b \right] \ge 0 . \qquad (4.34)$$

The macroscopic energy balance, defined by Eq. (4.20), can now be rewritten as

$$D_{\tau}^* + D_{\tau\tau}^* + D_{\tau\tau\tau} = E + W_2$$
 (4.35)

where the dissipation integrals D_{I} and D_{II} contain only contributions due to the viscous stresses. W_{2} , D_{III} and E are defined by Eqs. (4.26), (4.28), and (4.34), respectively. D_{I} and D_{II} are defined as follows

$$D_{r}' = 2\pi \int_{0}^{\pi} \int_{R_{d}}^{R} \eta \left[4 \left(\frac{u_{r}^{T}}{T} \right)^{2} + \left(\frac{\partial u_{r}^{T}}{\partial z} \right)^{2} \right] r dr dz \qquad (4.36)$$

$$D_{xx} = 2\pi \int_{0}^{\pi} \int_{0}^{R_{d}} <\eta> \left[2\left(\frac{\partial u_{x}^{xx}}{\partial r}\right)^{2} + 2\left(\frac{u_{x}^{xx}}{r}\right)^{2} + \left(\frac{\partial u_{x}^{xx}}{\partial r} + \frac{\partial u_{x}^{xx}}{\partial z}\right)^{2}\right]$$

$$+ 2\left(\frac{\partial u_z^{TT}}{\partial z}\right)^2 \quad] \quad r \, dr \, dz . \qquad (4.37)$$

Appendix C gives explicit equations for D_1 and D_{11} in terms of Q, ω , k, n, R, R_a , and H.

Eq. (4.35) can be used to estimate the volumetric flow rate, Q. Eqs. (4.36) and (4.37), together with the equations for the velocity components, show that D_r and

 D_{rr} are both proportional to Q^2 . Moreover, Eq. (4.28) shows that $D_{rrr} \propto Q^{n+1}$ and Eq. (4.26) indicates that $W_2 \propto Q$. Because E $\propto W_2$, it follows that E $\propto Q$ also. Thus, Eq. (4.35) has the following dependence on the flow rate

$$\hat{C}_1 Q^2 + \hat{C}_2 Q^{n+1} = \hat{C}_3 Q \tag{4.38}$$

where the dimensional coefficients \hat{c}_1 , \hat{c}_2 , and \hat{c}_3 are all positive. If a=0, W_2 and E are zero (see Eqs. (4.26) and (4.34)). Thus $\hat{c}_3=0$ also, and the only solution to Eq. (4.38) is Q=0. However, for $\hat{c}_3>0$, Eq. (4.38) has a unique solution. The qualitative behavior of Eq. (4.38), which represents a steady state power balance over the rotating die pre-pregger, will be summarized in the next section.

4.6 Dimensional Analysis

Eq. (4.38) determines the volumetric flow rate Q in terms of four geometric parameters, (R, R_a , L_a , H), a single operating parameter (ω), and four rheological coefficients (a,b,k,n). Dimensional analysis implies that Eq. (4.38) can be reduced to an equation containing seven dimensionless groups.

The rheological parameters and the angular velocity can be combined to form the following three dimensionless ratios

b, the dimensionless elasticity exponent;

n, the dimensionless viscosity exponent; and,

$$G = \frac{a}{k} \omega^{b-n} . \tag{4.39}$$

The dimensionless group G gives a measure of the relative importance of elastic and viscous effects in the rotating die. This follows by comparing a measure of the primary normal stress difference with a measure of the viscous shear stress. For instance, if Eq. (4.18) denotes a characteristic strain rate associated with the swirling flow, then a characteristic Weissenberg number can be identified as

We
$$\equiv \frac{N_1}{\tau_{\theta z}} = \frac{2\eta \lambda \dot{\gamma}_c^2}{\eta \dot{\gamma}_c} = \frac{a}{k} (\dot{\gamma}_c)^{b-n} = G(\frac{r}{H})^{b-n}$$
 (4.40)

Eq. (4.40) shows that G is closely associated with a local Weissenberg number, or equivalently, a local Deborah number (De $\approx \lambda \dot{\gamma}_c$). The utility of G as an independent group arises from the fact that it does not depend on the geometric scales of the pre-pregger.

For "Tanner" type fluids (b = 2n), Eq. (4.40) shows that

We
$$\alpha$$
 $(\dot{\gamma})^n$.

Therefore, with n=1, the increase in the ratio of normal to viscous stresses is proportional to the strain rate. For shear thinning fluids (n<1), the increase in We with $\dot{\gamma}_c$ is diminished. Although the exponent "b" for polymer melt is nominally less than two, $(b \le 2)$, Eq. (4.40) predicts more than a proportional increase in We with $\dot{\gamma}_c$ even for shear thinning fluids provided b>1+n. One of the constituents for the model fluids in this study (CTBN) has exponents of b=1.9 and n=0.5 (see Table 5.2).

The four geometric scales of the pre-pregger give three dimensionless ratios based on the radius of the outlet tube:

$$\beta_{R} = \frac{R}{R_{A}} \tag{4.41}$$

$$\beta_{L} = \frac{L_{d}}{R_{A}} \tag{4.42}$$

$$\beta_{\pi} = \frac{H}{R_{A}} \tag{4.43}$$

Eq. (4.10), with $r=R_d$ defines the remaining dimensionless group as a velocity ratio α ($\equiv \alpha(R_d)$). Thus, using the foregoing definitions, Eq. (4.38) can be rewritten as an equation for α ,

$$F(\alpha) = c_1 \alpha + c_2 \alpha^n - c_3 = 0$$
 (4.44)

Hereinafter, the symbol α denotes Eq. (4.10) evaluated at $r = R_a$. The coefficients in Eq. (4.44) are defined as follows (see Appendix C for a derivation of c_1 , c_2 , and c_3)

$$c_1(n, \beta_m, \beta_R) = -\frac{4}{\beta_L} \frac{1-\beta_R^{n-1}}{n-1} + \frac{8\beta_R}{5} \frac{1-\beta_R^{n-3}}{3-n}$$

$$+\frac{8}{3 \beta_{\rm m} (1+n)} \left[\frac{13 (1+3n)^2 n}{70 (1+n)^3} \beta_{\rm m}^4\right]$$

$$+ \frac{9 + 54n + 264n^{2} + 432n^{3} + 231n^{4} + 90n^{5}}{5 (1+n)^{3} (1+2n)} \beta_{n}^{2}$$

$$+\frac{1+14n+56n^2+74n^3+31n^4}{4(1+n)^2(1+3n)(1+5n)}$$
 (4.45)

$$C_2(n, \beta_H, \beta_L) = 2 \beta_L \left[\frac{2}{3} \beta_H^2 \frac{1+3n}{n} \right]^n$$
 (4.46)

$$c_3(n, \beta_R, \beta_R, G, b) = 2G\beta_R^{n-b} \frac{(1+b)\beta_R^b - 1}{2b}$$
 (4.47)

Note that the coefficient c_3 is proportional to G. The dimensionless gap width, β_R , and the viscosity exponent, n, appear in all three coefficients of Eq. (4.44).

Eq. (4.44) can be used to compute G in terms of the remaining six groups. A simple rearrangement of Eq. (4.44) yields

$$G = C_1 \cdot \alpha + C_2 \cdot \alpha^n \tag{4.48}$$

where

$$C_1' \equiv \frac{C_1}{C_3'} ,$$

$$C_2' \equiv \frac{C_2}{C_3'} ,$$

$$C_3' \equiv \frac{C_3}{G} .$$

 c_1^* depends on n, b, β_R^* , and β_R^* . On the other hand, c_2^* depends on n, b, β_R^* , and β_R^* as well as β_L^* . If n < 1, then Eq. (4.48) predicts that (see Eqs. (4.10) and (4.39))

$$Q \propto \frac{a}{k} (\omega)^{b-n+1}$$
 for $\alpha \to \infty$; and, (4.49)

$$Q \propto \left(\frac{a}{k}\right)^{\frac{1}{n}} (\omega)^{\frac{b}{n}}$$
 for $\alpha \to 0$. (4.50)

For the special case n=1 (i.e., constant viscosity fluid), Eq. (4.48) implies that $G \propto \alpha$ for all values of α . Thus,

$$Q \propto \frac{a}{k} \omega^b \text{ for } n = 1 . \tag{4.51}$$

The asymptotic results given by Eqs. (4.49) and (4.50) provide a means to compare the consistency between the flow model and the independently measured power exponents, n and b.

Eq. (4.44), or Eq. (4.48) determines the distribution of energy "transferred" to the fluid into two distinct channels: either viscous dissipation in Regions I and II or viscous dissipation in Region III (see Figure 3.1). The

equation can be rewritten as (cf. Eq. (4.38))

$$\frac{C_1}{C_3} \frac{\alpha^2}{\alpha} + \frac{C_2}{C_3} \frac{\alpha^{n+1}}{\alpha} = 1 \tag{4.44a}$$

where

$$X = \frac{c_1 \alpha^2}{c_3 \alpha} = \frac{\begin{pmatrix} \text{viscous dissipation in} \\ \text{Regions I and II} \end{pmatrix}}{\begin{pmatrix} \text{elastic transfer and} \\ \text{storage of energy} \end{pmatrix}}$$

$$1 - X = \frac{c_2 \alpha^{n+1}}{c_3 \alpha} = \frac{\begin{pmatrix} \text{viscous dissipation in} \\ \text{Region III} \end{pmatrix}}{\begin{pmatrix} \text{elastic transfer and} \\ \text{storage of energy} \end{pmatrix}}$$

The magnitude of X provides a quantitative measure of which dissipation process dominates the performance of the prepregger (see Section 4.8).

4.7 Flow Capacity for a Boger Fluid

The special case of Eq. (4.48) for which n = 1 and b = 2 (i.e., "Boger" fluid) implies that

$$Q_{BF} = K \frac{a}{k} \omega^2 \tag{4.52}$$

where

$$K = \frac{2\pi R_d^2 H}{3(c_1^* + c_2^*)} . (4.53)$$

The dimensionless coefficients c_1 ($\equiv c_1/c_3$) and c_2 ($\equiv c_2/c_3$) follow directly from Eqs. (4.45) - (4.47) by setting n=1 and b=2. The first term in Eq. (4.45) for n=1 reduces to

$$-\frac{4}{\beta_{R}} \lim_{n\to 1} \frac{1-\beta_{R}^{n-1}}{n-1} = +\frac{4}{\beta_{R}} \ln(\beta_{R}).$$

Therefore, Eqs. (4.45) through (4.47) for n = 1 and b = 2 are

$$c_{1}(1,\beta_{H},\beta_{R}) = \frac{4}{\beta_{H}} \ln(\beta_{R}) + \frac{4}{5} \beta_{H} (1 - \beta_{R}^{-2}) + \frac{4}{3\beta_{H}} (\frac{13}{35} \beta_{H}^{4} + 9 \beta_{H}^{2} + \frac{131}{384})$$
(4.54)

$$c_{2}(1,\beta_{H},\beta_{L}) = \frac{16}{3} \beta_{L} \beta_{H}^{2}$$
 (4.55)

$$c_3(1,\beta_H,\beta_R,G,2) = \frac{G}{2\beta_H}(3\beta_R^2 - 1) = c_3^* G.$$
 (4.56)

Eq. (4.52) shows that the volumetric flow rate of a viscoelastic fluid having a constant viscosity and a constant primary normal stress difference (i.e., $a/k = 2\lambda$

for n = 1 and b = 2) has a quadratic dependence on the angular velocity. As previously shown, the power law exponents $n \neq 1$ and $b \neq 2$ moderate this conclusion (see, for example, Eqs. (4.49) and (4.50)). Moreover, for small values of $\beta_{\rm m}$, the foregoing results also imply that $(c_1^* + c_2^*)$ is independent of $\beta_{\rm m}$. Thus, Eqs. (4.52) and (4.53) imply that

$$Q_{pp} \propto H\omega^2 \text{ for } H \rightarrow 0.$$
 (4.57)

In this limit, the dissipation in Region I balances the elastic storage and surface work term in Eq. (4.35). On the other hand, for large values of $\beta_{_{\rm H}}$,

$$\lim_{B_{2}\to\infty} (C_{1}^{*} + C_{2}^{*}) \propto B_{H}^{4} , \qquad (4.58)$$

which implies

$$Q_{BF} \propto \frac{\omega^2}{H^3} \text{ for } H \to \infty$$
 (4.59)

In this limit, the dissipation in Region II balances the elastic storage and surface work terms in Eq. (4.35). These theoretical observations anticipate that $Q_{\rm pp}$ attains a maximum value for some intermediate value of H.

4.8 Parametric Study

The velocity ratio, α , defined by Eq. (4.10), with $r=R_a$, depends on six dimensionless groups: β_R , β_R , β_L , G, n, and b. Eq.(4.44) is a power balance on the rotating die prepregger which determines α . An interval halving technique was developed to solve this equation for arbitrary values of the six groups listed above. Appendix D gives a listing of the computer code which accomplishes this task. The scope of the parametric study was limited to simulate the experimental equipment and the model fluids studied. Thus, the operating parameter G, defined by Eq. (4.39), ranges from 0 to 50. The geometric ratios examined covered the following range

$$1 \leq \beta_{p} \leq 50$$

$$0.1 \leq B_{L} \leq 100$$

$$0.1 \leq \beta_{R} \leq 3.5$$
.

The viscosity exponent n (see Eq. (3.6)), and the exponent b for the primary normal stress coefficient (see Eq. (3.7)) are related by b = 2n for "Tanner" fluids. (see Figure 4.2). These empirical exponents b and n were also varied independently to ascertain their individual effect on the velocity ratio α . Both the shear thinning (n < 1) and shear thickening (n > 1) fluids were simulated.

Figure 4.2 shows the effect of the gap width on the

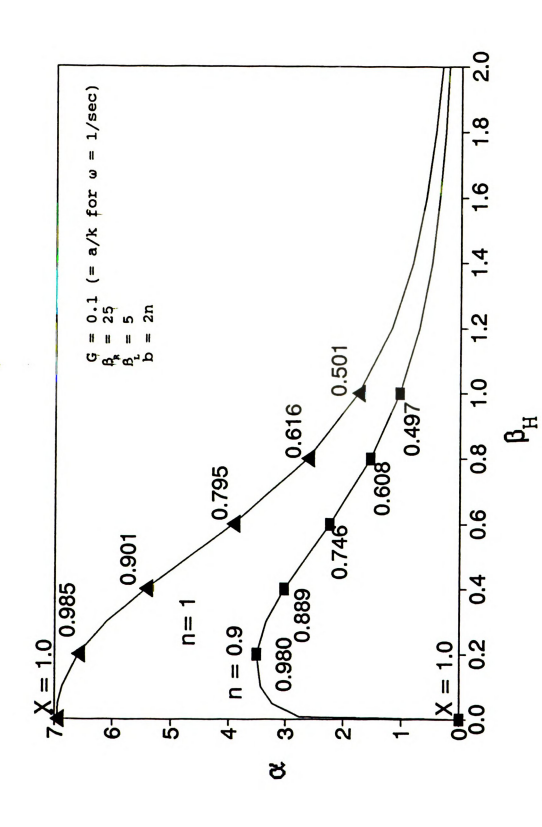


Figure 4.2: The Effect of the Viscosity Exponent on the Velocity Ratio.

velocity ratio α for two different "Tanner" fluids (i.e. b = 2n). The calculations show that the flow capacity of the pre-pregger can be significantly increased by decreasing the gap width H relative to the radius of the exit tube (i.e. $\beta_{\rm m} << 1$). The shear thinning fluid (n < 1) responds similarly, but the magnitude of α is less. For $\beta_{\rm m} \cong 0.1$, the velocity ratio for n = 0.9 is about a factor of two smaller than α for n = 1.0. This occurs because the large increase in the normal stresses, which occurs as the gap width decreases, is moderated by the shear thinning effect. This conclusion follows directly from Eq. (4.40), which shows that the incremental increase in the Weissenberg number with the shear rate depends on the exponent n.

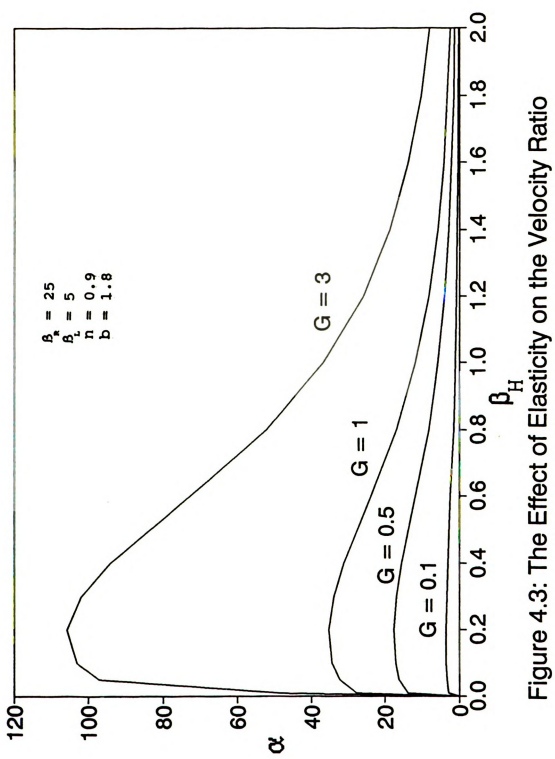
The parameterization of the α curves in Figure 4.2 by X (see Eq. (4.44a)) shows that the dissipation of energy in Region I (and II) determines α for $\beta_{_{\rm H}} < 1$ and that dissipation in Region III controls α for $\beta_{_{\rm H}} > 1$. It is noteworthy that the magnitude of X is distributed along the α curves in about the same way for the two cases n=1, and n=0.9, although the values of α differ significantly for small gap widths.

For the shear thinning fluid, α attains a maximum at $\beta_{\rm m}\cong 0.2$, where X = 0.980. For smaller values of $\beta_{\rm m}$, the velocity ratio decreases rapidly to zero because the balance between the viscous dissipation and the elastic work terms in the power balance cannot support a non-zero

flow rate. This follows by examining the behavior of Eq. (4.32) for $\beta_{\pi} \rightarrow 0$. Because $c_2 \rightarrow 0$ as $\beta_{\pi} \rightarrow 0$ (see Eq. (4.46)), Eq. (4.32) implies that

$$\lim_{\mathbf{B}_{-}\to 0} \alpha \propto (\mathbf{B}_{\mathbf{H}})^{1+n-b} . \tag{4.60}$$

Thus, for b = 2n and n < 1, the above result shows that α \rightarrow 0 for $\beta_{\mathbf{x}} \rightarrow$ 0. However, for b = 2n and n = 1, the velocity ratio approaches some non-zero value as $\beta_{\mu} \rightarrow 0$. Finally, for 1+n < b, α becomes unbounded as $\beta \rightarrow 0$. Figure 4.3 shows that the parameter G has a significant effect on the velocity ratio α . For fixed values of G, the α curves are similar to the shear thinning example portrayed by Figure 4.2. Once again, because 1+n > b, the flow rate suddenly drops to zero below a critical value of $\beta_{\rm L}$ < 0.20. Although the radial component of the velocity may be two orders of magnitude larger than the tangential velocity for β = 0.2 and G = 3, Figure 4.1 shows that the local orientation of the flow field changes rapidly to a predominantly tangential flow once $r/R_d > 10$. The effect on α of increasing the ratio of the die tube length to the die tube radius is seen in Figure 4.4. When the length of the die tube is increased, $\beta_{\!\scriptscriptstyle L}$ increases, and α decreases. However, for values of β_{π} below 0.1, the value of α becomes insensitive to the value of β . This occurs because the flow resistance in the narrow gap dominates



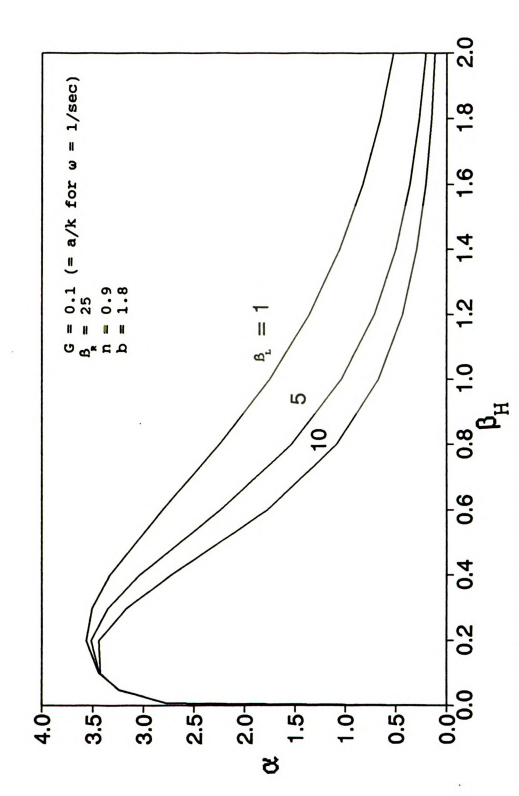


Figure 4.4: The Effect of Land Length on the Velocity Ratio

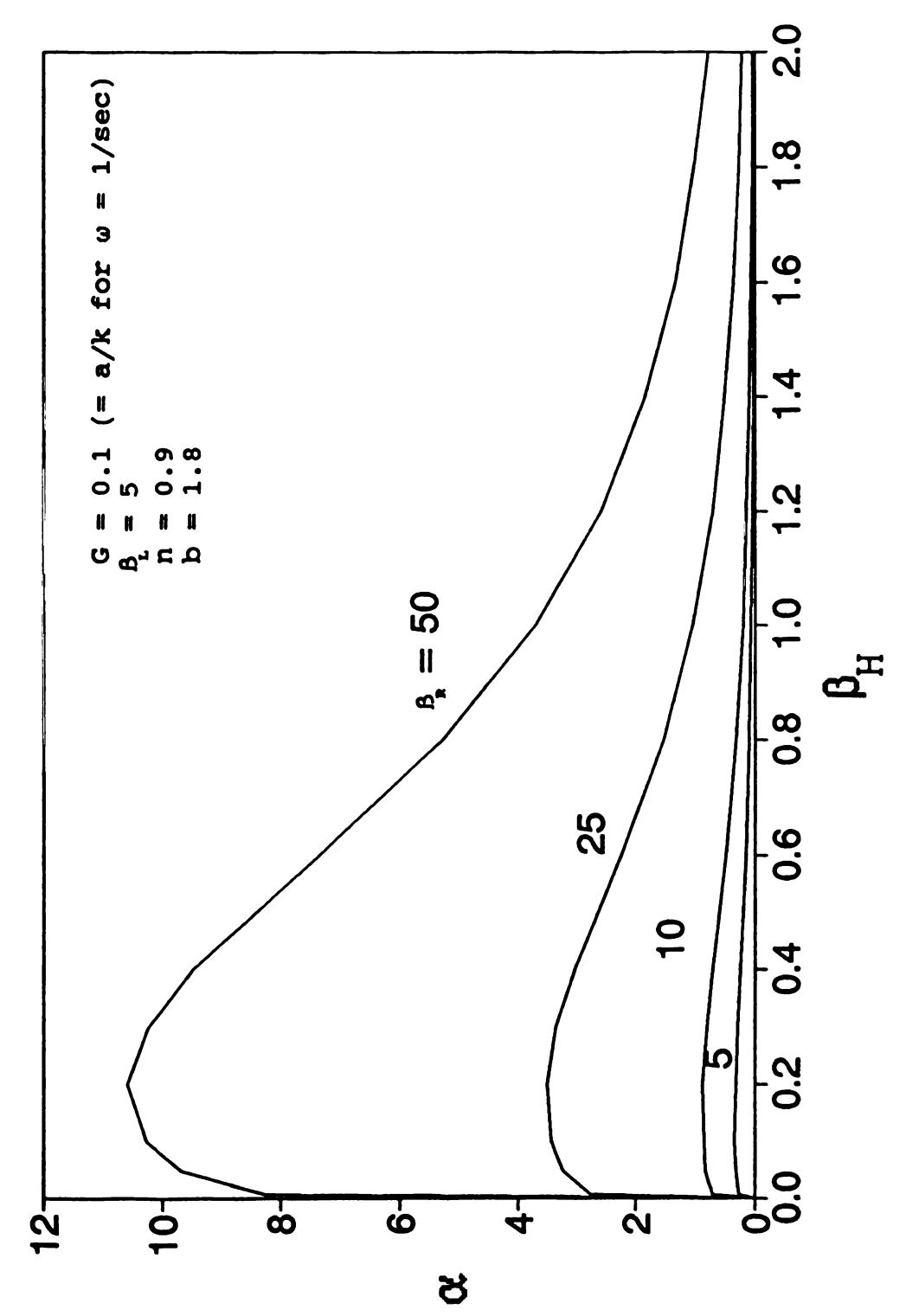


Figure 4.5: The Effect of the Disk Radius on the Velocity Ratio

(i.e., X is close to unity). Figure 4.4 also shows that the peak value of α occurs at larger values of $\beta_{\rm H}$ as $\beta_{\rm L}$ decreases. This illustrates the fact that the peak in α corresponds to a shifting of the dissipation domain from Regions I and II to Region III.

 β_R is the dimensionless ratio of the disk radius to the die tube radius. Figure 4.5 shows that for a fixed value of β_R , α increases as β_R increases. Doubling β_R from 25 to 50 almost triples α at low values of β_R . This means that the flow field becomes much more radial as β_R is decreased, and also as β_R is increased. Note that the peak value of α occurs at larger values of β_R as β_R increases. This shows that slightly larger gap widths are required to shift the dissipation from Regions I (and II) to Region III.

Figure 4.6 shows the effect of changing the viscosity exponent, n, on the velocity ratio, α . For fixed values of β and G (which is also a function of n), the value of α rises as the value of n decreases. Thus, a decrease in n increases the radial nature of the flow, and the fluid takes fewer spirals around the disk on its way from the periphery of the disk to the entry of the die tube. Note that the behavior of the family of curves changes near the origin, as n increases. This behavior is due to the fact that b=2 for these calculations. The asymptotic behavior of α for small values of β explains the different behavior for

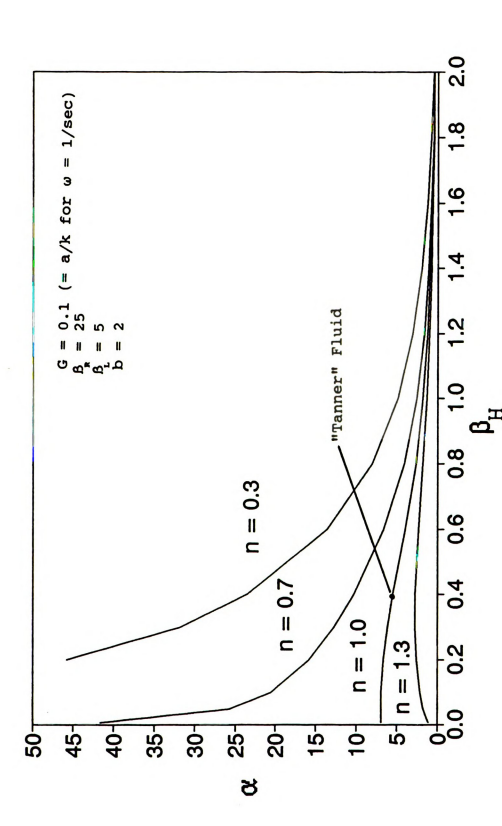


Figure 4.6: The Effect of the Viscosity Exponent on the Velocity Ratio

shear thinning (n < 1) and shear thickening (n > 1) fluids. It follows from Eq. (4.60) that $\alpha \to 0$ as $\beta_{\underline{n}} \to 0$ provided (1+n) > b; and $\alpha \to \infty$ as $\beta_{\underline{n}} \to 0$ for (1+n) < b. Thus, the calculations presented by Figure 4.6 for b = 2 illustrate these two limiting cases. Of course, Figure 4.2 already shows that for b = 2n and n < 1, the velocity ratio is bounded. The conclusion which stems from these calculations is that the parameter l = b - (1+n) has a dramatic effect on the behavior of the velocity ratio. For l = 0, $\alpha \to constant$ as $\beta_{\underline{n}} \to 0$. However, for l > 0, $\alpha \to \infty$ as $\beta_{\underline{n}} \to 0$; whereas for l < 0, $\alpha \to 0$ as $\beta_{\underline{n}} \to 0$.

The effect of the elasticity exponent, b, on the velocity ratio is shown in Figure 4.7. As b increases, α increases for a given value of $\beta_{\rm H}$. However, note that the curves change their nature near the origin in a manner analogous to that shown by Figure 4.6. Once again, an understanding of the three cases shown follows from Eq. (4.40).

The parametric study illustrates the interaction of the seven dimensionless groups that make up the flow equation. Practical questions about specific pre-pregger operations can now be answered. These results will be of assistance in the design and operation of the pre-pregger.

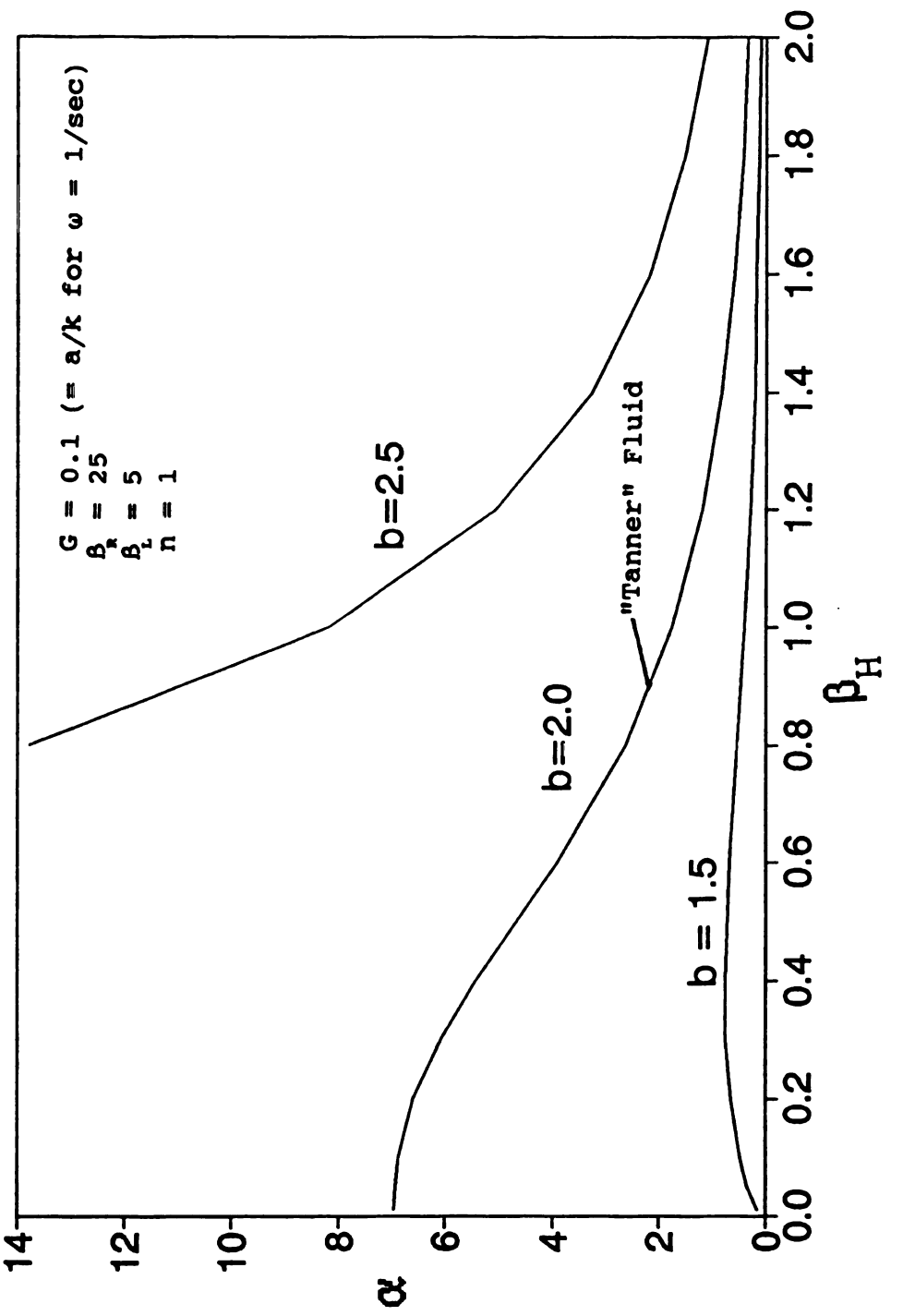


Figure 4.7: The Effect of the Normal Stress Coefficient Exponent on the Velocity Ratio.

Chapter 5 Experiments

5.1 Introduction

Experiments were conducted to determine the flow capacity of the rotating die prepregger in the absence of a fiber tow. Table 5.1 defines the model viscoelastic fluids used to simulate the rheological response of thermoplastic resins. For low strain rates, the PIB solution has a constant viscosity coefficient, whereas the two Separan AP-30 solutions show significant shear thinning behavior. These fluids also exhibit strong elastic behavior. The two blends of CTBN and Epon 828 show weak elastic behavior and constant viscosity, and the neat polybutene and neat Epon 828 showed insignificant elastic behavior and constant viscosity.

The 0.3 wt% PIB solution was prepared by dissolving solid polyisobutylene rubber in a known amount of kerosene while stirring over gentle heat. This solution was then mixed into the polybutene liquid to form a clear, visibly homogeneous solution. The solution was kept in a tightly covered glass jar for six months. This solution was similar to one used by Chmielewski (1990).

Table 5.1: Experimental Fluids; Constituents and Suppliers

Fluid Name	Density* (g/cm [*])	Constituents	Supplier
23 wt% CTBN in Epon 828	1.13	23 wt% Carboxy-Terminated Acrylonitrile/Butadiene Rubber (CTBN) (HYCAR 1300X13) M = 3200	B.F. Goodrich
		77 wt% Bisphenol A - Diglycidyl Ether Epoxide (DEGBA) (Epon 828) M _w = 340	Shell
40 wt% CTBN in Epon 828	1.09	40 wt% CTBN 60 wt% Epon 828	
0.3 wt% PIB in PB	688.0	0.3 wt% polyisobutylene (Vistanex L-12g) $\overline{M}_{w} = 1.66 \times 10$	Exxon
		4.4 wt% kerosene	
		95.3 wt% polybutene (Indopol H300) M ≈ 2000	Amoco
5 wt% Separan	1.18	5 wt% copolymer of polyacrylamide and polyacrylonitrile (Separan AP=30) $\overline{M}_{\infty} \approx 4 \times 10^6$	Dow
		42.5 wt% distilled water	
		42.5 wt% glycerol	

* Densities measured by gravimetric means.

The Separan AP-30 solution was prepared by following the protocol described by Good, et al. (1974). The solution was made by slowly mixing the Separan AP-30 powder into a mixture of glycerine and water. Care was taken to wet each particle and to avoid clumps. The solution showed very strong rod-climbing tendencies. After being allowed to stand for a week, the fluid appeared clear with no haziness or regions of dissimilar refractive index. The Separan AP-30 solution was tested after one week, and the remainder was kept for six months in a tightly capped glass jar for subsequent testing. These solutions are referred to as 'fresh' and 'aged' respectively.

The blends of CTBN and Epon 828 contained no curing agent. The two liquids mixed to form an optically clear, visibly homogeneous solution with a slight tendency to climb the shaft of the mixer. This rod-climbing behavior is a sign of an elastic nature, as discussed in Chapter 3. Both of the CTBN/Epon 828 blends were kept in tightly capped glass jars to prevent evaporation. Epon 828 and polybutene were tested as pure (neat) liquids.

The primary normal stress difference and the viscosity coefficients of these fluids were measured over a range of strain rates, as discussed in Section 5.2. The design and operating procedures for the rotating die prepregger are presented in Section 5.3, while the scope and the results of the experimental work are summarized in Section 5.4.

Section 5.5 provides an interpretation of the results as well as comparison with earlier experimental work and the model developed in Chapter 4.

5.2 Rheological Parameters

The rheological characterization experiments were done on a Rheometrics Mechanical Spectrometer Model 800 (also known as the RMS-800). Figure 5.1 shows a schematic of the cone and plate configuration used. The cone is kept stationary, and the torque and normal force necessary to keep it stationary are measured. The coordinate system is spherical, with its origin at the tip of the cone. The subscript r refers to the radial coordinate, while ϕ is the rotational coordinate, and θ is the azimuthal coordinate. The cone angle, θ , is made small enough that the approximation $\sin \theta \cong \theta$ can be used to simplify the derivation of the flow field (see Appendix A, and Bird, et al., p. 522, 1987).

To measure the rheological properties of a fluid, the fluid is loaded onto the plate, then the cone is lowered until the gap between the tip of the cone and the plate is 500 microns. Care is taken to ensure that the fluid in the tool contains no voids and that there is no excess fluid on the edges of the tool. For a steady shear test, the plate is rotated at a given radial velocity, and the signals from the torque and normal force transducers are read.

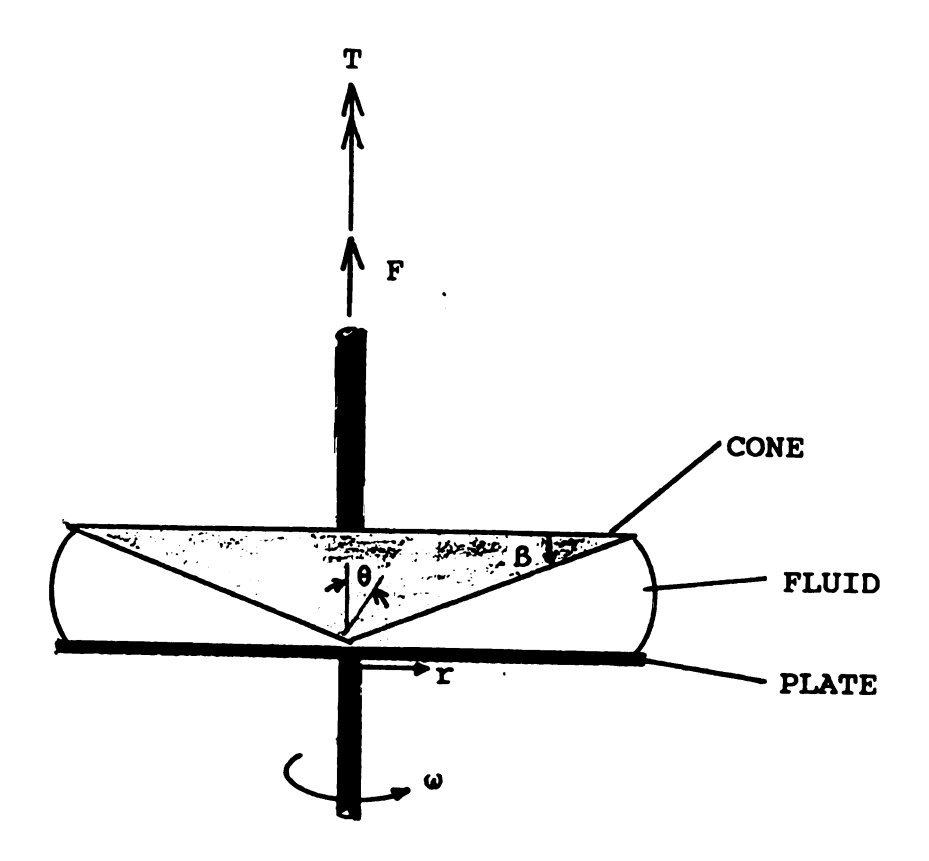


Figure 5.1: The Cone and Plate Rheometer

The shear stress, the viscosity coefficient, and the primary normal stress difference are calculated from readings of the transducers, which produce signals from calibrated strain gauges. The torque transducer has a range of ± 2000 grams, and is accurate to ± 2 grams. The lever arm of the torque transducer is fixed at 1.0 cm, so the 'torque' reading, M₁, from the torque transducer has units of gram-cm. M₁ is multiplied by the acceleration due to gravity to obtain the torque acting on the cone (T = M₁g). The servo-motor which rotates the bottom plate is driven by a controller which reads the angular velocity to 0.1%, but is not accurate at rotation rates above 100 radians per second.

The viscosity coefficient is calculated by relating the shear stress to the measured torque and the strain rate to the measured angular velocity. For the RMS-800 apparatus, the viscosity coefficient η is given by (see Figure 5.1 and p. 522 in Bird et al., 1987)

$$\eta = \frac{\tau_{\phi\theta}}{\dot{y}} = \frac{\left(\frac{3M_1g}{2\pi R^3}\right)}{\left(\frac{\omega}{B}\right)}$$
 (5.1)

where,

 $\tau_{e\theta}$ is the shear stress (dyne/cm²)

y is the strain rate (1/sec)

M, is the reading from the torque transducer (g-cm)

g is the acceleration due to gravity (cm/sec2)

ω is the angular velocity (sec⁻¹)

R is the radius of the plate (1.25 cm)

B is the cone angle (0.108 radians)

The reading, M_2 , from the normal force transducer has a range of ± 2000 grams, and is accurate to ± 0.1 %. However, readings are not accurate below 2 grams. The normal force acting on the apparatus is obtained by multiplying this reading by the acceleration due to gravity ($F = M_2$ g). The primary normal stress difference is given by (see Figure 5.1 and p. 523 in Bird et al., 1987)

$$N_1 = \frac{2M_2g}{\pi R^2} \tag{5.2}$$

where,

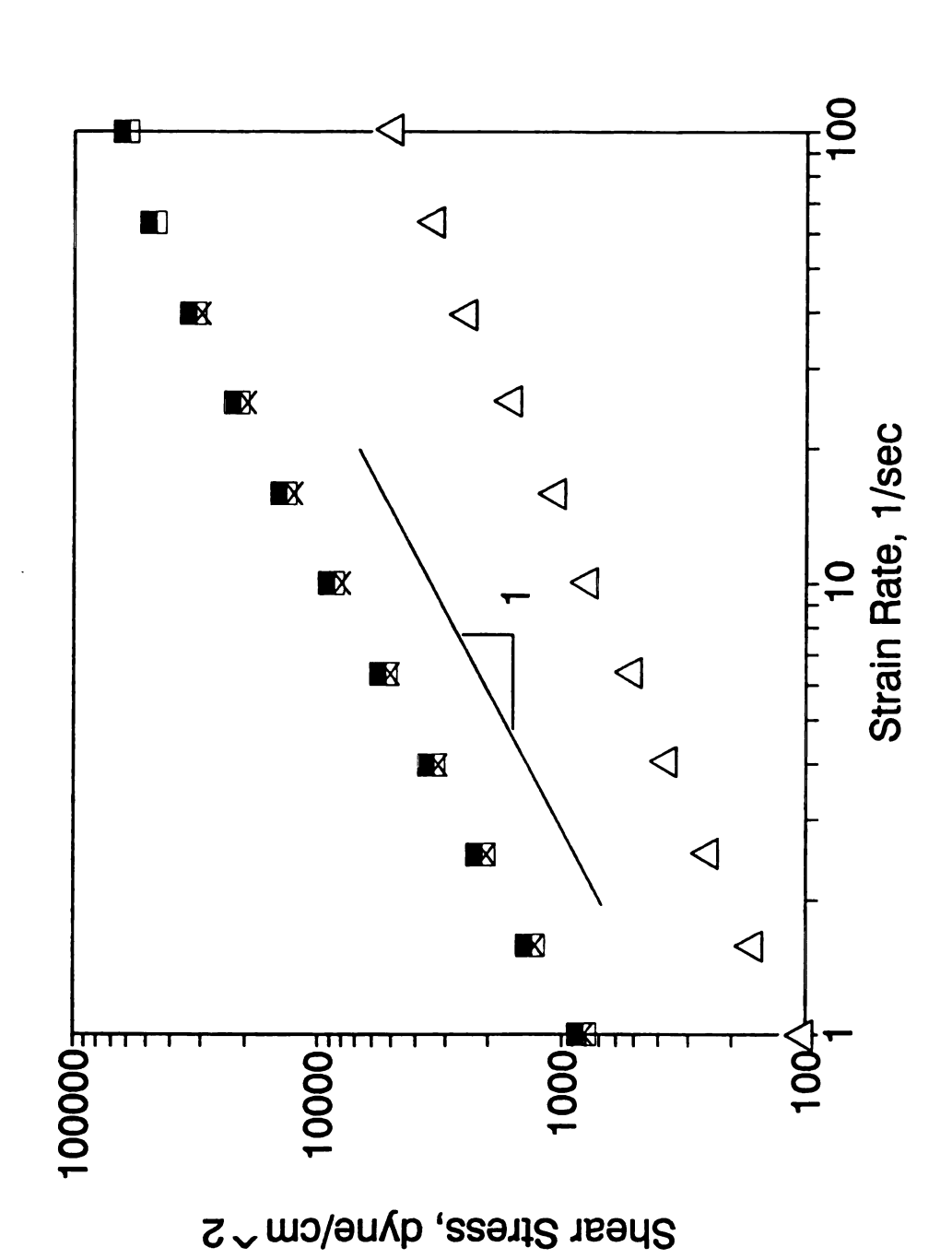
M₂ is the reading from the normal stress transducer (g)

g is the acceleration due to gravity (cm/sec2)

R is the radius of the plate (1.25 cm)

The viscosity coefficient and the primary normal stress difference were measured for all the test fluids over a range of strain rates.

Figure 5.2 shows a log-log plot of the shear stress, $\tau_{\theta z}$ against the strain rate, $(\dot{\gamma} = \frac{\omega}{B})$. The 23 and 40 wt% blends of CTBN and Epon 828 have very similar curves to the polybutene. The slope of the curves is the viscosity exponent, and slopes for these three fluids are equal to one. The value of the intercept gives the value of the viscosity coefficient, k, and values for all three fluids fall at about 800 dyne/cm². The curve for Epon 828 has a constant slope of less than one, and an intercept just over 100 dyne/cm².



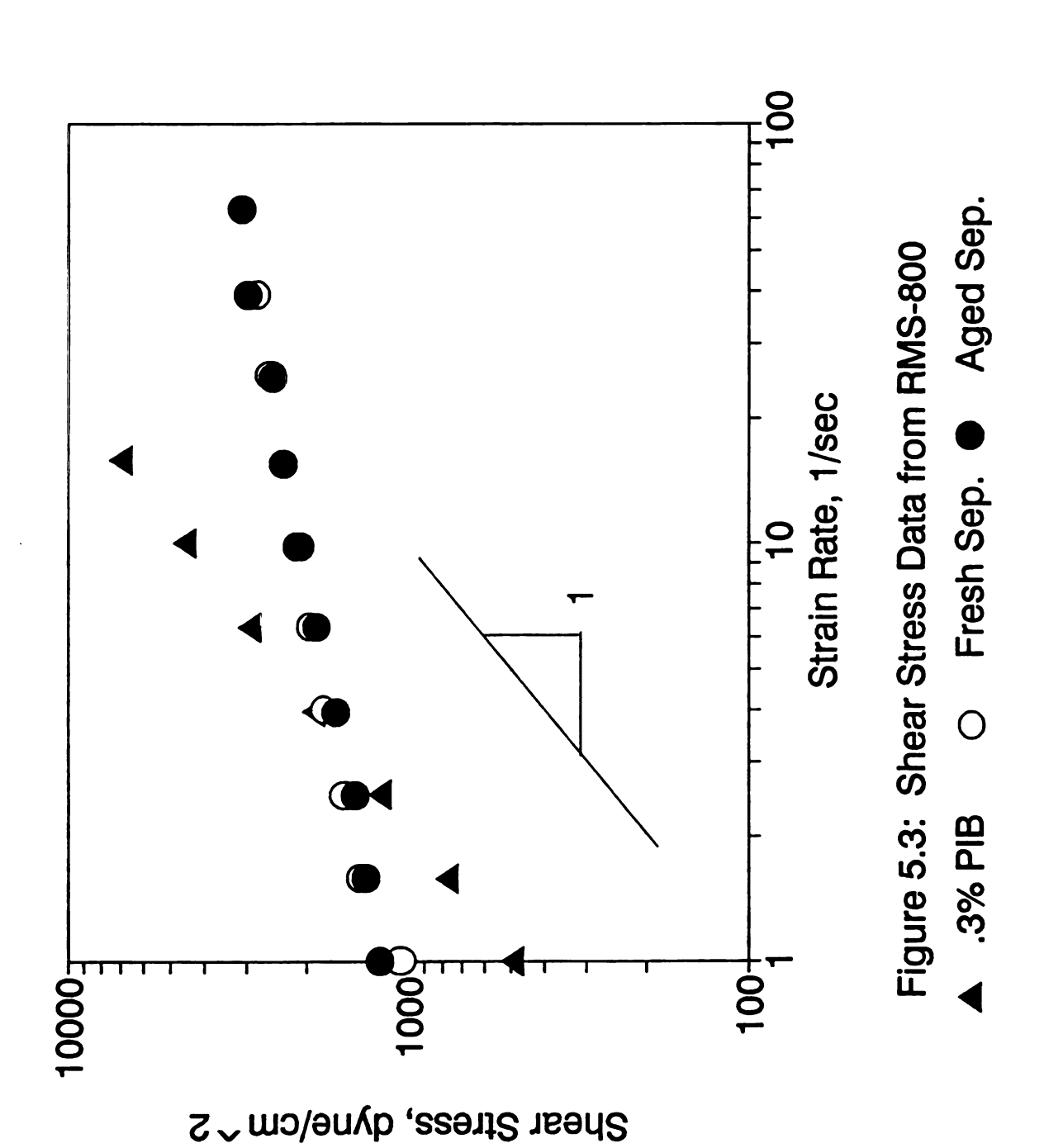
polybutene X Figure 5.2: Shear Stress Data from RMS-800 40% blend △ Epon 828 23% blend

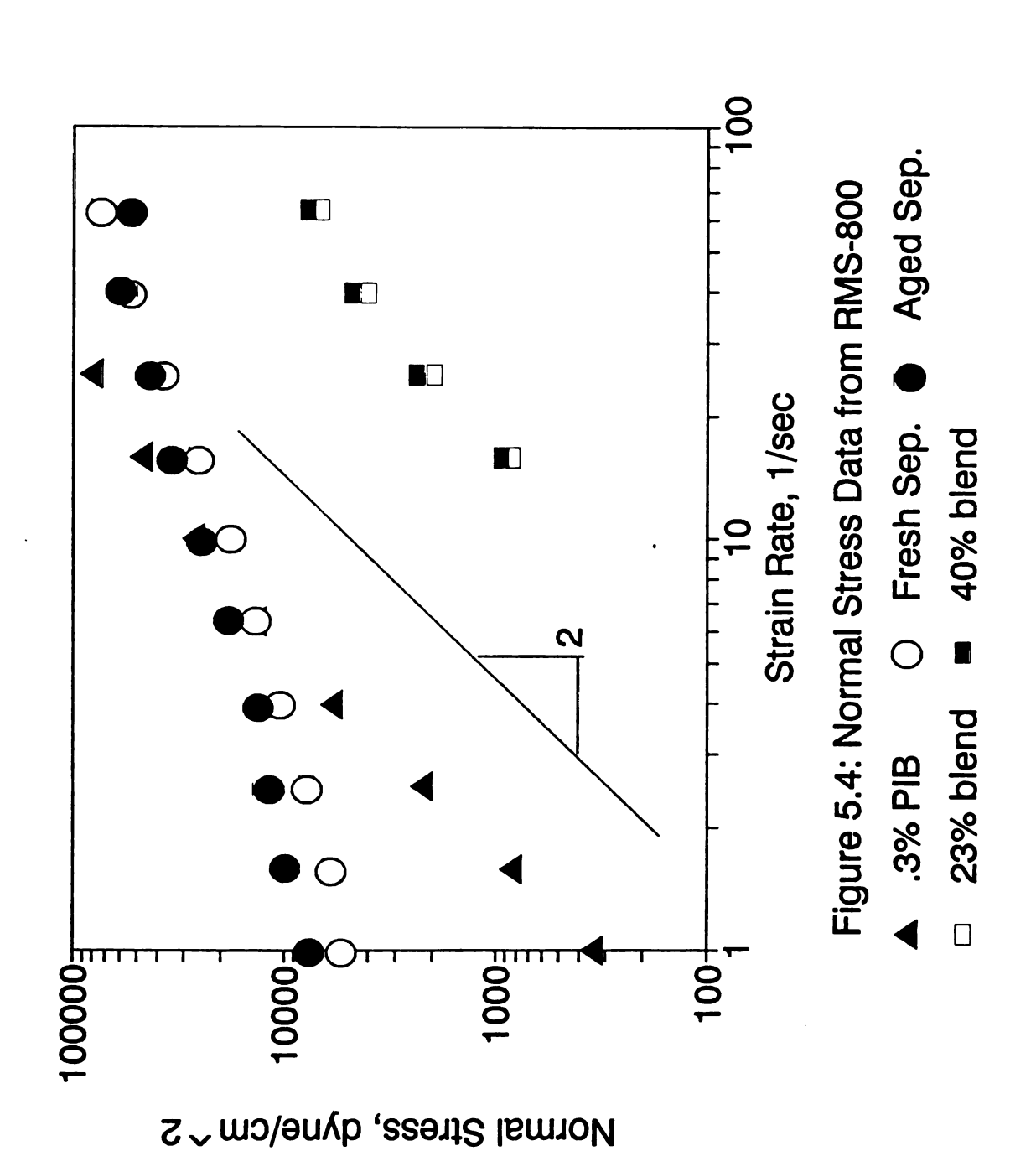
The shear stress versus strain rate data for the PIB and Separan solutions are plotted on log-log coordinates in Figure 5.3. The PIB data lie on a curve with a constant slope nearly equal to one, and an intercept at about 500 dyne/cm². The two Separan solutions have curves which have slopes very different from one, and intercepts at about 1000 dyne/cm².

The viscosity power-law parameters k and n (see Equation 4.4) were determined from the data depicted in Figures 5.2 and 5.3, using a linear regression program, where the slope was equal to n, and the intercept was equal to log(k). The constants are tabulated in Table 5.2.

Figure 5.4 shows the first normal stress difference, N₁, plotted against the strain rate on log-log coordinates.

Note that the curves for the two Separan solutions are mildly 'S' shaped. The curve for the PIB solution has a constant slope of 2 for low strain rates, but the slope decreases with increasing strain rate above 10/sec. The curves for the blends of CTBN and Epon 828 contain data at only large strain rates, because the normal stress difference was below the sensitivity of the RMS-800 at the lower strain rates. Despite the deviations from linearity, all of these curves were modeled as power laws (see Equation 4.5) and the linear regression program was used to obtain (slope = b) and (intercept = log(a)). The results are summarized in Table 5.2.





Rheological Constants for Experimental Fluids Table 5.2:

Fluid	کا [seg]	$\frac{k}{\text{dyne sec}^{n/\text{cm}^{2}}}$	r L	$[\mathrm{dyne\ sec}^{\mathrm{a}}/\mathrm{cm}^{2}]$	Q
Epon 828 Polybutene CTBN	0.003	120. 820. 8700.	1.0	45.	1.9
23 wt% CTBN in Epon 828 40 wt% CTBN in Epon 828	0.004	850. 950.	96.0	6.9	1.5
0.3 wt% PIB 5 wt% Separan, fresh 5 wt% Separan, aged	0.43 1.74 3.07	500. 1250. 1220.	0.96	430 4400 7500	1.7 0.66 0.53
<pre>5 wt% Polyacrylamide*</pre>	0.19	15.9 110.	0.69	6.0	1.10
Polyethylene **	26.5	8.69	0.40	4.6	0.79
0.3 wt% PIB in polybutene ## 1000 ppm PIB in polybutene ##	0.32	510. 400.	1.0	326.40 213.8	2.00
* Drom Cook of all (1024)	oned pouten	2 and horizon according to the factors of and	hir a fa		100

From Good, et al. (1974). Values have been corrected by a factor of πR^2 , to match normal force graphs given as Figures 3 and 4.

^{**} From Good, et al. (1974).

From Chmielewski (1990).

^{##} From Prilutski (1983).

The rheological characterizations summarized in Table 5.2 are valid over the test range of $1 \le \dot{\gamma} \le 100 \text{ sec}^{-1}$. The flow model assumes that the characterizations can be extrapolated to the shear rates encountered in the pre-pregger, the maximum of which is:

$$\dot{\gamma}_{\text{max}} = \left[\frac{R \omega_{\text{max}}}{H_{\text{min}}} \right] = \frac{2.5 \text{cm} \times 22 \text{sec}^{-1}}{0.1 \text{ cm}} = 550 \text{ sec}^{-1}$$
.

The mild 'S' shape of the N_1 versus $\dot{\gamma}$ curves for the Separan solutions suggests that the slope decreases as $\dot{\gamma}$ increases, i.e. b decreases. This could cause the flow model to overestimate Q at strain rates for which b is less than the value reported in Table 5.2. If n decreases with $\dot{\gamma}$, then the model will tend to underestimate Q. Equation (4.5) shows that the characteristic time, λ , for any given strain rate can be calculated if the viscosity and the first normal stress difference of the fluid are known at that strain rate:

$$\lambda = \frac{\Psi_1}{2\eta} = \frac{a \dot{\gamma}^{b-2}}{2k \dot{\gamma}^{n-1}} = \frac{a}{2k} \dot{\gamma}^{b-n-1}. \tag{5.3}$$

Note that λ is not a constant with respect to strain rate unless the viscosity and first normal stress coefficient are both constants with respect to strain rate (i.e. n=1 and

b=2). Chmielewski (1990) estimated λ for a similar 0.3 wt% PIB solution at strain rates sufficiently low that b = 2. However, strain rates as low as this were not investigated in this study. Instead, the values of λ reported in Table 5.2 were calculated for $\dot{\gamma}$ = 1/sec.

$$\lambda_{o} = \frac{a}{2k}. \tag{5.4}$$

The rheological constants of the test fluids are reported in Table 5.2, along with some values from the literature. Note that Epon 828 and polybutene are Newtonian fluids, and no elasticity constants are reported for them. Also note that the values of a for the blends of CTBN and Epon are small compared to the fluids that are considered strongly The PIB solution was formulated to imitate a solution studied by Chmielewski (1990), the constants of which appear in Table 5.2 for comparison. The values of a, k, and n are comparable, but the value of b reported for the present study is less than that reported by Chmielewski. This is because the values of a and b for the fluids of the present study were derived from a linear regression which included a part of the first normal stress difference curve that did not have a slope of 2. Chmielewski's value of b takes into account only that part of the curve where the slope is 2.

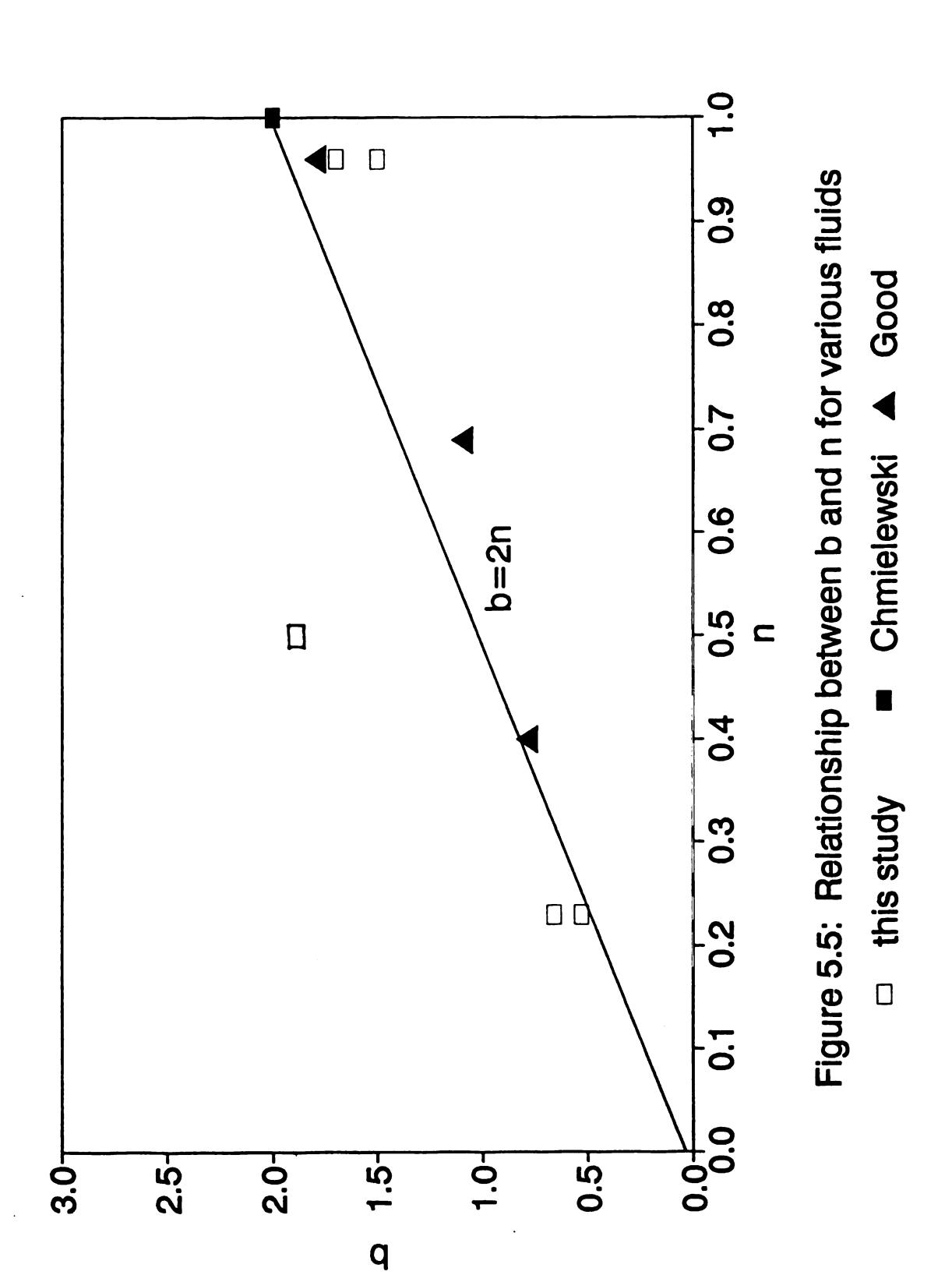
The Separan AP-30 solution was formulated following the

recipe given in Good (1974) for a polyacrylamide solution. Reference to Table 5.2 will show that the rheological constants of the two fluids are different by two orders of magnitude for k, and three orders of magnitude for a. The polyacrylamide solution has values of a and k which make it more similar to the CTBN/Epon 828 blends than to the Separan solutions. This large difference in rheological characters may be attributed to the fact that Separan AP-30 is a copolymer of polyacrylamide and acrylonitrile. The addition of acrylonitrile will affect the hydrogen bonding density of the polymer molecules with the water in the solution. If hydrogen bonds can be considered as a weak cross-link, then changing the hydrogen bonding density or strength will change the effective molecular weight of the polymer (Davidson).

From the discussion in Chapter 3, where a Tanner fluid was defined as a fluid where b=2n, and a Boger fluid was defined as having b=2, and n=1, it is apparent that the PIB solution is a Boger fluid at very low shear rates, and the Separan solutions are nearly Tanner fluids. Figure 5.5 shows graphically the relationship between b and n for the fluids of Table 5.2. Figure 5.5 shows that b=2n is a good approximation for the fluids of this study.

5.3 Experimental Apparatus and Procedure

Figure 5.6 shows a schematic of the rotating die pre-



pregger used in this study, while Figure 5.7 shows a schematic cross-section of the die. The pre-pregger consists of a cylinder which is rotated about its axis, and a dish which holds the fluid and provides the outlet tube. The bottom of the rotor, and the inside bottom surface of the dish provide the shearing surfaces of the pre-pregger, while the volume of the dish outside the disk region provides a reservoir of fluid to feed the pre-pregger. rotor is provided with 2 flights which serve to scrape the sides of the dish and keep partially melted polymer beads in motion against the heated surface of the dish. The flights were superfluous for runs with model fluids, but were not removed for these experiments. The hole in the center of the rotor, through which the tow would be drawn for impregnation runs, was plugged for these experiments. dish is mounted on a stand of adjustable height, through the center of which the long outlet tube of the die must pass.

Figure 5.7 shows the configuration of the pre-pregger exit tube in more detail. The die exit has a conical entry, a short cylindrical land of radius $R_{\rm d}$, and a long cylindrical exit of much larger radius. This die tube configuration was designed to ease the tow into the small radius section for consolidation. It is more complex than the shape of the die tube studied in Chapter 4, and the choice of $R_{\rm d}$ and $L_{\rm d}$ is discussed in Section 5.5.

The gap width, H, was a geometrical parameter which could

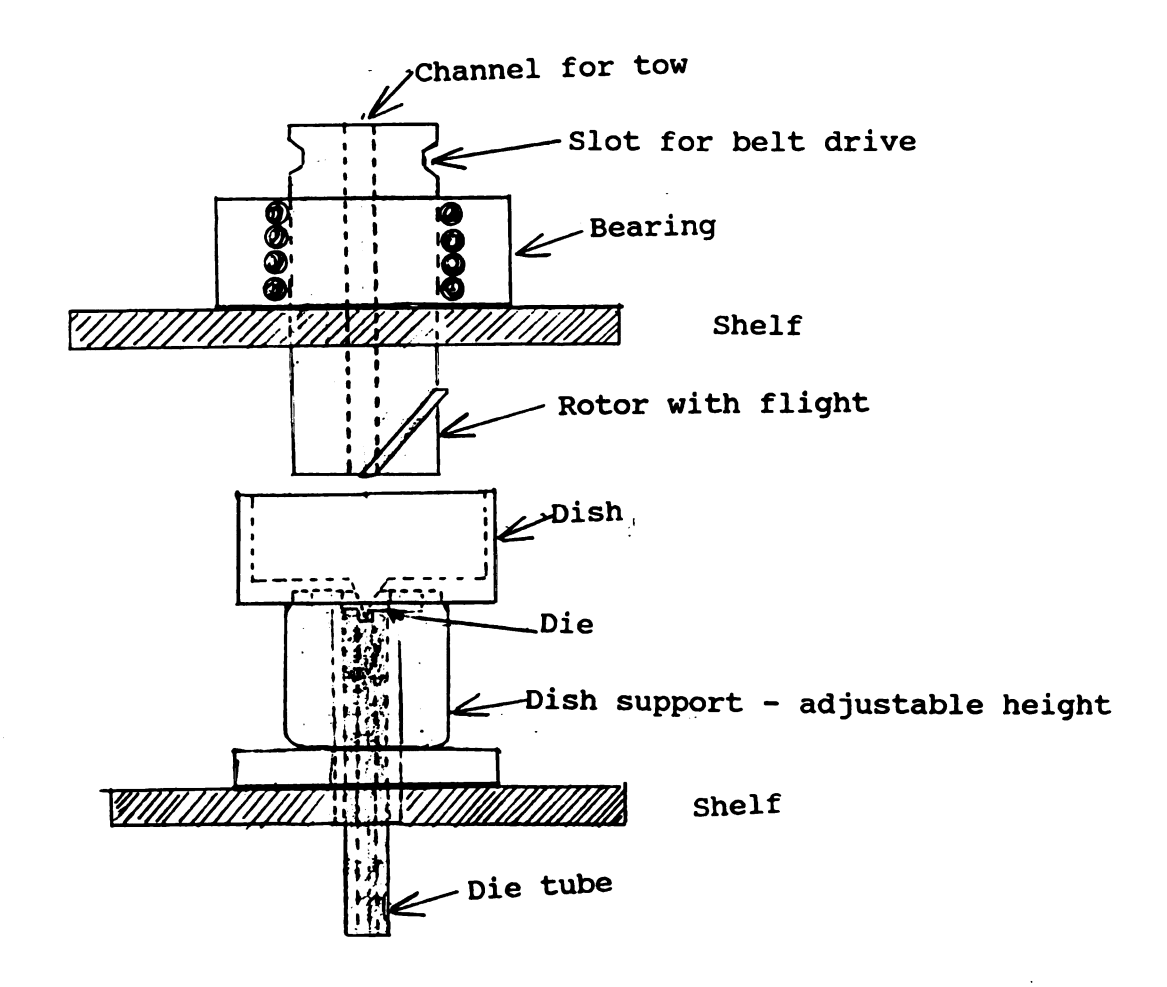


Figure 5.6: The Rotating Die Pre-Pregger

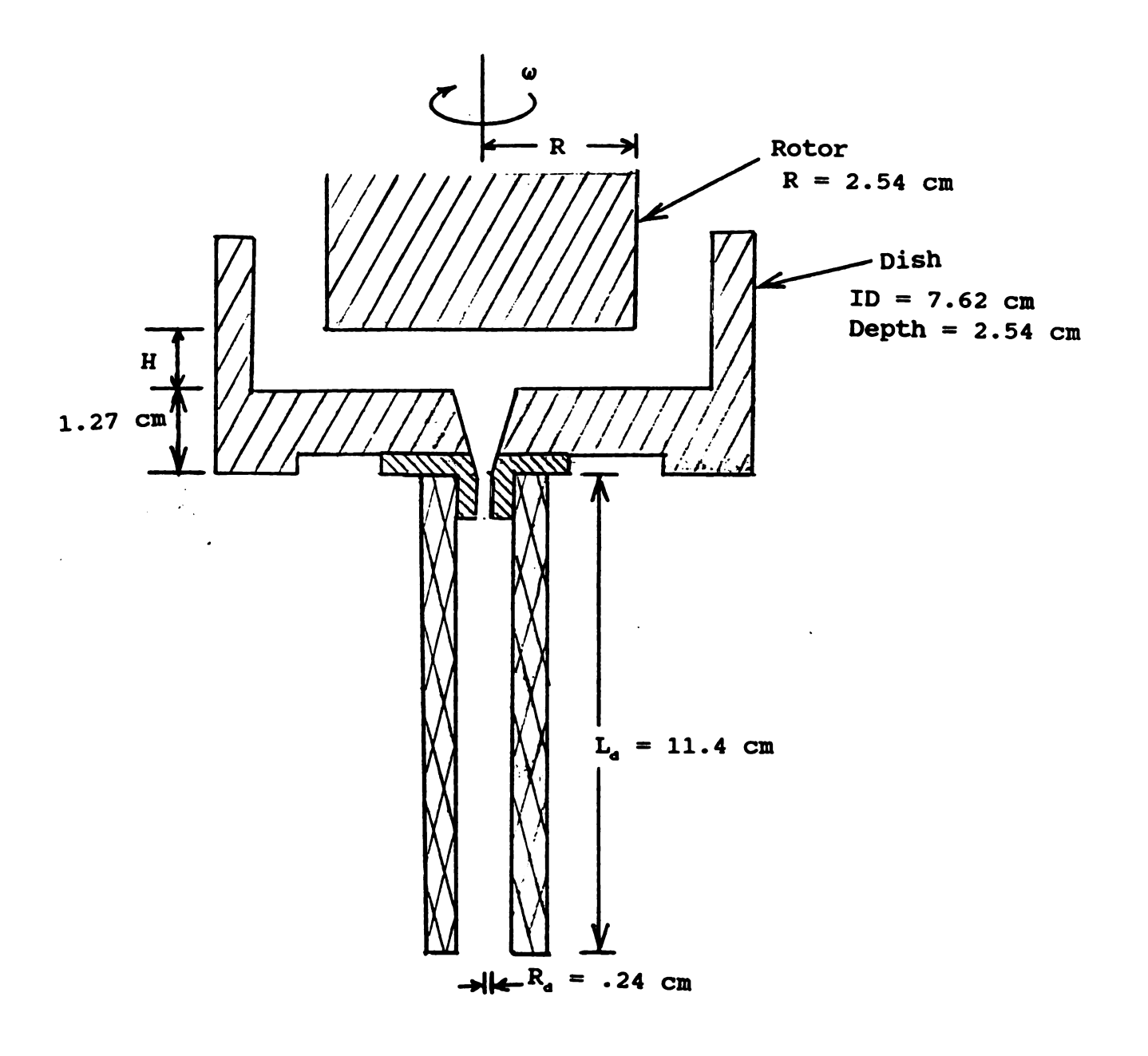


Figure 5.7: Schematic of Rotating Die Pre-Pregger

be varied from 0 to 10 cm, and which could be measured to $^{\pm}$ 0.0025 cm (0.001 in). However, the smallest gap that seemed to give reliable operation of the rotating die was 0.1 cm, and this was chosen as the smallest gap to be investigated in this study, with the other gaps chosen as simple multiples of 0.1 cm. At high rotation speeds, with fluid of low viscosity, the bottom dish of the rotating die tended to wobble on its stand $^{\pm}$ 0.006 cm (0.0025 in).

The rotation rate, ω , could be set with the variable speed motor controller and measured to within 1 rpm. The rotation rates for this study were chosen to span the range of the motor, and were varied from 90 to 200 rpm (9.4 to 21 rad/sec). The low viscosity fluids were also allowed to flow out of the rotating die when $\omega=0$ so that flow under hydrostatic conditions could be measured. The Separan solutions and the .3% PIB solution did not tend to flow when $\omega=0$.

The gap widths (0.1 to 0.4 cm) and rotation rates (9.4 to 21 rad/sec), used for this study complement the work reported earlier by Good et al. (1974), who studied gap widths of 0.05 to 0.2 cm, and rotation rates of 4 to 10 rad/sec.

The experimental procedure was as follows:

- 1. load fluid into the dish
- 2. adjust the height of the dish to set the gap
- 3. start the motor and adjust the rotation rate

- 4. fine-tune the gap width
- 5. remove the clamp from the outlet tube to allow fluid flow to start
- 6. wait for steady flow
- start timer and start collecting flow into sample beakers
- 8. take four time and weight samples
- 9. stop rotation and replace clamp
- 10. report results as graphs of weight by time

The two Separan solutions and the PIB solution had high enough viscosity that they did not flow out of the die tube when the pre-pregger was not running, so the clamp was not used with these fluids. Steady flow was judged by observing that the column of fluid running from the outlet tube to the weighing beaker was of a constant cross section, and that any pulsations in the flow were regular and consistent over a period of about 30 seconds. The total time to collect one sample was typically 2 minutes for the less elastic fluids, and about 30 seconds for the highly elastic fluids. The beakers and contents were weighed in a balance that was accurate to $^{\pm}0.1$ mg.

The dish was replenished with fluid either during a run or at the start of each run. With the gap width set at 0.2 cm, the volume of fluid contained in the gap would be 4.1 cm³, and the volume contained in the entire dish would be 69 cm³. At volume flow rates of 0.2 cm³/sec, the fluid

between the disks would have a residence time of about twenty seconds, and the volume in the dish would be exhausted in 300 seconds.

5.4 Experimental Results

Each of the experimental runs generated a set of data of the type shown in Figure 5.8, where accumulated mass of the sample is plotted versus the elapsed time of the run. If the flow rate is constant throughout the experiment, then the four points form a straight line, which passes through the x-axis at the start of the experiment. The slope of this line is the average mass flow rate for the run. However, the graphs of the data from the test fluids show that the data do not form straight lines, and so it is concluded that the experiments were unsteady. Both Separan solutions and the PIB solution had a very great tendency to climb the rotor of the rotating die, and it is speculated that the rod-climbing flow competes with the disk flow for the available fluid. If the balance is tipped in favor of the rod-climbing flow, then the disk flow may be starved of fluid as the run progresses, as depicted in Figure 5.9. Therefore, the mass flow rate for each run was taken to be the slope of the line linking the first two data points, ignoring transient behavior at start-up, and the possibility of starvation at the end. The volume flow rate was calculated from the mass flow rate and the density of the

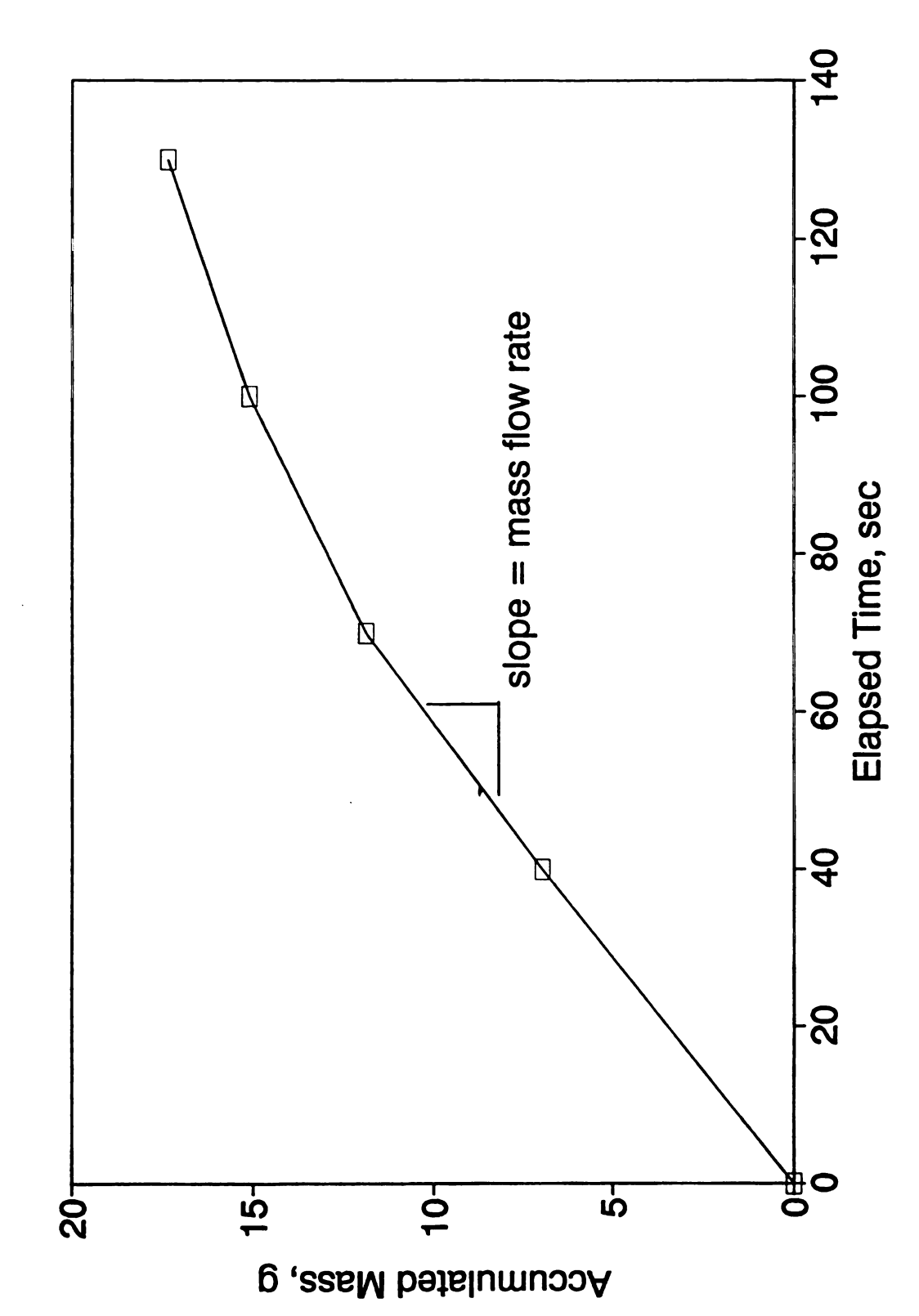


Figure 5.8: Typical Rotating Die Data

fluid from Table 5.2. Experiment data and calculations are reported in Appendix F.

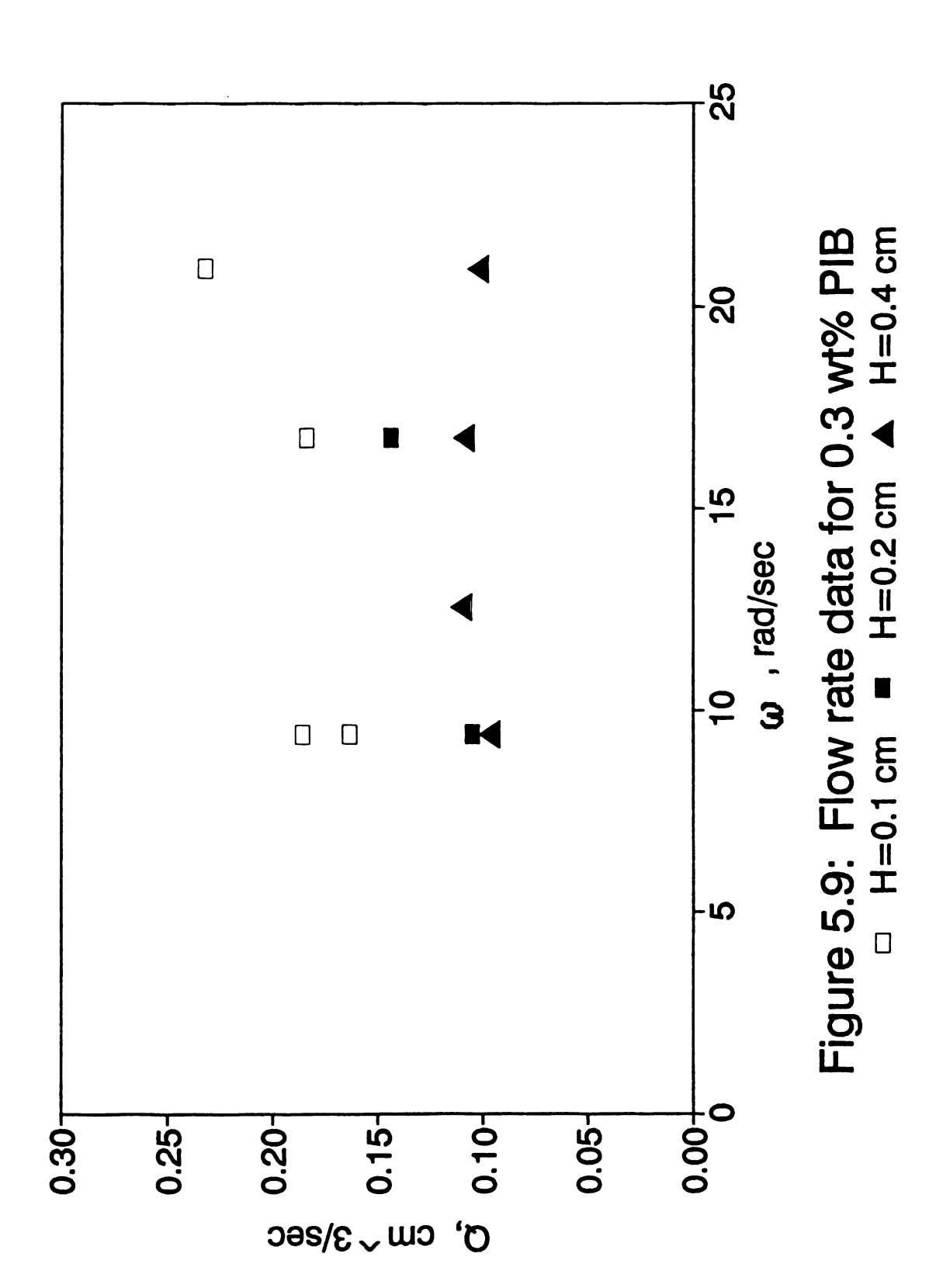
Flow rate experiments were performed with two Newtonian fluids: Epon 828 and polybutene. Two slightly elastic fluids with constant viscosity were also run: CTBN/Epon 828 blends. The three elastic fluids included a constant viscosity fluid: 0.3wt% PIB solution; and two shear-thinning fluids: fresh and aged Separan AP-30 solutions. Flow rates for both Newtonian fluids were calculated for the case of $\omega = 0$, i.e. flow induced through the prepregger by gravity only, to compare with the flow rate produced by the action of the rotor. The polybutene had a maximum flow rate of 0.021 cm³/sec, which is small compared to the flow rates of the elastic fluids, but still an order of magnitude larger than the flow rate recorded (.0012 cm³/sec) when $\omega = 0$. Likewise, the Epon 828 had a maximum flow rate of .023 cm3/sec when the die was running, and .0046 cm³./sec when $\omega = 0$. Neither of these fluids was pumped through the rotating die at rates that would allow sufficient fluid delivery to a tow being drawn through the pre-pregger at a rate of 20 cm/sec (see Chapter 3).

Since the CTBN/Epon blends showed rod-climbing behavior while being mixed, it was expected that they would be pumped by the rotating die at greater rates than the Newtonian fluids. The flow rate data are summarized in Appendix F.

The flow rates for the 23% blend were 0.012 cm³/sec maximum, with a gravity flow rate of 0.002 cm³/sec. The flow rates for the 40% blend were 0.015 cm³/sec maximum and 0.0021 cm³/sec under gravity. These flow rates are comparable to those attained with the Newtonian fluids, and are not satisfactory rates for the task of supplying resin to a tow. There is considerable scatter in the data, and although the trend is generally to increase Q as ω increases, there is no clear relationship between H and Q.

The volumetric flow rates for the PIB solution are plotted against the rotation rate of the die in Figure 5.9. The maximum flow rate was $0.23~\text{cm}^3/\text{sec}$, which is nearly equal to the goal of $0.24~\text{cm}^3/\text{sec}$. This maximum flow rate is produced at the highest ω and the smallest H with Q generally decreasing as ω decreases, and H increases. There is no indication of a critical gap width, as discussed in Chapter 4.

Figure 5.10 shows the experimental flow rates for the fresh Separan solution. The maximum flow rate was 0.165 cm³/sec, obtained at the highest value of ω , and at the intermediate value of H = 0.2 cm. As with the PIB solution, Q decreases with decreasing ω . However, the values of Q for the case of H = 0.1 cm are less than those for H = 0.2 cm, at low rotation rates, while values of Q for H = 0.4 cm are less than either of the other cases. This would seem to show that there is a critical gap width



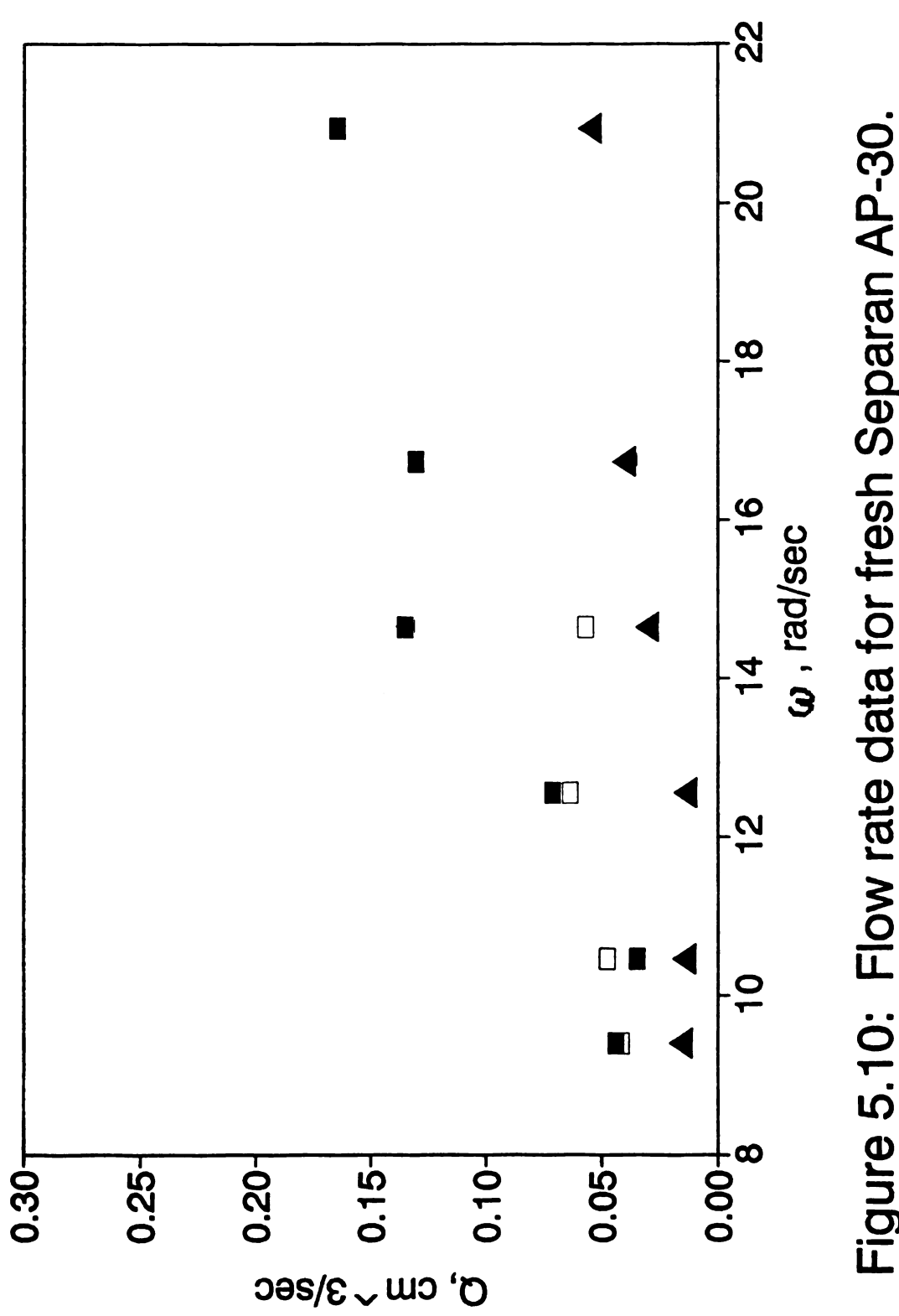


Figure 5.10: Flow rate data for fresh Separan AP-30.

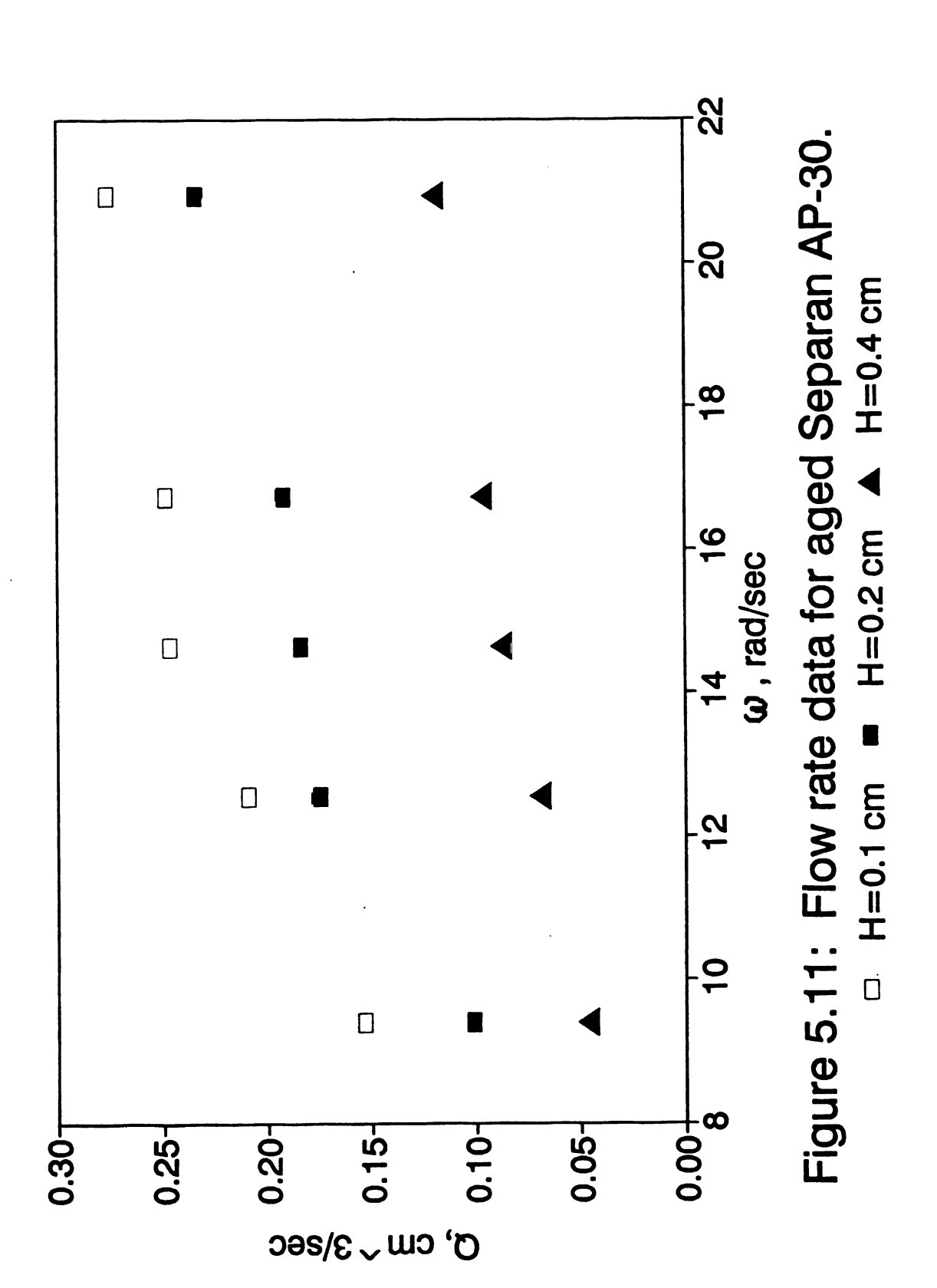
□ H=0.1 cm ■ H=0.2 cm ▲ H=0.4 cm

between H = 0.1 and 0.2 cm.

Values of the flow rate are plotted against rotation rate in Figure 5.11 for the aged Separan solution. The maximum Q is $0.27 \text{ cm}^3/\text{sec}$, which is adequate to impregnate 20 cm/sec of tow, as discussed in Chapter 3. Again, the top flow rates are achieved at narrow gaps and high rotation rates. Like the data for the fresh Separan, Q decreases with decreasing ω . However, the data for the aged Separan do not show the existence of a critical gap width, as the values of Q decrease monotonically with an increase of H.

5.5 Experimental Discussion

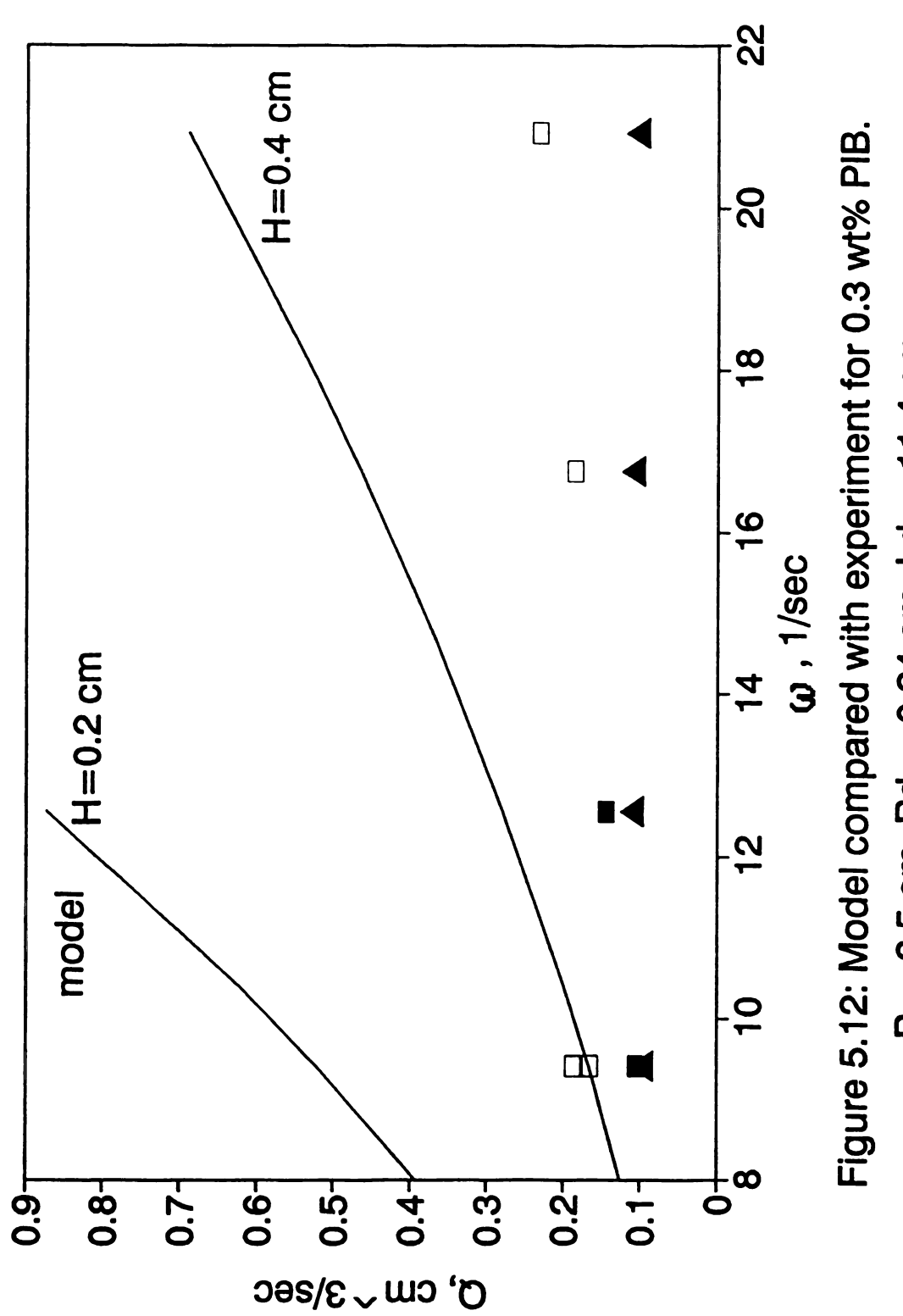
The model proposed in Chapter 4 predicts that flow rates for Newtonian fluids will be zero. However, the model does not take flow induced by gravity into account. Two Newtonian fluids, Epon 828, and polyisobutylene were loaded into the pre-pregger and allowed to flow through by gravity ($\omega = 0$). Small but measurable flow rates were produced, 0.0046 cm³/sec for Epon 828, and 0.0012 cm³/sec for polybutene. When the volumetric flow rate was measured with the pre-pregger running ($\omega > 0$), flow rates produced were an order of magnitude larger, at 0.023 cm³/sec for Epon 828, and 0.021 cm³/sec for polybutene. These flow rates are very small compared to the flow rates obtained with the elastic fluids, but they are not zero, as predicted for Newtonian fluids. It may be that the fluid has some elastic



character that is too small to be measured by the RMS-800, or it may be that flow is taking place because of secondary flows such as those reported by Blyler (1966). In either case, the model does not predict the flow rate behavior of the Newtonian fluids.

The flow rate data for the CTBN/Epon 828 blends have so much scatter that the quality of the fit to the model cannot be judged, but the fit can be improved by translating the model curves upward by the amount of the gravity-induced flow rate. It must be noted that although the CTBN/Epon 828 blends have measurable elastic properties, and that they flow through the pre-pregger at rates that match the prediction of the model, these flow rates are still very small, being of the same magnitude as those of the Newtonian fluids, and an order of magnitude below those of the strongly elastic fluids.

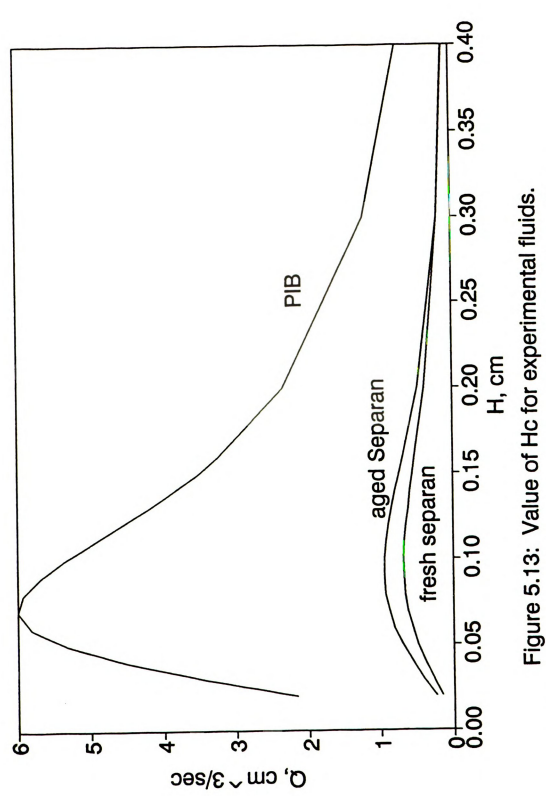
The comparison between the experimental data and the model calculations for the 0.3 wt% PIB solution is shown in Figure 5.12. Note that the value of L_d is not the length of the restriction in the die, 0.64 cm, but is taken as the full length of the die and outlet tube, 11.4 cm. As discussed in Chapter 4, the value of L_d has a very great influence upon Q. The choice of L_d and R_d for the experimental outlet die was not obvious. If R_d is chosen as the radius of the narrowest part of the outlet die, and L_d is chosen as the total die length, then the model



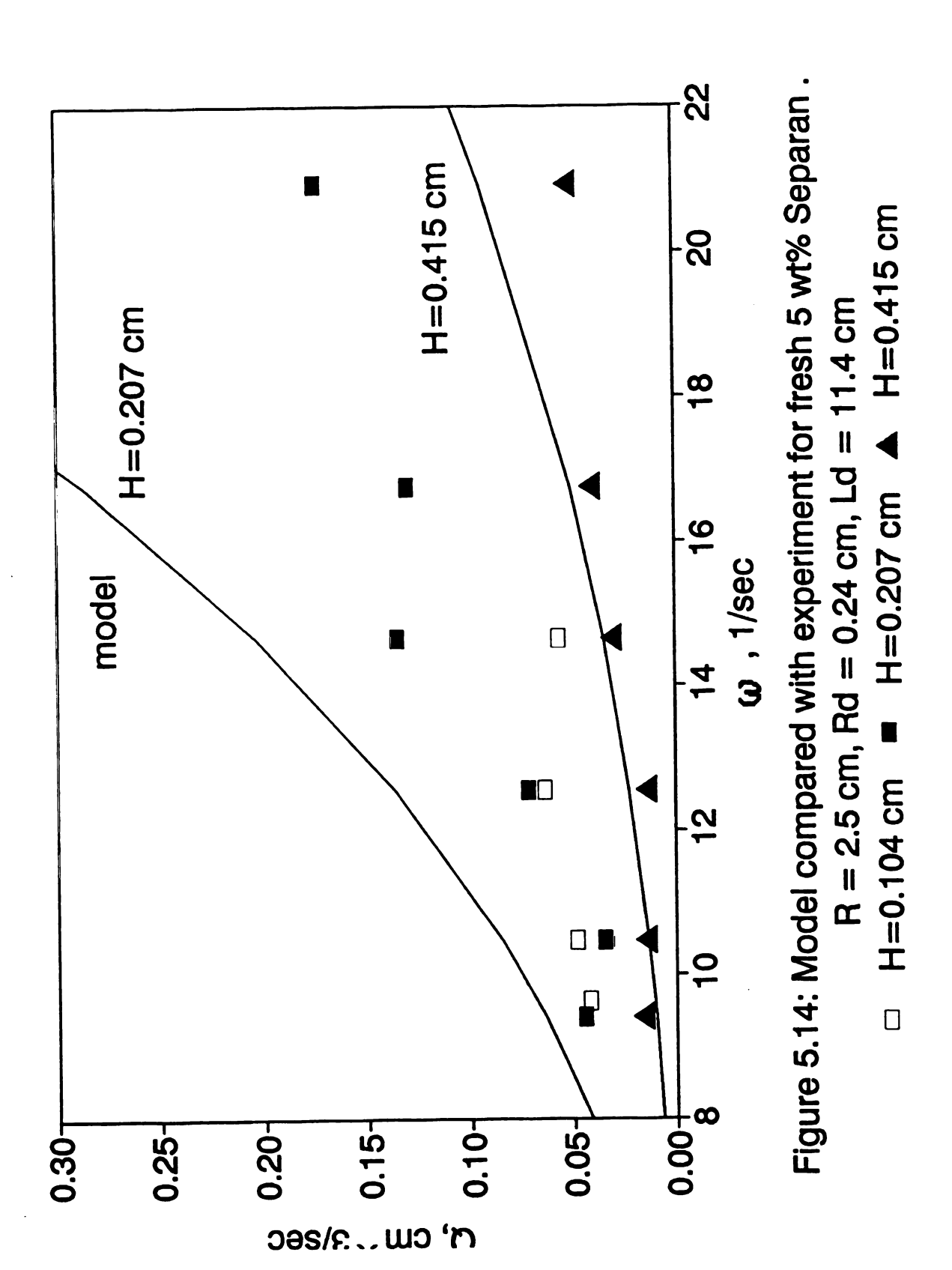
□ H=0.1 cm ■ H=0.2 cm ▲ H=0.4 cm R = 2.5 cm, Rd = 0.24 cm, Ld = 11.4 cm

calculations are the same order of magnitude as the experimental data of this study. Model values are from 2 to 10 times as great as experimental values. The model assumes that the rheological constants a, b, k, and n are constant with strain rate, as discussed in Section 5.2. If the strain rates in the pre-pregger are such that the constants vary appreciably from those reported in Table 5.2, then the model may over or under-predict Q at high rotation rates and low gap widths. The model also does not account for the tendency of the PIB solution to climb the rotor, and so will over-predict flow rates if the disk region is being deprived of feed, as discussed in Section 5.4. The model predicts that H_o for the PIB solution will fall at 0.07 cm (See Figure 5.13), which does not lie within the scope of the experimental data.

Figure 5.14 shows the comparison between the model predictions and the experimental data for the fresh Separan AP-30 solution. The model for H = 0.42 cm matches the data values quite well at low ω , but begins to deviate from data above ω = 16 rad/sec. The model for H = 0.21 cm does not match the data values, but gives values of Q a factor of 2 higher than the data. The explanation of starvation of the disk flow by the rotor-climbing tendency of the fluid may again be invoked to explain this phenomenon. An increase in ω will tend to increase the flow rates through the disk as well as up the rotor. An increase in gap width would not

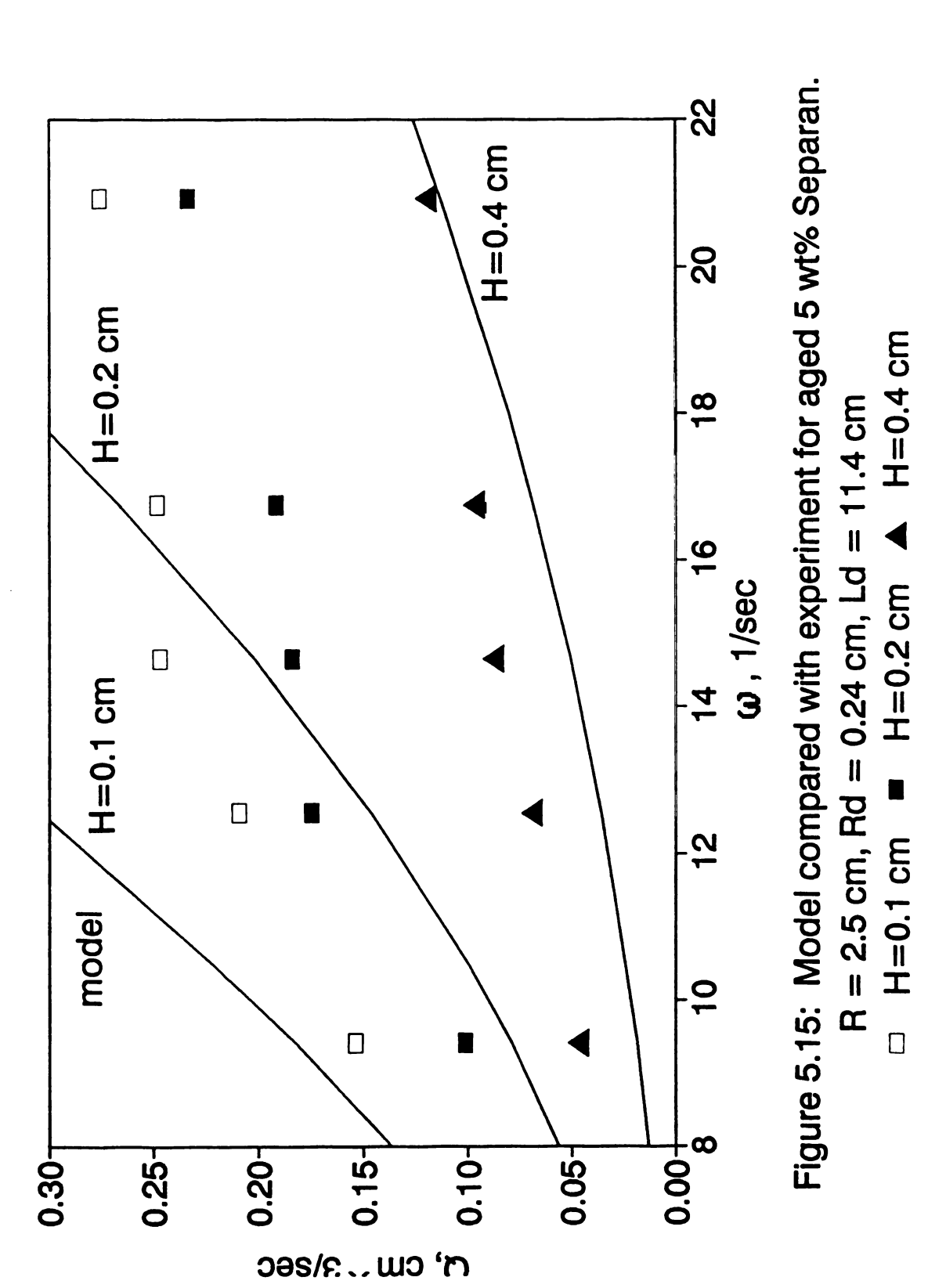


R = 2.5 cm, Rd = 0.24 cm, Ld = 11.4 cm, $\omega = 20 \text{ rad/sec}$



affect the rod-climbing flow, but would both decrease the volumetric flow rate through the disk by decreasing the strain rate that is driving flow, and increase the area by which new fluid can be taken into the disk flow around the periphery. Comparison of the model and data in Figure 5.14 suggests that a gap of 0.42 cm is wide enough to allow the disk flow to compete for fluid with the rod-climbing flow, because the model matches the data for low rotation rates. The balance apparently shifts at about $\omega = 16$ rad/sec, where the experimental flow rates begin to fail to keep up with the model flow rates. The rod-climbing field apparently dominates at all the narrower gap widths. Figure 5.13 shows that the optimum gap width for the fresh Separan solution is just greater than 0.10 cm, and this would seem to be confirmed by the experimental data which show H to be between 0.1 and 0.2 cm.

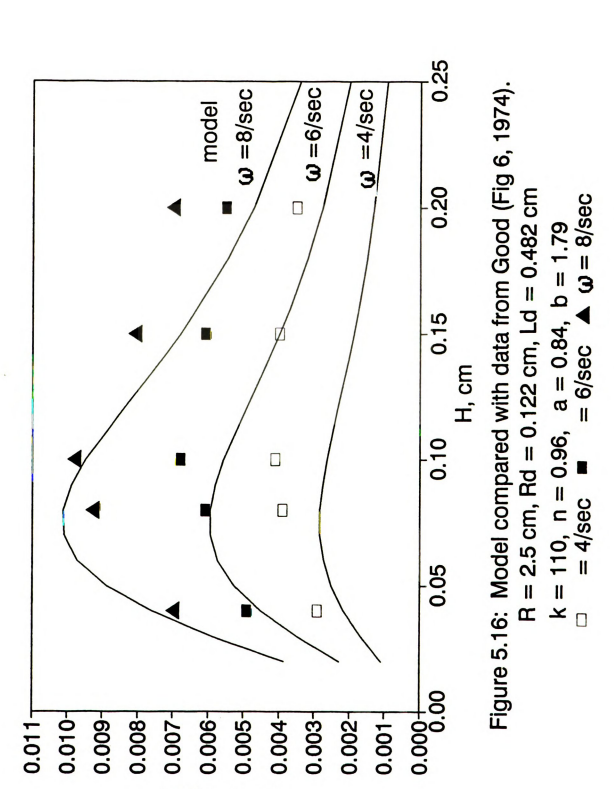
The comparison between the aged Separan experiments and model calculations is shown in Figure 5.15. Again, the model matches the data well for high gap widths and low rotation rates, but fails to match the data for narrow gaps and high ω . The fact that the elastic coefficient, a, for the aged Separan solution is nearly twice that of the fresh solution may be the reason that the model predictions for the aged solution are better than those for the fresh solution. The higher elasticity may help the disk flow compete with the rod-climbing flow up to smaller gaps and higher rotation



rates. Figure 5.13 shows that the model predicts that $\rm H_c$ = 0.09 cm for the aged Separan solution. This does not contradict the experimental data, which show that $\rm H_c$ < 0.1 cm.

Figure 5.16 shows the model calculation compared to data of Good, et al. (1974) for an 18 wt% solution of PIB in motor oil. Reference to Table 5.2 will show that this fluid has a low but nearly constant viscosity (k = 110 dyne sec/cm², n = .96), and that the elasticity coefficient, a, is equivalent to that for the CTBN/Epon blends. Flow rates of this solution are comparable to those for the CTBN/Epon blends, being less than 0.01 cm³/sec. The model predicts volumetric flow rates lower than the data shown, especially at the large gap widths. Also, the predicted H_c is less than that shown by the data.

Good (1974) mentions the tendency of the fluids to climb over the top disk of his centripetal pump at large ω , and other authors (Kocherov, 1973 and D'Amato, 1974) have noted that the centripetal pump runs successfully only when the problem of feeding the fluid or pellets into the shear zone is addressed. Figure 5.13 indicates that potential flow rates with the pre-pregger go as high as 0.8 cm³/sec for the Separan Ap-30 solutions, and 6 cm³/sec for the PIB solution at the critical gap width and ω = 20 rad/sec. These rates would be sufficient to deliver fluid to a tow drawn through the pre-pregger at rates of from 30 to 100



Q, cm ^ 3/sec

cm/sec, far in excess of the 20 cm/sec deemed sufficient for success, as discussed in Chapter 3.

Chapter 6 Conclusions

The model developed for the rotating die pre-pregger makes use of the Criminale-Ericksen-Fibley model with the second primary normal stress coefficient equal to zero. This representation provides a practical description of elastic effects for the problem of flow through the pre-pregger. The strain rate tensor S within Regions I and II (see Figure 4.1) was estimated by assuming a velocity field which satisfies continuity and no slip boundary conditions. The strain rate in the exit tube was predicted by solving the equation of motion for a power-law fluid.

An analysis of the mechanical energy balance shows that the work transferred to the pre-pregger across the rotating disk surface by the shearing action on the fluid is entirely balanced by the viscous dissipation due to the deformation of the fluid caused by the swirling motion of the fluid between the disks in Regions I and II (see Figure 4.1). The fluid entering the gap from the reservoir is spun up by the rotor, and the work transferred to the pre-pregger across the circumferential surface together with the stored elastic energy of the fluid balances the remaining dissipation

effects between the disks and in the exit tube. Thus, greater efficiency in feeding fluid to the gap may increase the flow rate of fluid through the pump.

The empirical fluid parameters that describe the viscous and elastic nature of the fluid (a, b, k, and n) can be obtained through rheological experiments. For the fluids studied, the ratio of b to n was shown to be approximately equal to two (see Figure 5.5). Because the flow model is very sensitive to the values of the rheological description, it is important that the above parameters be determined accurately for the full range of strain rates which will be encountered in the pre-pregger.

The ratio, α , of the radial velocity of the fluid in the pre-pregger to the tangential velocity gives a dimension-less measure of the spiral nature of the flow field. Increasing values of α indicate that the flow is more radial, i.e., that a particle of fluid travels in fewer circles on its way through the pre-pregger. The qualitative behavior of α at small values of H/R_d was found to depend on the sign of the fluid parameter l=b-(1+n). For instance, for $H/R_d \rightarrow 0$ and l>0, the flow ratio becomes unbounded; however, for l<0, $\alpha \rightarrow 0$. For l=0, α has a finite, non-zero value for $H/R_d \rightarrow 0$.

The model shows that the volumetric flow rate, Q, increases monotonically with the rotation rate, ω . The

model also shows that Q increases with the gap width, H, until H reaches a critical value, H_c , above which Q decreases with increasing H. As H increases from zero to H_c , Q increases because the energy dissipation in Region I, D_i^* , decreases. As H increases from H_c , Q decreases again, because the elastic term of the mechanical energy balance, E, decreases more quickly than D_i^* decreases.

The flow model produces curves that fit the data of Good et al. (1974) reasonably well, although different constitutive equations and simplifying assumptions were used. The flow model can be made to fit the experimental data of this study by choosing the geometric parameter L_d to be the length of the entire die tube, rather than the length of the die restriction only (see Figure 5.6).

The flow rates of the Newtonian fluids (Epon 828 and polybutene) through the pre-pregger were four to ten times as great while the pre-pregger was running, as when the fluid was draining by gravity only. The flow rates of the slightly elastic fluids (CTBN/Epon 828 blends) through the pre-pregger were the same magnitude as the flow rates for the Newtonian fluids. These fluids had measurable elasticity coefficients, and the flow model could predict the flow rates reasonably well.

The highly elastic fluids (polyisobutylene and Separan

AP-30 solutions) flowed through the pre-pregger at rates which would be adequate to impregnate a 3K carbon tow drawn through the pre-pregger at 20 cm/sec (i.e. Q > 0.22 cm³/sec). The flow model predicted flow rates of 6 cm³/sec for the polyisobutylene solution, and 0.8 cm³/sec for the Separan solutions. The flow rates predicted by the model may be brought more into line with those obtained by experiment, by investigating the following three phenomena. First, the rheological experiments were performed at strain rates below 100 sec-1, and the fluid characteristics a, b, k, and n were assumed to be constants for the strain rates produced by the pre-pregger, although they were as great as 550 sec-1. Second, the fluids' tendency to climb the rotor may have set up resistance to fluid entering the gap of the pre-pregger. Third, the model assumed steady state operation, and the experiments showed that the operation was not at steady state on the time scale that samples were being taken. mass flow graphs were not linear, and pulsing behavior was observed for all three elastic fluids.

Chapter 7 Recommendations

Although the flow model assumed a steady state of flow in the pre-pregger, experimental data (see Figure 5.8) showed that the flow had not generally reached steady state within the time frame of the run. In order to study steady state flows, the pre-pregger should be provided with a reservoir of fluid, and a means to feed the fluid directly into the gap. Some measure of whether steady state has been reached is needed. Steps should also be taken to prevent the fluid from climbing the rotor, as the rotor climbing effect may obscure experimental results.

When the rotating die pre-pregger was built, the die was designed with a conical section in imitation of pre-preggers with stationary dies. The flow model assumed that the flow in the die tube was a fully-developed laminar tube flow. Thus, the geometrical parameters of the die tube were simply the radius, R_a , and the length, L_a of a cylinder. When the model was compared to the experiments, the choice of dimensions from the pre-pregger to enter in the calculation was unclear. In order to more clearly evaluate the potential of resin melts to be pumped by a rotating die, the

experiments should be designed to reflect the less complex geometry of the model.

The fluids of the present study were all of the class of "Tanner" fluids (i.e., the first normal stress coefficient exponent, b, is approximately twice the viscosity exponent, n). A theoretical class of fluids was identified in the parametric study of the flow model for which the relationship b > 1+n is characteristic. Fluids of this class should be studied in the pre-pregger, because the model predicts that the behavior of the velocity ratio, α , changes drastically from that of the "Tanner" fluids at small gap widths.

The pre-pregger was designed and built for the purpose of making pre-preg. The present study was undertaken in order to better understand the operation of the pre-pregger without the tow. It is recommended that future studies focus on the operation of the pre-pregger with fiber tow and polymer melt. The question of whether the tow would be impregnated or only coated by the pre-pregger is of interest, as is the question of which parameters may be manipulated to assure the tow is impregnated by the pre-pregger, rather than being merely coated.

APPENDIX A KINEMATIC TENSORS

EQUATIONS OF MOTION

VELOCITY VECTORS

STRAIN RATE TENSORS

EQUATIONS OF MOTION:

Cylindrical coordinates, variable viscosity.

Equation of Continuity

$$\frac{D\rho}{Dt} = -\rho(\nabla \cdot \underline{\mathbf{v}})$$

$$\frac{\partial \rho}{\partial t} + \frac{1}{r} \frac{\partial}{\partial r} (\rho r v_r) + \frac{1}{r} \frac{\partial}{\partial \theta} (\rho v_\theta) + \frac{\partial}{\partial z} (\rho v_z) = 0$$

Equation of Motion

$$\rho \frac{D\mathbf{v}}{D\mathbf{t}} = -\nabla \mathbf{p} + [\nabla \cdot \underline{\mathbf{r}}] + \rho \underline{\mathbf{g}}$$

r component:

$$\rho \left(\frac{\partial v_{r}}{\partial t} + v_{r} \frac{\partial v_{r}}{\partial r} + \frac{v_{\theta}}{r} \frac{\partial v_{r}}{\partial \theta} - \frac{v_{\theta}^{2}}{r} + v_{r} \frac{\partial v_{r}}{\partial z} \right) =$$

$$-\frac{\partial p}{\partial r} + \left(\frac{1}{r} \frac{\partial}{\partial r} (r \tau_{rr}) + \frac{1}{r} \frac{\partial \tau_{r\theta}}{\partial \theta} - \frac{\tau_{\theta\theta}}{r} + \frac{\partial \tau_{rr}}{\partial z} \right) + \rho g_{r}$$

θ component:

$$\rho \left(\frac{\partial v_{\theta}}{\partial t} + v_{r} \frac{\partial v_{\theta}}{\partial r} + \frac{v_{\theta}}{r} \frac{\partial v_{\theta}}{\partial \theta} + \frac{v_{r}v_{\theta}}{r} + v_{r} \frac{\partial v_{\theta}}{\partial z} \right) =$$

$$-\frac{1}{r} \frac{\partial p}{\partial \theta} + \left(\frac{1}{r^{2}} \frac{\partial}{\partial r} (r^{2} \tau_{r\theta}) + \frac{1}{r} \frac{\partial \tau_{\theta\theta}}{\partial \theta} + \frac{\partial \tau_{\theta\tau}}{\partial z} \right) + \rho g_{\theta}$$

z component:

$$\rho \left(\frac{\partial v_{z}}{\partial t} + v_{r} \frac{\partial v_{z}}{\partial r} + \frac{v_{\theta}}{r} \frac{\partial v_{z}}{\partial \theta} + v_{z} \frac{\partial v_{z}}{\partial z} \right) =$$

$$-\frac{\partial p}{\partial z} + \left(\frac{1}{r} \frac{\partial}{\partial r} (r \tau_{rz}) + \frac{1}{r} \frac{\partial \tau_{\theta z}}{\partial \theta} + \frac{\partial \tau_{zz}}{\partial z} \right) + \rho g_{z}$$

Substantial Time Derivative

$$\frac{DC}{Dt} = \frac{\partial C}{\partial t} + (\underline{v} \cdot \nabla C)$$

ROTATING DIE PRE-PREGGER, DISK REGION

Cylindrical coordinates:
$$v_1 = v_\theta$$

 $v_2 = v_r$
 $v_3 = v_1$

Velocity Vector

Assumptions:

$$\frac{v_r^{\rm I}}{r} = -\frac{\partial v_r^{\rm I}}{\partial r} \qquad \text{(Continuity)}$$

$$\frac{\partial}{\partial \theta} = 0 \qquad \text{(Axisymmetry)}$$

$$\frac{\partial v^{\rm I}}{\partial r} << \frac{\partial v^{\rm I}}{\partial z} \qquad \text{(Lubrication approximation)}$$

Strain Rate Tensor

$$S_{\theta\theta}^{I} = \frac{1}{2} [\nabla y^{I} + (\nabla y^{I})^{T}]$$

$$S_{\theta\theta}^{I} = \frac{V_{r}^{I}}{T}$$

$$S_{rr}^{I} = \frac{\partial V_{r}^{I}}{\partial r}$$

$$S_{\theta r}^{I} = S_{r\theta}^{I} = 0$$

$$S_{\theta r}^{I} = S_{r\theta}^{I} = \frac{1}{2} \frac{\partial V_{\theta}^{I}}{\partial z}$$

$$S_{rr}^{I} = S_{rr}^{I} = \frac{1}{2} \frac{\partial V_{r}^{I}}{\partial z}$$

First Invariant of S^T

$$tr \underline{s}^{r} = \frac{v_{r}^{r}}{r} + \frac{\partial v_{r}^{r}}{\partial r} = 0$$

Second Invariant of S^I

$$2(\underline{S}^{r}:\underline{S}^{r}) = 4\left(\frac{v_{r}^{r}}{T}\right)^{2} + \left(\frac{\partial v_{\theta}^{r}}{\partial z}\right)^{2} + \left(\frac{\partial v_{r}^{r}}{\partial z}\right)^{2}$$

Third Invariant of ST

$$\det \mathbf{S}^{\mathbf{r}} = -2 \frac{\mathbf{v}_{\mathbf{r}}^{\mathbf{r}}}{\mathbf{r}} \left[\left(\frac{\partial \mathbf{v}_{\theta}^{\mathbf{r}}}{\partial \mathbf{z}} \right)^{2} + \left(\frac{\partial \mathbf{v}_{\mathbf{r}}^{\mathbf{r}}}{\partial \mathbf{z}} \right)^{2} \right]$$

$$\frac{\delta \underline{S}}{\delta \underline{t}} = \frac{\partial \underline{S}}{\partial \underline{t}} + \underline{v} \cdot \nabla \underline{S} - \{\nabla \underline{v}^{\underline{r}} \cdot \underline{S} + \underline{S} \cdot \nabla \underline{v}\}$$

$$\left(\frac{\delta S^{I}}{\delta t}\right)_{\theta\theta} = -4\left(\frac{v_{r}^{I}}{r}\right)^{2} - \left(\frac{\partial v_{\theta}^{I}}{\partial r}\right)^{2}$$

$$\left(\frac{\delta S^{r}}{\delta t}\right)_{r} = -\left(\frac{\partial v_{r}^{r}}{\partial r}\right)^{2} - \left(\frac{\partial v_{r}^{r}}{\partial z}\right)^{2}$$

$$\left(\frac{\delta S^{x}}{\delta t}\right)_{x} = 0$$

$$\left(\frac{\delta S^{r}}{\delta t}\right)_{n,n} = \left(\frac{\delta S^{r}}{\delta t}\right)_{n,n} = -\left(\frac{\partial v_{\theta}^{r}}{\partial z}\frac{\partial v_{r}^{r}}{\partial z}\right)$$

$$\left(\frac{\delta S^{r}}{\delta t}\right)_{rr} = \left(\frac{\delta S^{r}}{\delta t}\right)_{rr} = 0$$

$$\left(\frac{\delta S^{r}}{\delta t}\right)_{a} = \left(\frac{\delta S^{r}}{\delta t}\right)_{a} = 0$$

ROTATING DIE PRE-PREGGER, DIE TUBE

Cylindrical coordinates:
$$v_1 = v_2$$

$$v_2 = v$$

$$v_3 = v_6$$

Velocity Vector

$$\underline{v}^{\text{III}} = v^{\text{III}}_{z}(r)\underline{e}_{z}$$

$$v_z^{\text{III}} = \frac{Q}{\pi R_d^2} \frac{3n+1}{n+1} \left[1 - \left(\frac{r}{R_d} \right)^{\frac{1+n}{n}} \right]$$

$$v_r^{\text{rr}} = v_\theta^{\text{rr}} = 0$$

Strain Rate Tensor

$$\underline{S}^{\text{rrr}} = \frac{1}{2} [\nabla \underline{v}^{\text{rrr}} + (\nabla \underline{v}^{\text{rrr}})^{\text{T}}]$$

$$S_{rz}^{III} = S_{zr}^{III} = \frac{1}{2} \frac{\partial V_{z}^{III}}{\partial r}$$

$$S_{\theta\theta}^{\text{III}} = S_{\text{rr}}^{\text{III}} = S_{\text{rr}}^{\text{III}} = 0$$

$$S_{\theta z}^{\text{rrr}} = S_{z\theta}^{\text{rrr}} = 0$$

$$S_{r\theta}^{III} = S_{\theta r}^{III} = 0$$

First Invariant of S'''

$$tr \underline{s}^{ii} = 0$$

Second Invariant of S'II

$$5(\bar{S}_{111};\bar{S}_{111}) = \left(\frac{9h_{111}}{3h}\right)_{5}$$

Third Invariant of STIT

$$\det S = 0$$

$$\frac{\delta S}{\delta t} = \frac{\partial S}{\partial t} + y \cdot \nabla S - ((\nabla y)^{T} \cdot S) + S \cdot \nabla y)$$

$$\left(\frac{\delta S^{III}}{\delta t}\right)_{\theta\theta} = \left(\frac{\delta S^{III}}{\delta t}\right)_{rr} = 0$$

$$\left(\frac{\delta S^{III}}{\delta t}\right)_{r\theta} = -\left(\frac{\partial V^{III}}{\partial r}\right)^{2}$$

$$\left(\frac{\delta S^{III}}{\delta t}\right)_{r\theta} = \left(\frac{\delta S^{III}}{\delta t}\right)_{\theta r} = 0$$

$$\left(\frac{\delta S^{III}}{\delta t}\right)_{r} = \left(\frac{\delta S^{III}}{\delta t}\right)_{r} = 0$$

$$\left(\frac{\delta S^{III}}{\delta t}\right)_{\theta} = \left(\frac{\delta S^{III}}{\delta t}\right)_{\theta} = 0$$

ROTATING DIE PRE-PREGGER, TRANSITION REGION

Cylindrical Coordinates:
$$v_1 = v_0$$

 $v_2 = v_r$
 $v_3 = v_1$

Velocity Vector

Assumptions:

$$\frac{\mathbf{v}_{\mathbf{r}}^{\text{II}}}{\mathbf{r}} = -\frac{\partial \mathbf{v}_{\mathbf{r}}^{\text{II}}}{\partial \mathbf{r}} \qquad \text{(Continuity)}$$

$$\frac{\partial}{\partial \theta} = 0 \qquad \qquad \text{(Axisymmetry)}$$

$$\frac{\partial \mathbf{v}^{\text{II}}}{\partial \mathbf{r}} << \frac{\partial \mathbf{v}^{\text{II}}}{\partial \mathbf{z}} \qquad \text{(Lubrication approximation)}$$

Strain Rate Tensor

$$S_{\theta\theta}^{II} = \frac{1}{2} [\nabla \underline{v}^{II} + (\nabla \underline{v}^{II})^{T}]$$

$$S_{\theta\theta}^{II} = \frac{V_{r}^{II}}{T}$$

$$S_{rr}^{II} = \frac{\partial V_{r}^{II}}{\partial r}$$

$$S_{rr}^{II} = \frac{\partial V_{r}^{II}}{\partial z}$$

$$S_{r\theta}^{II} = S_{\theta r}^{II} = 0$$

$$S_{r\theta}^{II} = S_{\theta r}^{II} = \frac{1}{2} \frac{\partial V_{\theta}^{II}}{\partial z}$$

$$S_{rr}^{II} = S_{rr}^{II} = \frac{1}{2} \left(\frac{\partial V_{r}^{II}}{\partial r} + \frac{\partial V_{r}^{II}}{\partial z} \right)$$

First Invariant of S

$$tr S^{II} = \frac{V_r^{II}}{r} + \frac{\partial V_r^{II}}{\partial r} + \frac{\partial V_i^{II}}{\partial z}$$

Second Invariant of S^{rr}

$$2(\underline{S}^{II}:\underline{S}^{II}) = 2\left(\frac{\partial v_{\theta}^{II}}{\partial z}\right)^{2} + 2\left(\frac{\partial v_{z}^{II}}{\partial r} + \frac{\partial v_{z}^{II}}{\partial z}\right)^{2} + 4\left(\frac{\partial v_{z}^{II}}{\partial r}\right)^{2} + 4\left(\frac{\partial v_{z}^{II}}{\partial z}\right)^{2}$$

Third Invariant of ST

$$\begin{split} \text{det } \underline{s}^{\text{II}} &= \frac{1}{2} \ \frac{v_{\text{r}}^{\text{II}}}{r} \ \left(\frac{\partial v_{\text{r}}^{\text{II}}}{\partial r} + \frac{\partial v_{\text{r}}^{\text{II}}}{\partial z} \right) \! \left(\frac{\partial v_{\text{r}}^{\text{II}}}{\partial r} - \frac{\partial v_{\text{r}}^{\text{II}}}{\partial z} \right) \\ &- \frac{1}{4} \ \left(\frac{\partial v_{\text{r}}^{\text{II}}}{\partial r} \right) \! \left(\frac{\partial v_{\theta}^{\text{II}}}{\partial z} \right)^{2} \end{split}$$

CONE AND PLATE VISCOMETER

Spherical coordinates:
$$v_1 = v_{\phi}$$

 $v_2 = v_{\theta}$
 $v = v$

Velocity Vector

$$\underline{v} = v_{\phi}(\theta, r) \underline{e}_{\phi}$$

$$v_{\phi} = \frac{r\omega\alpha}{\beta}$$

$$v_{\theta} = v_{r} = 0$$

Strain Rate Tensor

$$S = \frac{1}{2} [\nabla \underline{v} + \nabla \underline{v}^{T}]$$

$$S_{\phi\theta} = S_{\theta\phi} = \frac{1}{2} \left(\frac{1}{r} \frac{\partial V_{\phi}}{\partial \theta} - \frac{V_{\phi}}{r} \cot \theta \right)$$

$$S_{\phi r} = S_{r\phi} = \frac{1}{2} \left(\frac{\partial V_{\phi}}{\partial r} - \frac{V_{\phi}}{r} \right)$$

$$S_{\phi\phi} = S_{\theta\theta} = S_{rr} = 0$$

$$S_{\theta r} = S_{r\theta} = 0$$

Let $v_{\phi} = \frac{r\omega\alpha}{\beta}$.

Since $0 \le \alpha \le \beta \le 4^{\circ}$, and $\cot \theta = \tan \alpha \cong \alpha$, then S reduces to:

$$S_{\phi\theta} = S_{\theta\phi} = -\frac{1}{2} \frac{\omega}{B}$$

Strain Rate

$$\dot{\gamma} = \sqrt{2 \text{ S:S}} = \frac{\omega}{B}$$

First Invariant of S

$$tr S = 0$$

Second Invariant of S

$$(\underline{S}:\underline{S}) = \frac{1}{2} \left(\frac{\underline{\omega}}{B}\right)^2$$

Third Invariant of S

$$\det S = 0$$

$$\frac{\delta \underline{\underline{s}}}{\delta \underline{t}} = \frac{\partial \underline{\underline{s}}}{\partial \underline{t}} + \underline{\underline{v}} \cdot \nabla \underline{\underline{s}} - \{ \nabla \underline{\underline{v}}^{\underline{r}} \cdot \underline{\underline{s}} + \underline{\underline{s}} \cdot \nabla \underline{\underline{v}} \}$$

$$\left(\frac{\delta \underline{\underline{s}}}{\delta \underline{t}} \right)_{\theta \theta} = \left(\frac{\delta \underline{\underline{s}}}{\delta \underline{t}} \right)_{rr} = 0$$

$$\left(\frac{\delta \underline{\underline{s}}}{\delta \underline{t}} \right)_{\theta \theta} = -\dot{\gamma}^{2}$$

$$\left(\frac{\delta \underline{\underline{s}}}{\delta \underline{t}} \right)_{r\theta} = \left(\frac{\delta \underline{\underline{s}}}{\delta \underline{t}} \right)_{\theta r} = 0$$

$$\left(\frac{\delta \underline{\underline{s}}}{\delta \underline{t}} \right)_{r\phi} = \left(\frac{\delta \underline{\underline{s}}}{\delta \underline{t}} \right)_{\phi r} = 0$$

$$\left(\frac{\delta \underline{\underline{s}}}{\delta \underline{t}} \right)_{\theta \phi} = \left(\frac{\delta \underline{\underline{s}}}{\delta \underline{t}} \right)_{\phi \theta} = 0$$

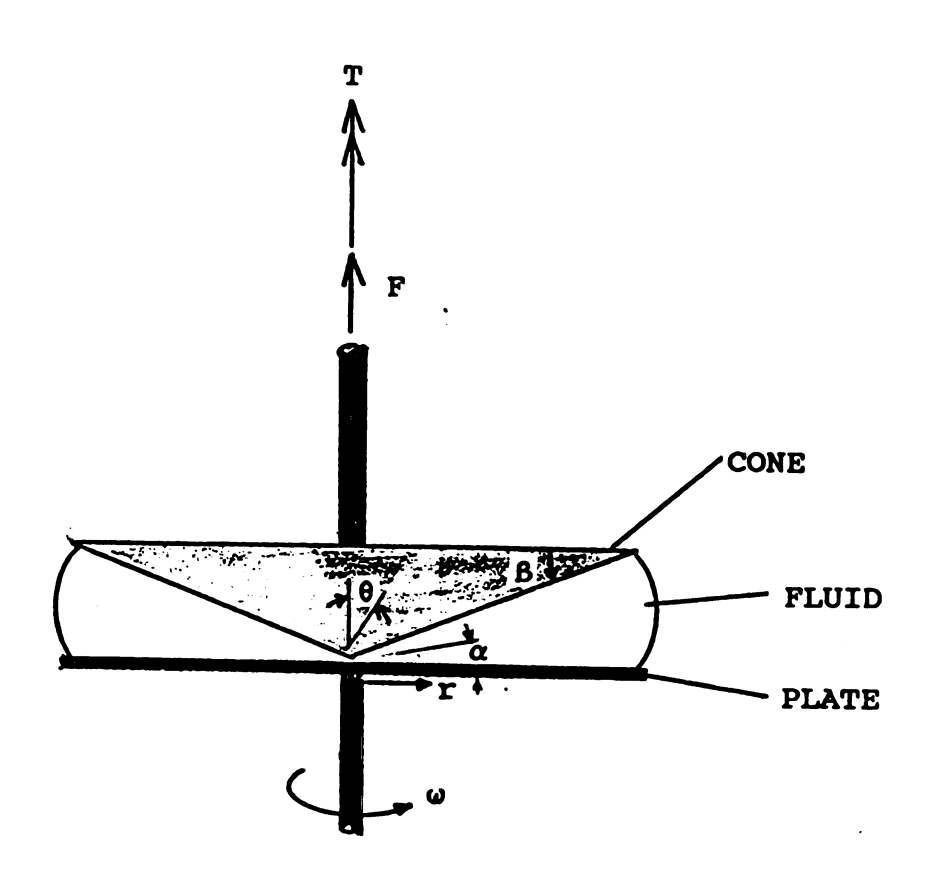


Figure A.1: The Cone and Plate Rheometer

PLATE AND PLATE VISCOMETER

Cylindrical Coordinates:
$$v_1 =$$

$$v_2 = v_r$$
 $v_3 = v_z$

$$V_3 = V_1$$

Velocity Vector

$$\underline{\mathbf{v}} = \mathbf{v}_{\theta}(\mathbf{r}, \mathbf{z})\underline{\mathbf{e}}_{\theta}$$

$$v_{\theta} = r\omega \left(1 - \frac{z}{H}\right)$$

Strain Rate Tensor

$$\underline{S} = \frac{1}{2} [\nabla \underline{v} + \nabla \underline{v}^{T}]$$

$$S_{\theta\theta} = S_{rr} = S_{rr} = 0$$

$$S_{\theta r} = S_{\theta r} = 0$$

$$S_{rz} = S_{zr} = 0$$

$$S_{\theta z} = S_{z\theta} = \frac{1}{2} \frac{\partial V_{\theta}}{\partial z}$$

First Invariant of S

$$tr S = 0$$

Second Invariant of S

$$2(S:S) = \frac{\partial v_{\theta}}{\partial z}$$

Third Invariant of S

$$\det S = 0$$

$$\frac{\delta \underline{S}}{\delta \underline{t}} = \frac{\partial \underline{S}}{\partial \underline{t}} + \underline{v} \cdot \nabla \underline{S} - \{(\nabla \underline{v})^{\mathrm{T}} \cdot \underline{S}\} + \underline{S} \cdot \nabla \underline{v}\}$$

$$\left(\frac{\delta \underline{S}}{\delta \underline{t}}\right)_{\theta \theta} = -\left(\frac{\partial \underline{v}_{\theta}}{\partial z}\right)^{2}$$

$$\left(\frac{\delta \underline{S}}{\delta \underline{t}}\right)_{rr} = \left(\frac{\delta \underline{S}}{\delta \underline{t}}\right)_{rr} = 0$$

$$\left(\frac{\delta \underline{S}}{\delta \underline{t}}\right)_{\theta r} = \left(\frac{\delta \underline{S}}{\delta \underline{t}}\right)_{r\theta} = 0$$

$$\left(\frac{\delta \underline{S}}{\delta \underline{t}}\right)_{\theta r} = \left(\frac{\delta \underline{S}}{\delta \underline{t}}\right)_{r\theta} = 0$$



Rotating Die Pre-pregger, Disk Region

$$\underline{\tau}^{\mathrm{I}} = 2\eta \underline{S}^{\mathrm{I}} - \underline{\Psi}_{1} \frac{\delta \underline{S}^{\mathrm{I}}}{\delta t}$$

$$\tau_{\theta\theta}^{\mathrm{I}} = 2\eta \frac{v_{\mathrm{I}}^{\mathrm{I}}}{T} - \underline{\Psi}_{1} \left[-4\left(\frac{v_{\mathrm{I}}^{\mathrm{I}}}{T}\right)^{2} - \left(\frac{\partial v_{\theta}^{\mathrm{I}}}{\partial z}\right)^{2} \right]$$

$$\tau_{\mathrm{II}}^{\mathrm{I}} = 2\eta \frac{\partial v_{\mathrm{I}}}{\partial r} + \underline{\Psi}_{1} \left(\frac{\partial v_{\mathrm{I}}^{\mathrm{I}}}{\partial z}\right)^{2}$$

$$\tau_{\mathrm{II}}^{\mathrm{I}} = 0$$

$$\tau_{\mathrm{II}}^{\mathrm{I}} = \tau_{\mathrm{I}\theta}^{\mathrm{I}} = \underline{\Psi}_{1} \frac{\partial v_{\theta}^{\mathrm{I}}}{\partial z} \frac{\partial v_{\mathrm{I}}^{\mathrm{I}}}{\partial z}$$

$$\tau_{\theta \mathrm{I}}^{\mathrm{I}} = \tau_{\mathrm{I}\theta}^{\mathrm{I}} = \eta \frac{\partial v_{\theta}^{\mathrm{I}}}{\partial z}$$

$$\tau_{\mathrm{II}}^{\mathrm{I}} = \tau_{\mathrm{II}}^{\mathrm{I}} = \eta \frac{\partial v_{\theta}^{\mathrm{I}}}{\partial z}$$

Rotating Die Pre-pregger, Die Tube Region

$$\underline{\tau} = 2\eta \underline{S} - \underline{\Psi}_1 \frac{\delta \underline{S}}{\delta \underline{t}}$$

$$\tau_{zz}^{III} = \underline{\Psi}_1 \left(\frac{\partial \mathbf{V}_z^{III}}{\partial \mathbf{r}} \right)^2$$

$$\tau_{zx}^{III} = \tau_{rz}^{III} = \eta \frac{\partial \mathbf{V}_z^{III}}{\partial \mathbf{r}}$$

$$\tau_{rx}^{III} = \tau_{\theta\theta}^{III} = 0$$

$$\tau_{z\theta}^{III} = \tau_{\thetaz}^{III} = 0$$

$$\tau_{r\theta}^{III} = \tau_{\thetaz}^{III} = 0$$

Rotating Die Pre-Pregger, Transition Region

$$\underline{\tau}^{\text{II}} = 2 < \eta > \underline{S}$$

$$\tau_{\theta\theta}^{\text{II}} = 2 < \eta > \underline{V_{x}^{\text{II}}}$$

$$\tau_{rr}^{\text{II}} = 2 < \eta > \frac{\partial V_{r}^{\text{II}}}{\partial r}$$

$$\tau_{zz}^{\text{II}} = 2 < \eta > \frac{\partial V_{z}^{\text{II}}}{\partial z}$$

$$\tau_{r\theta}^{ii} = \tau_{\theta r}^{ii} = 0$$

$$\tau_{z\theta}^{\text{rr}} = \tau_{\theta z}^{\text{rr}} = \langle \eta \rangle \frac{\partial V_{\theta}^{\text{rr}}}{\partial z}$$

$$\tau_{rz}^{\text{II}} = \tau_{zr}^{\text{II}} = \langle \eta \rangle \left(\frac{\partial v_z^{\text{II}}}{\partial r} + \frac{\partial v_z^{\text{II}}}{\partial z} \right)$$

Cone and Plate Viscometer

$$\underline{\tau} = 2\eta \underline{S} - \Psi_1 \frac{\delta \underline{S}}{\delta \underline{t}}$$

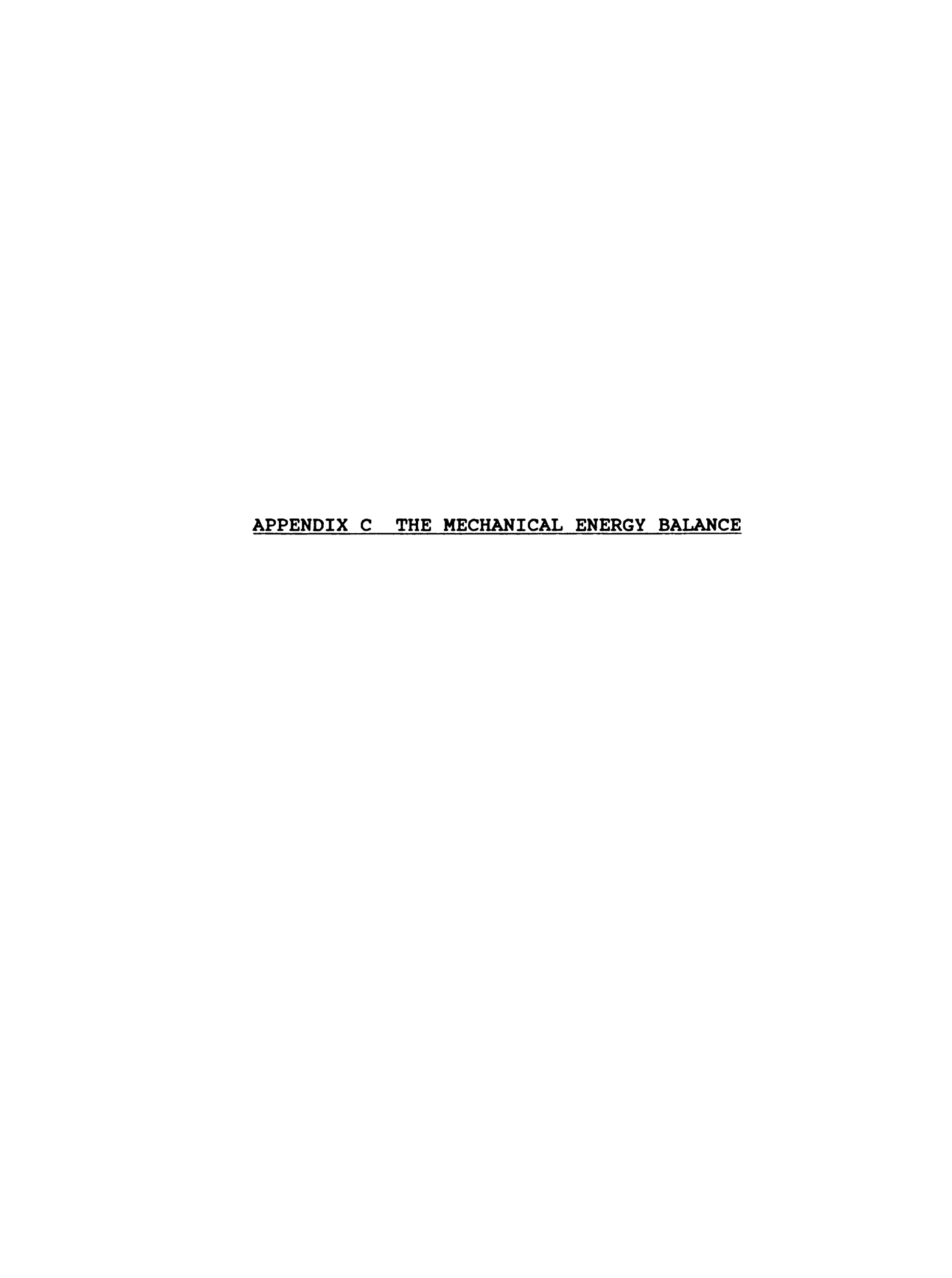
$$\tau_{\phi\phi} = \Psi_1 \left(\frac{\omega}{\beta}\right)^2$$

$$\tau_{\phi\theta} = \tau_{\theta\phi} = \eta \frac{\omega}{B}$$

$$\tau_{\theta\theta} = \tau_{rr} = 0$$

$$\tau_{\phi r} = \tau_{r\phi} = 0$$

$$\tau_{\theta r} = \tau_{r\theta} = 0$$



$$D = W_1 + W_2 \tag{C.1}$$

$$D = \iiint_{V} \underline{\tau} : \nabla \underline{u} \ dV$$
 (C.2)

$$= D_{r} + D_{rr} + D_{rrr}$$
 (C.3)

Dissipation in disk region.

$$D_{r} = 2\pi \int_{0}^{\pi} \int_{R_{d}}^{R} \underline{\tau}^{r} : \nabla \underline{v}^{r} dr dz \qquad (C.4)$$

Dissipation in transition region.

$$D_{ii} = 2\pi \int_{0}^{\pi} \int_{0}^{R} \underline{\tau}^{ii} : \nabla \underline{v}^{ii} r dr dz \qquad (C.5)$$

Dissipation in die tube region.

$$D_{iii} = 2\pi \int_{R}^{t+R} \int_{0}^{R} \underline{\tau}^{iii} : \nabla \underline{v}^{iii} r dr dz$$
 (C.6)

Work put in by rotating disk.

$$W_1 = -2\pi \int_0^R \left[\tau_{z\theta} V_{\theta} \right]_{z=0} r dr \qquad (C.7)$$

Work brought in by entering fluid.

$$W_2 = 2\pi \int_0^{R} \left[\tau_{r\theta} V_{\theta} \right]_{r=R} dz$$
 (C.8)

$$W_{1} = -2\pi \int_{0}^{R} (\tau_{z\theta} v_{\theta})_{z=0} r dr$$

from Appendix A:
$$r_{i\theta} = \eta \frac{\partial v_{\theta}}{\partial z}$$

$$v_{\theta} = r\omega(1-\frac{Z}{H})$$
and: $\eta = k \left(\frac{r\omega}{H}\right)^{n-1}$

$$W_{1} = -2\pi \int_{0}^{R} -k \left(\frac{r\omega}{H}\right)^{n} r dr$$

$$= \frac{2\pi R^{2} k}{n+2} \left(\frac{R\omega}{H}\right)^{n} \qquad (C.9)$$

$$W_{2} = 2\pi R \int_{0}^{R} \left[\tau_{r\theta} v_{\theta} \right]_{r=R} dz$$

from Appendix A:
$$\tau_{r\theta} = - \Psi_1 \frac{\partial v_{\theta}}{\partial z} \frac{\partial v_r}{\partial z}$$

$$v_{\theta} = r\omega(1 - \frac{z}{H})$$

$$v_r = - \frac{3Q}{\pi r H} \frac{z}{H} \left(1 - \frac{z}{H}\right)$$
 and:
$$\Psi_1 = a \left(\frac{r\omega}{H}\right)^{b-2}$$

$$W_2 = - Q a \left(\frac{R\omega}{H}\right)^b$$
 (C.10)

$$D_{r} = 2\pi \int_{0}^{R} \int_{R_{d}}^{R} \eta \left[\left(\frac{\partial v_{\theta}}{\partial z} \right)^{2} + 4 \left(\frac{v_{r}}{r} \right)^{2} + \left(\frac{\partial v_{r}}{\partial z} \right)^{2} \right] r dr dz$$

$$-2\pi \int_{0}^{R} \int_{R_{A}}^{R} \Psi_{1} \frac{V_{r}}{\Gamma} \left[\left(\frac{\partial V \theta}{\partial z} \right)^{2} + 4 \left(\frac{V_{r}}{\Gamma} \right)^{2} - \left(\frac{\partial V_{r}}{\partial z} \right)^{2} \right] r dr dz$$

Note: First term of first integral balances with $\left[W_{1}\right]_{R_{A}}^{R}$.

$$D_{r} = \left[W_{1}\right]_{R_{d}}^{R} + D_{r}^{*} - E \qquad (C.11)$$

$$-E = 2\pi \int_{0}^{R} \int_{R_{d}}^{R} \Psi_{1} \frac{V_{r}}{r} \left[\left(\frac{\partial V \theta}{\partial z} \right)^{2} + 4 \left(\frac{V_{r}}{r} \right)^{2} - \left(\frac{\partial V_{r}}{\partial z} \right)^{2} \right] r dr dz$$

$$= Q \frac{a}{b} \left(\frac{R_d \omega}{H}\right)^b \left[\left(\frac{R}{R_d}\right)^b - 1\right]$$
 (C.12)

$$D_{r}^{*} = 2\pi \int_{0}^{H} \int_{R_{d}}^{R} \eta \left[4 \left(\frac{V_{r}}{T} \right)^{2} + \left(\frac{\partial V_{r}}{\partial Z} \right)^{2} \right] r dr dz$$

$$\eta = k \left(\frac{r\omega}{H} \right)^{n-1}$$

$$V_{r} = -\frac{3Q}{\pi r H} \frac{Z}{H} \left(1 - \frac{Z}{H} \right)$$

For $n \neq 1$,

$$D_{I}' = \frac{6kQ^{2}}{\pi H^{3}} \left(\frac{R_{d}\omega}{H}\right)^{n-1} \left[\frac{2}{5(n-3)} \left(\frac{H}{R_{d}}\right)^{2} \left[\left(\frac{R}{R_{d}}\right)^{n-3} -1\right] + \frac{1}{n-1} \left[\left(\frac{R}{R_{d}}\right)^{n-1} -1\right]\right]$$
(C.13)

For n = 1,

$$D_{r}^{*} = \frac{6kQ^{2}}{\pi H^{3}} \left[\frac{1}{5} \left(\frac{H}{R_{d}} \right)^{2} \left[1 - \left(\frac{R_{d}}{R} \right)^{2} \right] + \ln \left(\frac{R}{R_{d}} \right) \right]$$
 (C.14)

$$D_{rr} = 2\pi \int_{0}^{R} \int_{0}^{R_{d}} <\eta> \left[\left(\frac{\partial v_{\theta}}{\partial z} \right)^{2} + 2 \left(\frac{v_{r}}{r} \right)^{2} + 2 \left(\frac{\partial v_{r}}{\partial r} \right)^{2} \right] + \left(\frac{\partial v_{r}}{\partial r} + \frac{\partial v_{r}}{\partial z} \right)^{2} + 2 \left(\frac{\partial v_{z}}{\partial z} \right)^{2}$$

Note: First term of integral balances with $\left[W_{1}\right]_{0}^{R_{d}}$.

$$D_{II} = \left[W_{I}\right]_{0}^{R_{d}} + D_{II}^{*}$$

$$D_{rr}^{*} = 2\pi \int_{0}^{\pi} \int_{0}^{R_{d}} \langle \eta \rangle \left[2\left(\frac{V_{r}}{r}\right)^{2} + 2\left(\frac{\partial V_{r}}{\partial r}\right)^{2} + \left(\frac{\partial V_{z}}{\partial r} + \frac{\partial V_{r}}{\partial z}\right)^{2} + 2\left(\frac{\partial V_{z}}{\partial z}\right)^{2} \right] r dr dz$$

from Appendix A:

$$v_r = -\frac{3Q}{\pi R_d H} \frac{3n+1}{n+1} \frac{r}{R_d} \left[1 - \frac{2n}{2n+1} \left(\frac{r}{R_d} \right)^{\frac{n+1}{n}} \right] \frac{z}{H} \left(1 - \frac{2}{3} \frac{z}{H} \right)$$

$$\mathbf{v}_{z} = \frac{3Q}{\pi R_{d}^{2}} \frac{3n+1}{n+1} \left[1 - \left(\frac{\mathbf{r}}{R_{d}}\right)^{\frac{n+1}{n}} \right] \left(\frac{\mathbf{z}}{H}\right)^{2} \left(1 - \frac{2}{3} \frac{\mathbf{z}}{H}\right)$$

and:

$$<\eta> = \frac{2k}{n+1} \left(\frac{R_d \omega}{H}\right)^{n-1}$$

$$D_{II} = \frac{2Q^{2}}{\pi H^{3}} \left[\frac{2k}{n+1} \left(\frac{R_{d}\omega}{H} \right)^{n-1} \right] \left[\frac{13}{70} \frac{n(3n+1)^{2}}{(n+1)^{3}} \left(\frac{H}{R_{d}} \right)^{4} \right]$$

$$+ \frac{9 + 54n + 264n^{2} + 432n^{3} + 231n^{4} + 90n^{5}}{5(n+1)^{3}(2n+1)} \left(\frac{H}{R_{d}} \right)^{2}$$

$$+ \frac{1 + 14n + 56n^{2} + 29n^{3} + 31n^{4}}{4(n+1)^{2}(3n+1)(5n+1)}$$
(C.15)

$$D_{rr} = 2\pi L_d \int_0^{R_d} \tau_{rr} \left(\frac{\partial v_r}{\partial r} + \frac{\partial v_r}{\partial z} \right) r dr$$

from Appendix A:

$$v_{z} = \frac{Q}{\pi R_{a}^{2}} \frac{3n+1}{n+1} \left[1 - \left(\frac{r}{R_{d}}\right)^{\frac{n+1}{n}} \right]$$

and:

$$\tau_{xz} = \eta \left(\frac{\partial v_z}{\partial r} \right) = k \left(\frac{\partial v_z}{\partial r} \right)^n$$

$$\left(\frac{\partial V_{r}}{\partial z}\right) \ll \left(\frac{\partial V_{t}}{\partial r}\right)$$

$$D_{rrr} = 2kL_{d} \frac{Q^{n+1}}{R_{d}^{3n+1}} \left(\frac{3n+1}{\pi n}\right)^{n}$$
 (C.16)

Let:
$$\hat{c}_{1} Q^{2} = D_{1} + D_{11}$$

 $\hat{c}_{2} Q^{n+1} = D_{111}$
 $\hat{c}_{3} = E + W_{2}$

Then:
$$\hat{C}_1 Q^2 + \hat{C}_2 Q^{n+1} = \hat{C}_3 Q$$

 $\hat{C}_1 Q + \hat{C}_2 Q^n - \hat{C}_3 = 0$

Non-dimensionalize with:

$$\alpha = \frac{3Q}{\pi R_{d}^{2} \omega H}$$

$$G = \frac{a}{k} \omega^{b-n}$$

$$\beta_{H} = \frac{H}{R_{d}}$$

$$\beta_{R} = \frac{R}{R_{d}}$$

$$\beta_{L} = \frac{L_{d}}{R_{d}}$$

To get:
$$c_1 \alpha + c_2 \alpha^n - c_3 = 0$$
 (C.17)

$$c_2 = 2 \beta_L \left(\frac{2}{3} \beta_R^2 \frac{3n+1}{n}\right)^n$$
 (C.18)

$$c_3 = G \beta_{H}^{n-b} \left(\frac{b+1}{b} \beta_{R}^{b} - \frac{1}{b} \right)$$
 (C.19)

When $n \neq 1$:

$$c_{1} = \frac{8}{5(3-n)} \beta_{H} \left(1-\beta_{R}^{n-1}\right) + \frac{4}{\beta_{H}(n-1)} \left(1-\beta_{R}^{n-1}\right)$$

$$+ \frac{8}{3(n+1)\beta_{H}} \left[\frac{13}{70} \frac{n(3n+1)^{2}}{(n+1)^{3}} \beta_{H}^{4}\right]$$

$$+ \frac{9+54n+264n^{2}+432n^{3}+231n^{4}+90n^{5}}{5(n+1)^{3}(2n+1)} \beta_{H}^{2}$$

$$+ \frac{1+14n+56n^{2}+29n^{3}+31n^{4}}{4(n+1)^{2}(3n+1)(5n+1)} \left[(C.20) \right]$$

When n = 1

$$c_{1} = \frac{4}{5} \beta_{H} (1-\beta_{H}^{-2}) + \frac{4}{\beta_{H}} \ln(\beta_{R}) + \frac{4}{3\beta_{H}} \left(\frac{13}{35} \beta_{H}^{4} + 9 \beta_{H}^{2} + \frac{131}{384}\right)$$
(C.21)



```
С
      Nancy Losure Oct 3, 1990
C
C
      Program File: ARNOLD.FOR
C
      Data Input File: ARNOLD.DAT
C
      Data Output File: ARNOLD.OUT
C
C
      THIS PROGRAM SOLVES A NON-LINEAR EQUATION FOR THE
C
      DIMENSIONLESS FLOW RATE FROM A CENTRIPETAL PUMP, BY
C
      INTERVAL HALVING
C
C
      INPUT:
C
       AA IS THE ELASTICITY COEFFICIENT [DYNE*SEC^B/CM^2]
C
       AB IS THE ELASTICITY EXPONENT
C
       AK IS THE VISCOSITY COEFFICIENT [DYNE*SEC^N/CM^2]
C
       AN IS THE VISCOSITY EXPONENT
C
       BRD IS THE RADIUS OF THE DIE [CM]
C
       BR IS THE RADIUS OF THE DISK [CM]
C
       BL IS THE LENGTH OF THE DIE [CM]
C
       BW IS THE ROTATION RATE OF THE DISK [RAD/SEC]
C
       BETAR IS DISK RADIUS/DIE RADIUS
C
       BETAH IS GAP WIDTH/DIE RADIUS
C
       BETAL IS DIE LENGTH/DIE RADIUS
C
               (a/k) (omega)**b-n
C
       ATOL IS THE TOLERANCE WITH WHICH ALPHA AND ALEPH ARE
C
          REQUIRED TO MATCH
C
       NW IS THE NUMBER OF VALUES OF OMEGA WHICH WILL BE
C
          CALCULATED
C
       NH IS THE NUMBER OF VALUES OF BH WHICH WILL BE
C
          CALCULATED
C
       BH(X) IS THE ARRAY WHICH CONTAINS A LIST OF GAP
C
          WIDTHS TO BE CALCULATED [CM]
C
       ANSW(X) IS THE ARRAY WHICH CONTAINS THE FLOW RATES
C
          CALCULATED FOR EACH BH(X) [CM-3/SEC]
C
       ALPHA IS THE TRIAL VALUE OF THE DIMENSIONLESS FLOW
С
          RATE
C
       ALEPH IS THE CALCULATED VALUES OF THE DIMENSIONLESS
C
          FLOW RATE
C
       C1, C2, C3 ARE INTERMEDIATE CALCULATIONS
      IMPLICIT REAL*4(A-H, O-Z)
      DIMENSION BH(100), BW(100), ANSW(100)
C
      OPEN (UNIT=5, FILE='ARNOLD.DAT')
      OPEN (UNIT=6, FILE='ARNOLD.OUT', STATUS='UNKNOWN',
        ACCESS='append')
      OPEN (UNIT=7, FILE='CON')
      READ DATA AND WRITE DATA AND HEADINGS TO OUTPUT FILE.
C
C
10
     WRITE(6,9000)
```

```
READ(5,*)AA,AB,AK,AN,BR,BRd,BL,ATOL,NW,NH
      WRITE(6,9001)AA, BR, ATOL, AB, BRD, NW, AK, BL, NH, AN
C
      DO 12 I=1,NW
      READ(5,*)BW(I)
12
      CONTINUE
      DO 14 I=1,NH
      READ(5,*)BH(I)
14
      CONTINUE
      BETAR = BR/BRD
      BETAL = BL/BRD
      WRITE(6,9002)BETAR, BETAL
      DO 120 K=1,NW
20
      DO 100 I=1,NH
      ANSW(I) = 0.000001
      ALPHA = 0.0001
      J = 0
      BETAH = BH(I)/BRD
      GG=AA/AK*BW(K)**(AB-AN)
      if (an. EQ. 1) then
      cla= 4*alog(pr)
      else
      C1a = 4/(1-AN)*(1-BETAR**(AN-1))
      endif
      c1b = 1.60/(3-AN)*BETAH**2*(1-BETAR**(AN-3))
      C1C= 52*(1+3*AN)**2*AN*BETAH**4/105/(1+AN)**4
      cld= 8*(9+54*AN+264*AN**2+432*AN**3+231*AN**4+90*
           AN**5)*BETAH**2 /15/(1+AN)**4/(1+2*AN)
      cle= 2*(1+14*AN+56*AN**2+74*AN**3+31*AN**4)/3/
           (1+AN)**3/(1+3*AN)/(1+5*AN)
      cl = (cla+clb+clc+cld+cle)/ph
      C2 = 2*BETAL*(2*BETAH**2*(1+3*AN)/3/AN)**AN
      C3 = AA/AK*(BW(K)/BETAH)**(AB-AN)*((AB+1)/AB-1/pR**
           (AB)/AB)*BETAR**AB
60
      IF(AN.EQ.1)THEN
      ALEPH = C3/(C2+C1)
      ANSW(I) = ALEPH*2.094*BRD**2*BW(K)*BH(I)
      WRITE(6,9003)BW(K),BH(I),ANSW(I),GG,BETAH,ALEPH
      GO TO 100
      ENDIF
      START INTERVAL HALVING
C
      FIRST FIND LOW AND HIGH GUESSES
           NFLAG=0
           G1=.00001
           G2=1
65
           FA1=C1*G1+C2*G1**AN-C3
70
           FA2=C1*G2+C2*G2**AN-C3
              IF((FA1*FA2).GE.O.AND.NFLAG.NE.1) THEN
                                129
```

```
G2=G2*2
               GO TO 70
              ELSE
               NFLAG=1
              ENDIF
        G3=(G1+G2)/2
        FA3 = C1*G3+C2*G3**AN-C3
C
       write(7,*)'g1',g1,'
                              fal',fal
C
       write(7,*)'g2',g2,'
                              fa2',fa2
C
       write(7,*)'q3',q3,'
                              fa3',fa3
      IF(ABS(FA3).LT.ATOL)THEN
         ALEPH=G3
         ANSW(I)=ALEPH*2.094*BRD**2*BW(K)*BH(I)
         WRITE(6,9003)BW(K),BH(I),ANSW(I),GG,BETAH,ALEPH
         GO TO 100
      ELSE
                   IF((FA1*FA3).LT.0)THEN
                    G1=G1
                    G2=G3
                    G3=(G1+G2)/2
                    GO TO 65
                   ELSE
                    G1=G3
                    G2=G2
                    G3=(G1+G2)/2
                    GO TO 65
                   ENDIF
      ENDIF
100
      CONTINUE
120
      CONTINUE
9000
      FORMAT(3X, "NANCY LOSURE', 10X, 'ARNOLD. FOR', 10X,
          'Oct. 6, 1990"')
      FORMAT(/,/,3X,'" a="',f8.2,',',10x,'" R="',f8.4,',',
9001
                  10x, '"atol="', f8.6,',',/,3x,'" b="',f8.2,
     æ
                  ',',10x,'"Rd="',f8.4,',',10x,'" NW="',
                  12,/,3x,''' k=''',f8.2,',',10x,''' L=''',f8.4,''
     æ
                  ',',10X,'" NH="',i2,/,
     æ
                  3x,'" n="',f8.2,',',10x)
      FORMAT(1X, '"R/Rd="', F8.2,',',7X,'"L/Rd="', F6.2,/,/
9002
                  3X, '"OMEGA"', 6X, '"H"', 15x, '"Q"', 3X, '"G"',
                  5X,"H/Rd"',5X,"ALPHA"')
9003
     FORMAT(1X,F6.2,',',5X,F6.2,',',5X,F12.8,',',5X,F8.4,
                 ',',5X,F8.4,',',5X,F8.4)
9004
     FORMAT(5x,'G1',3x,f12.6,10x,'G2',3x,f12.6,10X,'G3',3X,
                F12.6)
      STOP
      END
```

"NANCY	LOSURE	ARNO	LD.FOR	MAY 4, 1	.991 "
" a="	432.00,	" R="	2.5000,	"atol="0	.001000,
" b="	1.73,	"Rd="	0.1500,	" NW="	•
" k="	502.00,	" L="	0.5000,	" NH="1	
" n="	0.96,		0.3000,		
"R/Rd="	•	"L/R	d=" 3.33		
"OMEGA"	ı ııHıı	"Q"	"G"	"H/Rd"	"ALPHA"
8.00,	0.02,	0.0972,	4.2674,	0.1333,	12.9005
8.00,	0.04,	0.2106,	4.2674,	0.2667,	13.9685
8.00,	0.06,	0.3015,	4.2674,	0.4000,	13.3320
8.00,	0.08,	0.3549,	4.2674,	0.5333,	11.7700
8.00,	0.10,	0.3727,	4.2674,	0.6667,	9.8874
8.00,	0.12,	0.3653,	4.2674,	0.8000,	8.0771
8.00,	0.14,	0.3439,	4.2674,	0.9333,	6.5170
8.00,	0.16,	0.3164,	4.2674,	1.0667,	5.2461
8.00,	0.18,	0.2876,	4.2674,	1.2000,	4.2384
8.00,	0.20,	0.2599,	4.2674,	1.3333,	3.4477
8.00,	0.25,	0.2013,	4.2674,	1.6667,	2.1366
8.00,	0.30,	0.1581,	4.2674,	2.0000,	1.3979
8.00,	0.35,	0.1265,	4.2674,	2.3333,	0.9591
8.00,	0.40,	0.1032,	4.2674,	2.6667,	0.6847
10.00,	0.02,	0.1444,	5.0673,	0.1333,	15.3193
10.00,	0.04,	0.3127,	5.0673,	0.2667,	16.5901
10.00,	0.06,	0.4478,	5.0673,	0.4000,	15.8395
10.00,	0.08,	0.5273,	5.0673,	0.5333,	13.9902
10.00,	0.10,	0.5540,	5.0673,	0.6667,	11.7589
10.00,	0.12,	0.5434,	5.0673,	0.8000,	9.6111
10.00,	0.14,	0.5118,	5.0673,	0.9333,	7.7585
10.00,	0.16,	0.4710,	5.0673,	1.0667,	6.2481
10.00,	0.18,	0.4283,	5.0673,	1.2000,	5.0497
10.00,	0.20,	0.3872,	5.0673,	1.3333,	4.1090
10.00,	0.25,		5.0673,	1.6667,	2.5479
10.00,	0.30,	0.2357,		2.0000,	1.6676
10.00,	0.35,	0.1887,	-	•	1.1444
10.00,	0.40,	0.1540,	5.0673,	2.6667,	0.8171
12.00,	0.02,	0.1993,	5.8311,	0.1333,	17.6286
12.00,	0.04,		5.8311,	0.2667,	19.0933
12.00,	0.06,	· ·	5.8311,	0.4000,	18.2344
12.00,	0.08,		5.8311,	· ·	
12.00,	0.10,	0.7660,	-		
12.00,	0.12,		5.8311,		
12.00,	0.14,	0.7081,		0.9333,	8.9465
12.00,	0.16,	0.6520,	5.8311,	1.0667,	7.2073
12.00,	0.18,	•	5.8311,	1.2000,	5.8266
12.00,	0.20,	0.5362,	5.8311,	· · · · · · · · · · · · · · · · · · ·	4.7423
12.00,	0.25,	0.4158,	5.8311,	*	2.9419

12.00,	0.30,	0.3267,	5.8311,	2.0000,	1.9261
12.00,	0.35,	0.2616,	5.8311,	2.3333,	1.3221
12.00,	0.40,	0.2135,	5.8311,	2.6667,	0.9441
14.00,	0.02,	0.2619,	6.5660,	0.1333,	19.8506
14.00,	0.04,	0.5673,	6.5660,	0.2667,	21.5023
14.00,	0.06,	0.8129,	6.5660,	0.4000,	20.5396
14.00,	0.08,	0.9580,	6.5660,	0.5333,	18.1546
14.00,	0.10,	1.0073,	6.5660,	0.6667,	15.2715
•	•	· · · · · · · · · · · · · · · · · · ·		<u> </u>	12.4921
14.00,	0.12,	0.9888,	6.5660,	0.8000,	
14.00,	0.14,	0.9319,	6.5660,	0.9333,	10.0916
14.00,	0.16,	0.8583,	6.5660,	1.0667,	8.1322
14.00,	0.18,	0.7808,	6.5660,	1.2000,	6.5760
14.00,	0.20,	0.7062,	6.5660,	1.3333,	5.3534
14.00,	0.25,	0.5479,	6.5660,	1.6667,	3.3223
14.00,	0.30,	0.4305,	6.5660,	2.0000,	2.1757
14.00,	0.35,	0.3448,	6.5660,	2.3333,	1.4937
14.00,	0.40,	0.2815,	6.5660,	2.6667,	1.0668
16.00,	0.02,	0.3317,	7.2770,	0.1333,	22.0006
16.00,	0.04,	0.7187,	7.2770,	0.2667,	23.8333
16.00,	0.06,	1.0299,	7.2770,	0.4000,	22.7708
16.00,	0.08,	1.2141,	7.2770,	0.5333,	20.1323
16.00,	0.10,	1.2770,	7.2770,	0.6667,	16.9406
16.00,	0.12,	1.2540,	7.2770,	0.8000,	13.8618
16.00,	0.14,	1.1822,	7.2770,	0.9333,	11.2014
16.00,	0.16,	1.0890,	7.2770,	1.0667,	9.0288
16.00,	0.18,	0.9909,	7.2770,	1.2000,	7.3026
16.00,	0.20,		· ·		
	•	0.8965,	7.2770,	1.3333,	5.9459
16.00,	0.25,	0.6957,	7.2770,	1.6667,	3.6913
16.00,	0.30,	0.5468,	7.2770,	2.0000,	2.4179
16.00,	0.35,	0.4381,	7.2770,	2.3333,	1.6603
16.00,	0.40,	0.3576,	7.2770,	2.6667,	1.1859
18.00,	0.02,	0.4086,	7.9678,	0.1333,	24.0895
18.00,	0.04,	0.8853,	7.9678,	0.2667,	26.0983
18.00,	0.06,	1.2690,	7.9678,	0.4000,	24.9390
18.00,	0.08,	1.4963,	7.9678,	0.5333,	22.0549
18.00,	0.10,	1.5743,	7.9678,	0.6667,	18.5635
18.00,	0.12,	1.5463,	7.9678,	0.8000,	15.1941
18.00,	0.14,	1.4581,	7.9678,	0.9333,	12.2810
18.00,	0.16,	1.3435,	7.9678,	1.0667,	9.9012
18.00,	0.18,	1.2227,	7.9678,	1.2000,	8.0097
18.00,	0.20,	1.1064,	7.9678,	1.3333,	6.5228
18.00,	0.25,	0.8588,	7.9678,	1.6667,	4.0506
18.00,	0.30,	0.6752,	7.9678,	2.0000,	2.6538
18.00,	0.35,	0.5410,	7.9678,	2.3333,	1.8225
18.00,	0.40,	0.4416,	7.9678,	2.6667,	1.3019
20.00,	0.02,	0.4924,	8.6412,	0.1333,	26.1256
20.00,	0.04,	1.0669,	8.6412,	0.2667,	28.3062
20.00,	0.06,	1.5295,	8.6412,	0.4000,	27.0530
20.00,	0.08,	1.8039,	8.6412,	0.5333,	23.9296
20.00,	0.00,	· · · · · · · · · · · · · · · · · · ·	8.6412,	0.6667,	20.1466
•	•	1.8984,	•		
20.00,	0.12,	1.8651,	8.6412,	0.8000,	16.4939

20.00,	0.14,	1.7591,	8.6412,	0.9333,	13.3347
20.00,	0.16,	1.6212,	8.6412,	1.0667,	10.7528
20.00,	0.18,	1.4757,	8.6412,	1.2000,	8.7001
20.00,	0.20,	1.3354,	8.6412,	1.3333,	7.0860
20.00,	0.25,	1.0369,	8.6412,	1.6667,	4.4016
20.00,	0.30,	0.8153,	8.6412,	2.0000,	2.8842
20.00,	0.35,	0.6533,	8.6412,	2.3333,	1.9810
20.00,	0.40,	0.5334,	8.6412,	2.6667,	1.4152
22.00,	0.02,	0.5828,	9.2992,	0.1333,	28.1153
22.00,	0.04,	1.2631,	9.2992,	0.2667,	30.4639
22.00,	0.06,	1.8110,	9.2992,	0.4000,	29.1193
22.00,	0.08,	2.1363,	9.2992,	0.5333,	25.7625
22.00,	0.10,	2.2487,	9.2992,	0.6667,	21.6946
22.00,	0.12,	2.2097,	9.2992,	0.8000,	17.7653
22.00,	0.14,	2.0846,	9.2992,	0.9333,	14.3655
22.00,	0.16,	1.9215,	9.2992,	1.0667,	11.5862
22.00,	0.18,	1.7493,	9.2992,	1.2000,	9.3758
22.00,	0.20,	1.5833,	9.2992,	1.3333,	7.6373
22.00,	0.25,	1.2296,	9.2992,	1.6667,	4.7452
22.00,	0.30,	0.9670,	9.2992,	2.0000,	3.1098
22.00,	0.35,	0.7750,	9.2992,	2.3333,	2.1362
22.00,	0.40,	0.6328,	9.2992,	2.6667,	1.5262



FLUID: NEAT POLYBUTENE

GEOMETRY: Cone and Plate RADIUS [mm]: 12.5 CONE ANGLE [rad]: 0.108

<pre>gammadot strain rate [1/sec]</pre>	log strain rate	tau shear stress [dyne/cm^2]	log shear stress	N1 normal stress [dyne/cm^2]	log normal stress
1.000	0.000	811	2.909		
1.585	0.200	1285	3.109		
2.512	0.400	2024	3.306		
3.981	0.600	3196	3.505	252.2	2.402
6.310	0.800	5045	3.703	300.4	2.478
10.000	1.000	7956	3.901	229.3	2.360
15.850	1.200	12530	4.098	134.6	2.129
25.120	1.400	19540	4.291	474.7	2.676
39.810	1.600	30220	4.480	1511	3.179

Regression Output:

Constant 2.912827416
Std Err of Y Est 0.003873764
R Squared 0.999954815
No. of Observations 9
Degrees of Freedom 7

X Coefficient(s) 0.984176586 Std Err of Coef. 0.002500511

LOG(TAU) = CONSTANT + X COEFF*LOG(GAMMADOT)

k = 10^CONSTANT = 818.14 n = X COEFF = 0.98

Regression Output: fluid constants:

Constant
Std Err of Y Est
R Squared
No. of Observations
Degrees of Freedom

a= 74.00
b= 0.61
k= 818.14

X Coefficient(s) 0.607463763 Std Err of Coef. 0.374669108

LOG(N1) = CONSTANT + X COEFF*LOG(GAMMADOT)

a = 10^CONSTANT = 74.00 b = X COEFF = 0.61

FLUID: NEAT EPON 828

GEOMETRY: Cone and Plate RADIUS [mm]: 12.5 CONE ANGLE [rad]: 0.108

gammadot		tau		N1	
strain	log	shear	log	normal	log
rate	strain	stress	shear	stress	normal
[1/sec]	rate	[dyne/cm^2]	stress	[dyne/cm^2]	stress
1.000	0.000	115	2.061		
1.468	0.167	176	2.246		
2.154	0.333	262	2.417		
3.162	0.500	379	2.578		
4.642	0.667	551	2.741		
6.813	0.833	811	2.909		
10.000	1.000	1184	3.073		
14.680	1.167	1740	3.241		
21.540	1.333	2543	3.405		
31.620	1.500	3722	3.571		
46.420	1.667	5409	3.733	187.9	2.274
68.130	1.833	7782	3.891	218.5	2.339
100.000	2.000	10970	4.040	267.4	2.427

Regression Output:

Constant 2.080546032 Std Err of Y Est 0.009405885 R Squared 0.99980331 No. of Observations 13 Degrees of Freedom 11

0.989183198 X Coefficient(s) Std Err of Coef. 0.004183258

LOG(TAU) = CONSTANT + X COEFF*LOG(GAMMADOT)

120.38 fluid constants: $k = 10^{\text{CONSTANT}} =$ n = X COEFF =0.99

31.91 **b=** 0.46 Regression Output: k= 120.38 n= Constant 1.50394871 0.99

3=

Std Err of Y Est 0.009051788 0.993069556 R Squared 3 No. of Observations Degrees of Freedom 1

X Coefficient(s) 0.459758815 Std Err of Coef. 0.038407918

LOG(N1) = CONSTANT + X COEFF*LOG(GAMMADOT)

a = 10^CONSTANT = 31.91 0.46 b = X COEFF =

FLUID: NEAT CTBN

GEOMETRY: Cone and Plate RADIUS [mm]: 12.5 CONE ANGLE [rad]: 0.108

gammadot strain rate [1/sec]	log strain rate	tau shear stress [dyne/cm^2]	log shear stress	N1 normal stress [dyne/cm^2]	log normal stress
1.000	0.000	5679	3.754	[dyne/cm 2]	201622
1.585	0.200	8930	3.951		
2.512	0.400	14120	4.150		
3.981	0.600	22250	4.347		
6.310	0.800	34900	4.543	1315	3.119
10.000	1.000	55940	4.748	4105	3.613
15.850	1.200	84130	4.925	9516	3.978
25.120	1.400	10500	4.021	18380	4.264

Regression Output:

Constant 3.941196936
Std Err of Y Est 0.346071786
R Squared 0.386887277
No. of Observations 8
Degrees of Freedom 6

X Coefficient(s) 0.519524755 Std Err of Coef. 0.26699834

LOG(TAU) = CONSTANT + X COEFF+LOG(GAMMADOT)

k = 10^CONSTANT = 8733.67 fluid constants: n = X COEFF = 0.52 a= 8733.67

Constant 1.652959333
Std Err of Y Est 0.07415355
R Squared 0.98500733
No. of Observations 4
Degrees of Freedom 2

X Coefficient(s) 1.900693812 Std Err of Coef. 0.16581237

LOG(N1) = CONSTANT + X COEFF*LOG(GAMMADOT)

a = 10°CONSTANT = 44.97 b = X COEFF = 1.90

FLUID: 23% CTBN IN EPON 828

GEOMETRY: Cone and Plate RADIUS [mm]: 25
CONE ANGLE [rad]: 0.04

gammadot		tau		N1	
strain	log	shear	log	normal	log
rate	strain	stress	shear	stress	normal
[l/sec]	rate	[dyne/cm^2]	stress	[dyne/cm^2]	stress
1.585	0.200	1267	3.103		
2.512	0.400	2042	3.310		
3.981	0.600	3233	3.510		
6.310	0.800	5158	3.712		
10.000	1.000	8503	3.930		
15.850	1.200	13390	4.127		
25.120	1.400	20860	4.319	833.3	2.921
39.810	1.600	31510	4.498	1960	3.292
63.100	1.800	45160	4.655	3993	3.601
100.000	2.000	58770	4.769	6708	3.827

Regression Output:

 Constant
 2.931181167

 Std Err of Y Est
 0.040569108

 R Squared
 0.996378144

 No. of Observations
 11

 Degrees of Freedom
 9

X Coefficient(s) 0.962359666 Std Err of Coef. 0.019340587 fluid contstants:

k = 10 CONSTANT =	X COEFF+LOG(GAMMADOT) 853.46	a= b= k= n=	6.88 1.51 853.46 0.96
n = X COEFF =	0.96	u-	0.96

Regression Output:

Constant 0.837736651
Std Err of Y Est 0.051782667
R Squared 0.988425183
No. of Observations 4
Degrees of Freedom 2

X Coefficient(s) 1.513226605 Std Err of Coef. 0.115790821

LOG(N1) = CONSTANT + X COEFF*LOG(GAMMADOT)

a = 10°CONSTANT = 6.88 b = X COEFF = 1.51

FLUID: 40% CTBN IN EPON 828

GEOMETRY: Cone and Plate RADIUS [mm]: 12.5 CONE ANGLE [rad]: 0.108

gammadot strain rate [1/sec]	log strain rate	tau shear stress [dyne/cm^2]	log shear stress	N1 normal stress [dyne/cm^2]	log normal stress
1.000	0.000	882	2.945		
1.585	0.200	1427	3.154		
2.512	0.400	2264	3.355		
3.989	0.601	3599	3.556		
6.310	0.800	5647	3.752		
10.000	1.000	9234	3.965		
15.850	1.200	14560	4.163		
25.120	1.400	22640	4.355	935	2.971
39.810	1.600	34300	4.535	2377	3.376
63.100	1.800	49300	4.693	4775	3.679
100.000	2.000	64290	4.808	7720	3.888

Regression Output:

Constant 2.979206393
Std Err of Y Est 0.037741773
R Squared 0.996817999
No. of Observations 11
Degrees of Freedom 9

X Coefficient(s) 0.95545423 Std Err of Coef. 0.017994131

fluid constants:

LOG(TAIL) = CONSTANT	X COEFF*LOG(GAMMADOT)	a=	7.64
$k = 10^{\circ}CONSTANT =$	953.25	b=	1.53
n = X COEFF =	0.96	k=	953.25
n - A COBIL -	0.90	n=	0.96

Regression Output:

Constant 0.882956551
Std Err of Y Est 0.069510267
R Squared 0.979690909
No. of Observations 4
Degrees of Freedom 2

X Coefficient(s) 1.526697413 Std Err of Coef. 0.15543137

LOG(N1) = CONSTANT + X COEFF+LOG(GAMMADOT)

a = 10°CONSTANT = 7.64 b = X COEFF = 1.53

FLUID: .3% POLYISOBUTYLENE IN POLYBUTENE WITH 4.4% KEROSENE

GEOMETRY: Cone and Plate RADIUS [mm]: 25
CONE ANGLE [rad]: 0.04

gammadot		tau		N1	
strain	log	shear	log	normal	log
rate	strain	stress	shear	stress	normal
[1/sec]	rate	[dyne/cm^2]	stress	[dyne/cm^2]	stress
1.000	0.000	495	2.695	347.3	2.541
1.585	0.200	772	2.888	842.6	2.926
2.512	0.400	1216	3.085	2226	3.348
3.981	0.600	1909	3.281	6000	3.778
6.310	0.800	2965	3.472	13680	4.136
10.000	1.000	4571	3.660	26760	4.427
15.850	1.200	7009	3.846	47760	4.679
25.120	1.400	10700	4.029	82220	4.915

Regression Output:

 Constant
 2.700781072

 Std Err of Y Est
 0.006415462

 R Squared
 0.999838921

 No. of Observations
 8

 Degrees of Freedom
 6

X Coefficient(s) 0.955193258 Std Err of Coef. 0.004949602

fluid constants:

		9=	432.49
		b=	1.73
LOG(TAU) = CONSTANT	+ X COEFF*LOG(GAMMADOT)	k=	50 2.09
$k = 10^{\circ}CONSTANT =$	502.09	n=	0.96
n = X COEFF =	0.96		

Regression Output:

Constant 2.635979628
Std Err of Y Est 0.101790505
R Squared 0.987720941
No. of Observations
Degrees of Freedom 6

X Coefficient(s) 1.725281023 Std Err of Coef. 0.078532539

LOG(N1) = CONSTANT + X COEFF*LOG(GAMMADOT)

a = 10°CONSTANT = 432.49 b = X COEFF = 1.725281023

FLUID: 5% SEPARAN AP 30 IN 50/50 GLYCEROL AND WATER, FRESH

GEOMETRY: Cone and Plate RADIUS [mm]: 12.5
CONE ANGLE [rad]: 0.108

17C AMMAN		tau		N1	
strain	log	shear	log	normal	log
rate	strain	stress	shear	stress	normal
[l/sec]	rate	[dyne/cm^2]	stress	[dyne/cm^2]	stress
1.000	-0.000	1054	3.023	5238	3.719
1.259	0.100	1339	3.127	5600	3.748
1.585	0.200	1390	3.143	6116	3.786
1.995	0.300	1493	3.174	6867	3.837
2.512	0.400	1573	3.197	7863	3.896
3.162	0.500	1716	3.235	8980	3.953
3.980	0.600	1815	3.259	10400	4.017
5.011	0.700	1880	3.274	11950	4.077
6.308	0.800	1987	3.298	13560	4.132
7.942	0.900	2120	3.326	15540	4.191
9.998	1.000	2168	3.336	17850	4.252
12.590	1.100	2304	3.362	20910	4.320
15.850	1.200	2399	3.380	26350	4.421
19.950	1.300	2443	3.388	31110	4.493
25.110	1.400	2614	3.417	37720	4.577
31.610	1.500	2804	3.448	45580	4.659
39.800	1.600	2848	3.455	55290	4.743
50.100	1.700	3013	3.479	62360	4.795
63.080	1.800	3121	3.494	76040	4.881

Regression Output:

Constant 3.097970066
Std Err of Y Est 0.022456146
R Squared 0.97263321
No. of Observations 19
Degrees of Freedom 17

X Coefficient(s) 0.231215057 Std Err of Coef. 0.009406521

fluid constants

LOG(TAU) = CONSTANT +	X COEFF*LOG(GAMMADOT)	a=	4357.98
k = 10^CONSTANT =	1253.05	b=	0.66
n = X COEFF =	0.23	k= n=	1253.05 0.23

Regression Output:

 Constant
 3.639285409

 Std Err of Y Est
 0.037638737

 R Squared
 0.990501795

 No. of Observations
 19

 Degrees of Freedom
 17

X Coefficient(s) 0.663835021 Std Err of Coef. 0.015766266

LOG(N1) = CONSTANT + X COEFF*LOG(GAMMADOT) a = 10^CONSTANT = 4357.98

a = 10°CONSTANT = 4357.98 b = X COEFF = 0.663835021

FLUID: 5% SEPARAN AP 30 IN 50/50 GLYCEROL AND WATER, AGED

GEOMETRY: Cone and Plate RADIUS [mm]: 12.5 CONE ANGLE [rad]: 0.108

gammadot		tau		N1	
strain	log	shear	log	normal	log
rate	strain	stress	shear	stress	normal
[l/sec]	rate	[dyne/cm^2]	stress	[dyne/cm^2]	stress
1.000	0.000	1222	3.087	7754	3.890
1.585	0.200	1372	3.137	10080	4.003
2.512	0.400	1464	3.166	11930	4.077
3.980	0.600	1642	3.215	13570	4.133
6.308	0.800	1882	3.275	18470	4.266
9.998	1.000	2086	3.319	25190	4.401
15.850	1.200	2339	3.369	34520	4.538
25.110	1.400	2522	3.402	42990	4.633
39.800	1.600	2923	3.466	61330	4.788
63.080	1.800	3023	3.480	55950	4.748

Regression Output:

Constant 3.086367363
Std Err of Y Est 0.010437745
R Squared 0.994948125
No. of Observations 10
Degrees of Freedom 8

X Coefficient(s) 0.228086867
Std Err of Coef. 0.005746208 fluid constants:

LOG(TAU) = CONSTANT + X COEFF*LOG(GAMMADOT) b= 0.53 k = 10^CONSTANT = 1220.02 k= 1220.02 n = X COEFF = 0.23 n= 0.23

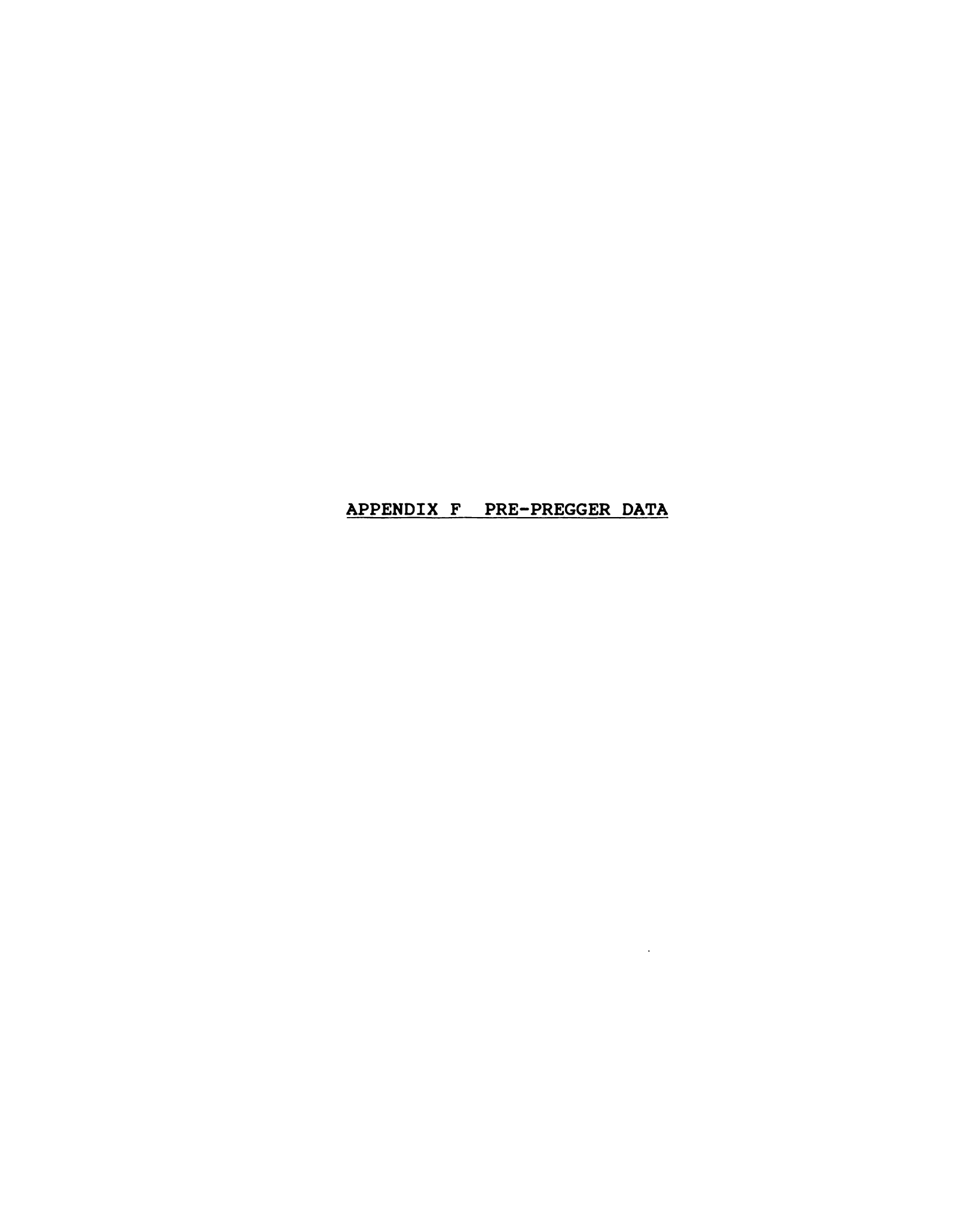
Regression Output:

Constant 3.874527315
Std Err of Y Est 0.046190195
R Squared 0.981630064
No. of Observations 10
Degrees of Freedom 8

X Coefficient(s) 0.525762426 Std Err of Coef. 0.025428717

LOG(N1) = CONSTANT + X COEFF*LOG(GAMMADOT)

a = 10°CONSTANT = 7490.78 b = X COEFF = 0.53



144	147	150	153	156
145	148	151	154	157
146	149	152	155	158

Figure F.1 Spreadsheet Diagram

SAMPLE CALCULATIONS

Data

ROTATION
$$\frac{\text{rad}}{\text{SeC}} = \omega = \frac{\text{ROTATION } \frac{\text{rev}}{\text{min}} * 2\pi \frac{\text{rad}}{\text{rev}}}{60 \frac{\text{sec}}{\text{min}}}$$

GAMMA.DOT
$$\frac{\text{rad}}{\text{sec}} = \dot{\gamma} = \frac{\text{R cm * } \omega \text{ rad/sec}}{\text{H cm}}$$

Least Squares Calculations For Fitting Data to a Line

y = b + m x

$$m = SLOPE = \frac{n \sum x_i y_i - (\sum x_i)(\sum y_i)}{n \sum x_i^2 - (\sum x_i)^2}$$

$$b = INTERCEPT = \frac{\sum y_i - m \sum x_i}{n}$$

n = NO.SAMPLE

$$\sum x_i = SUM \ 1 = TIME \ 1 + TIME \ 2 + TIME \ 3 + TIME \ 4$$

$$\sum y_i = SUM \ 2 = WEIGHT \ 1 + WEIGHT \ 2 + WEIGHT \ 3 + WEIGHT \ 4$$

$$\sum x_i y_i = \text{SUM } 3 = (\text{TIME } 1 * \text{WEIGHT } 1) + (\text{TIME } 2 * \text{WEIGHT } 2) + (\text{TIME } 3 * \text{WEIGHT } 3) + (\text{TIME } 4 * \text{WEIGHT } 4)$$

$$\sum x_1^2 = SUM \ 4 = (TIME \ 1)^2 + (TIME \ 2)^2 + (TIME \ 3)^2 + (TIME \ 4)^2$$

STANDARD
ERROR OF
ESTIMATE = + OR - =
$$\sqrt{\frac{\sum[y_i - (INTERCEPT + SLOPE * x_i)]^2}{n - 2}}$$

VOLUMETRIC FLOW RATE

$$Q \frac{Cm^3}{SEC} = \rho \frac{g}{Cm^3} * SLOPE \frac{g}{SEC}$$

INDEX	FLUID	GAP		ROTATION	
		(cm)	(rpm)	(rad/sec)	
4	fresh Separan	0.104	140	14.658	352.356
1	fresh Separan	0.104	92	9.632	231.548
3	fresh Separan	0.104	120	12.564	302.019
2	fresh Separan	0.104	100	10.470	251.683
8	fresh Separan	0.182	140	14.658	201.346
15	fresh Separan	0.207	200	20.940	252.899
9	fresh Separan	0.207	140	14.658	177.029
14	fresh Separan	0.207	160	16.752	202.319
6	fresh Separan	0.208	100	10.470	125.841
5	fresh Separan	0.208	90	9.423	113.257
7	fresh Separan	0.208	120	12.564	151.010
17	fresh Separan	0.415	200	20.940	126.145
13	fresh Separan	0.415	120	12.564	75.687
11	fresh Separan	0.415	90	9.423	56.765
10	fresh Separan	0.415	140	14.658	88.301
16	-	0.415			
12	fresh Separan		160	16.752	100.916
12	fresh Separan	0.415	100	10.470	63.072
20	23% CTBN/Epon	0.104	0	0.000	0.000
21	23% CTBN/Epon	0.104	90	9.423	226.514
23	23% CTBN/Epon	0.104	110	11.517	276.851
22	23% CTBN/Epon	0.104	110	11.517	276.851
24	23% CTBN/Epon	0.104	120	12.564	302.019
25	23% CTBN/Epon	0.104	160	16.752	402.692
36	23% CTBN/Epon	0.104	160	16.752	402.692
26	23% CTBN/Epon	0.104	200	20.940	503.365
19	23% CTBN/Epon	0.207	200	20.940	252.899
33	23% CTBN/Epon	0.208	90	9.423	113.257
34	23% CTBN/Epon	0.208	120	12.564	151.010
35	· •	0.208	160	16.752	201.346
37	· · · · · · · · · · · · · · · · · · ·	0.312	0	0.000	0.000
	23% CTBN/Epon				
38	23% CTBN/Epon	0.312	90	9.423	75.505
39	23% CTBN/Epon	0.312	110	11.517	92.284
40	23% CTBN/Epon	0.312	140	14.658	117.452
41	23% CTBN/Epon	0.312	160	16.752	134.231
42	23% CTBN/Epon	0.312	200	20.940	167.788
29	23% CTBN/Epon	0.417	0	0.000	0.000
30	23% CTBN/Epon	0.417	90	9.423	56.493
31	23% CTBN/Epon	0.417	110	11.517	69.047
32	23% CTBN/Epon	0.417	120	12.564	75.324
28	23% CTBN/Epon	0.417	160	16.752	100.432
27	23% CTBN/Epon	0.417	200	20.940	125.540
79	NEAT EPON	0.2	0	0.000	0.000
80	NEAT EPON	0.2	90	9.423	117.788
81	NEAT EPON	0.2	110	11.517	143.963
82	NEAT EPON	0.2	140	14.658	183.225
83	NEAT EPON	0.2	160	16.752	209.400
55	WINT DIOM	0.2	100	20.752	2021400

INDEX	FLUID	GAP	ROTATION (rpm)	ROTATION (rad/sec)	
84	NEAT EPON	0.2	200	20.940	261.750
85	NEAT EPON	0.4	200	20.940	130.875
86	NEAT EPON	0.4	0	0.000	0.000
87	NEAT EPON	0.4	90	9.423	58.894
88	NEAT EPON	0.4	110	11.517	71.981
89	NEAT EPON	0.4	140	14.658	91.613
90	NEAT EPON	0.4	160	16.752	104.700
91	discard	0.2	90	9.423	117.788
92	0.3% PIB	0.2	0	0.000	0.000
93	discard	0.2	120	12.564	157.050
94	discard	0.2	160	16.752	209.400
95	discard	0.2	200	20.940	261.750
96	discard	0.4	90	9.423	58.894
97	0.3% PIB	0.4	0	0.000	0.000
98	0.3% PIB	0.4	120	12.564	78.525
99	0.3% PIB	0.4	160	16.752	104.700
100	0.3% PIB	0.4	200	20.940	130.875
111	0.3% PIB	0.4	90	9.423	58.894
112	0.3% PIB	0.1	90	9.423	235.575
113	discard	0.1	120	12.564	314.100
114	discard	0.1	160	16.752	418.800
115	0.3% PIB	0.1	200	20.940	523.500
116	0.3% PIB	0.1	90	9.423	235.575
117	0.3% PIB	0.4	90	9.423	58.894
118	0.3% PIB	0.2	90	9.423	117.788
119	0.3% PIB	0.2	120	12.564	157.050
101	neat polybutene	0.2	0	0.000	0.000
102	neat polybutene	0.2	90	9.423	117.788
103	neat polybutene	0.2	120	12.564	157.050
104	neat polybutene	0.2	160	16.752	209.400
105	neat polybutene	0.2	200	20.940	261.750
106	neat polybutene	0.4	0	0.000	0.000
107	neat polybutene	0.4	90	9.423	58.894
108	neat polybutene	0.4	120	12.564	78.525
109	neat polybutene	0.4	160	16.752	104.700
110	neat polybutene	0.4	200	20.940	130.875
43	40% CTBN/Epon	0.1	90	9.423	235.575
44	40% CTBN/Epon	0.1	110	11.517	287.925
45	40% CTBN/Epon	0.1	140	14.658	366.450
46	40% CTBN/Epon	0.1	160	16.752	418.800
47	40% CTBN/Epon	0.1	200	20.940	523.500
48	40% CTBN/Epon	0.1	110	11.517	287.925
49	40% CTBN/Epon	0.1	0	0.000	0.000
50	40% CTBN/Epon	0.2	90	9.423	117.788
51	40% CTBN/Epon	0.2	110	11.517	143.963

INDEX	FLUID	GAP		ROTATION (
5 0	AGE CORDY (December	(cm)	(rpm)	(rad/sec)	(1/sec)
52	40% CTBN/Epon	0.2	120	12.564	157.050
53	40% CTBN/Epon	0.2	160	16.752	209.400
54	40% CTBN/Epon	0.2	200	20.940	261.750
55 5.6	40% CTBN/Epon	0.2	0	0.000	0.000
56	40% CTBN/Epon	0.2	140	14.658	183.225
57 5.0	40% CTBN/Epon	0.3	110	11.517	95.975
58	40% CTBN/Epon	0.3	140	14.658	122.150
59	40% CTBN/Epon	0.3	160	16.752	139.600
60	40% CTBN/Epon	0.3	90	9.423	78.525
61	40% CTBN/Epon	0.3	200	20.940	174.500
62	40% CTBN/Epon	0.3	0	0.000	0.000
64	40% CTBN/Epon	0.4	90	9.423	58.894
65	40% CTBN/Epon	0.4	110	11.517	71.981
66	40% CTBN/Epon	0.4	140	14.658	91.613
67	40% CTBN/Epon	0.4	160	16.752	104.700
68	40% CTBN/Epon	0.4	0	0.000	0.000
69	40% CTBN/Epon	0.4	200	20.940	130.875
70	40% CTBN/Epon	0.4	120	12.564	78.525
71	40% CTBN/Epon	0.2	90	9.423	117.788
72	40% CTBN/Epon	0.2	110	11.517	143.963
73	40% CTBN/Epon	0.2	160	16.752	209.400
74	40% CTBN/Epon	0.2	200	20.940	261.750
75	40% CTBN/Epon	0.2	160	16.752	209.400
76	40% CTBN/Epon	0.2	160	16.752	209.400
77	40% CTBN/Epon	0.2	160	16.752	209.400
78	40% CTBN/Epon	0.2	160	16.752	209.400
120	aged Separan	0.4	140	14.658	91.613
121	aged Separan	0.1	140	14.658	366.450
122	aged Separan	0.1	160	16.752	418.800
123	aged Separan	0.1	200	20.940	523.500
124	aged Separan	0.2	200	20.940	261.750
125	aged Separan	0.2	160	16.752	209.400
126	aged Separan	0.2	140	14.658	183.225
127	aged Separan	0.2	120	12.564	157.050
128	aged Separan	0.2	90	9.423	117.788
129	aged Separan	0.1	90	9.423	235.575
130	aged Separan	0.1	120	12.564	314.100
131	aged Separan	0.4	120	12.564	78.525
132	aged Separan	0.4	90	9.423	58.894
133	aged Separan	0.4	160	16.752	104.700
134	aged Separan	0.4	200	20.940	130.875
			-		

INDEX	Q	+ or -	CORRCOEF	NO.SAMPLE	TIME 1	TIME 2
	(cc/sec)	(cc/sec)			(sec)	(sec)
4	0.067855	0.004037	0.998	3	120	240
1		0.000402	1.000	4	210	450
3		0.005188	0.999	3	120	240
2		0.000638	1.000	4	120	300
8		0.002144	0.987	4	90	180
15		0.026116	0.999	3	50	110
9		0.002587	0.995	4	100	180
14		0.015602	0.997	3	90	150
6		0.000557	0.996	4	150	300
5		0.000534	1.000	4	180	360
7		0.001091	1.000	4	120	240
17		0.001052	0.997	4	90	180
13		0.000584	1.000	3	170	330
11		0.000145	0.999	4	230	430
10		0.001789	1.000	3	150	300
16	0.036061	0.002482	0.998	3 3 3	110	220
12	0.017173	0.000539	0.995	3	270	600
20	0.00186	3.58E-05	0.980	3	290	690
21	0.009406	0.000113	0.992	4	130	230
23	0.007969	0.000118	0.997	4	140	280
22	0.009863	0.000122	0.997	4	100	270
24	0.00986	0.000104	0.998	4	220	400
25	0.005977	9.5E-05	0.997	4	180	290
36	0.005538	9.35E-05	0.973	4	190	300
26	0.012092	0.000185	0.999	4	160	300
19	0.007051	0	1.000	2	130	310
33	0.009193	0.000197	0.997	4	90	180
34		0.000175	0.999	4	140	280
35	0.007085	0.000105	0.997	4	100	260
37	0.00169	1.64E-05	0.971	4	180	440
38	0.003259	0.000146	1.000	3	220	400
39	0.002081	2.65E-05	1.000	4	140	290
40	0.00462	6.72E-05	0.988	4	100	220
41	0.006616	0.000113	0.998	4	120	240
42		5.81E-05	0.985	4	100	210
29	0.00138	6.7E-06	0.999	4	350	640
30		7.27E-05	0.990	4	200	340
31		6.59E-05	1.000	4	210	370
32		4.57E-05	0.999	4	130	400
28		0.000122	0.999	4	140	240
27	0.009869	0.000168	0.999	4	240	340
79	0.004629	9.57E-05	1.000	3	340	660
80		0.000122	0.998	4	100	240
81		0.000109	0.992	4	180	310
82		6.54E-05	0.957	4	210	380
83		3.59E-05	0.993	4	140	360

INDEX	Q	+ or -	CORRCOEF	NO.SAMPLE		TIME 2
	(cc/sec)	(cc/sec)			(sec)	(sec)
84	0.022576	0.000388	0.996	4	90	210
85	0.004143	3.19E-05	1.000	4	390	630
86		8.65E-05	1.000	3	720	1270
87	0.007213	9.44E-05	0.999	4	140	280
88	0.017123	0.000239	0.999	4	130	260
89	0.009531	0.000126	0.997	4	210	360
90	0.015085	0.000192	0.984	4	190	340
91		0.013458	0.946	3	60	120
92	0.004821	3.58E-05	1.000	4	290	560
93	0.01732	0.002392	0.994	3	30	100
94	0.013697	0.00028	0.989	4	60	140
95	0.015428	0.000424	0.975	4	50	120
96	0.007384	9.16E-05	0.981	4	110	270
97	ERR	0	ERR	1	350	
98		0.003294	0.974	4	80	140
99	0.05741	0.008557	0.926	3	110	160
100	0.05668	0.012731	0.908	3	40	80
111	0.150442	0.045055	0.996	3	60	90
112		0.033816	1.000	4	30	60
113	0.142613	0.08542	1.000	2	30	60
114		0.024288	0.985	4	40	70
115	0.218227	0.041334	0.998	4	20	50
116		0.030939	1.000	4	30	60
117		0.015998	0.996	4	30	60
118		0.019742	1.000	4	30	60
119	0.13756	0.026055	1.000	4	30	60
101	0.001183	1.54E-05	0.998	4	160	320
102	0.019784	0.000423	1.000	4	90	180
103		0.000326	1.000	4	110	220
104	0.010742	0.00015	0.995	4	150	300
105		0.000328	0.997	4	100	210
106		2.07E-05	0.998	4	280	390
107	0.011842		0.999	4	160	310
108		0.000131	0.999	4	130	240
109		0.000204	0.997	4	140	280
110	0.020808	0.000342	0.994	4	110	220
43		0.000117	0.994	4	140	360
44		0.000246	0.991	3	190	370
45		0.000212	0.997	4	110	220
46		0.001218	1.000	3	210	320
47		0.000266	0.996	4	130	230
48		0.000117	0.995	4	230	340
49		3.39E-05	0.998	3	5017	5707
50		8.74E-05	0.997	4	110	260
51	0.011264	0.000147	0.999	4	120	240

INDEX	Q	+ or -	CORRCOEF	NO.SAMPLE		TIME 2
	(cc/sec)	(cc/sec)			(sec)	(sec)
52	0.009816	0.000154	0.998	4	120	240
53	0.005765	9.25E-05	0.997	4	120	240
54	0.005598	4.42E-05	0.977	4	160	300
55	0.00245	0	1.000	2	410	630
56	0.013384	0.000925	1.000	3	170	300
57	0.004167	5.63E-05	1.000	4	140	290
58	0.009396	0.000126	0.991	4	130	250
59	0.012466	0.000195	1.000	4	130	260
60	0.009519	0.000134	1.000	4	160	300
61	0.013819	0.000204	0.999	4	130	250
62	0.004088	1.95E-05	0.998	4	260	710
64	0.005689	5.46E-05	1.000	4	190	350
65	0.008524	0.000109	1.000	4	140	300
66	0.009056	0.000123	1.000	4	140	280
67	0.009332	0.000123	0.999	4	170	320
68	0.002821	4.04E-05	0.997	3	260	540
69	0.010382	0.000135	1.000	4	250	420
70	0.009057	0.000109	0.999	4	170	310
71	0.009694	0.000155	1.000	4	130	250
72	0.009914	0.00015	1.000	4	160	290
73	0.009649	0.000117	0.994	4	180	310
74	0.006806	8.12E-05	0.992	4	210	400
75		4.61E-05	0.993	4	170	410
76	0.006386	7.95E-05	0.998	4	230	350
77	0.009036	9.45E-05	0.994	4	180	370
78	0.006275	0.000104	0.998	4	220	310
120	0.078345	0.00272	0.999	4	60	120
121	0.225325	0.014844	0.998	3	50	100
122	0.209778	0.009286	0.997	4	40	80
123	0.264298	0.029019	1.000	3	40	70
124	0.226527	0.012727	1.000	4	30	60
125	0.19583	0.008159	1.000	4	40	90
126	0.180821	0.009417	1.000	4	40	80
127	0.173925	0.007247	1.000	4	50	100
128	0.095443	0.003748	0.998	4	60	120
129	0.156937	0.005816	1.000	4	50	100
130	0.210531	0.010965	1.000	4	40	80
131	0.069969	0.002017	1.000	4	60	120
132	0.045682	0.001303	1.000	4	70	140
133	0.096198	0.003028	1.000	4	60	120
134	0.109552	0.003804	0.998	4	60	120

INDEX	TIME 3	TIME 4			WEIGHT 3	
4	(sec)	(sec)	(g) 10.5768	(g)	(g) 34.4013	(g)
4	420	010		18.6168		40.2261
1 3	660 360	810	10.2841 9.0126	22.0683 18.0159	32.4162 28.6373	40.2261
2	450	570	7.4061	17.5573	26.9107	33.7450
8	290	372	17.4316	27.2709	38.0078	54.2505
15	170	3/2	10.4642	27.2709	35.1600	54.2505
9	270	360	14.3305	27.0832	40.8655	49.8615
14	220	300	11.7332	20.9730	29.1271	49.0015
6	450		7.8269	13.9549	23.5827	
5	540	660	9.6352	19.0433	28.2203	35.3986
7	360	480	9.8556	19.9510	28.7994	39.0221
17	280	370	7.3956	13.2799	20.0199	24.1374
13	600	370	3.1132	5.7258	10.2783	24.13/4
11	660	1010	4.0844	7.7953	13.4016	21.8594
10	460	1010	5.9176	11.3375	17.2108	21.0334
16	370		5.7348	10.9902	16.8545	
12	840		4.5768	10.3212	16.2324	
	0.10		4.5700	10.3212	10.2324	
20	1220		0.8550	2.0581	2.8418	
21	400	600	2.0500	3.6313	5.4601	7.1401
23	410	530	2.0769	3.0772	4.4153	5.5408
22	370	580	1.6829	3.5905	5.0092	6.9848
24	530	780	1.3998	3.6359	5.1491	7.6560
25	420	540	0.7273	1.5914	2.4905	3.1549
36	420	530	2.5568	3.7071	4.0000	4.8460
26	420	540	1.7455	3.8798	5.4615	6.9461
19			1.5931	3.0273		
33	270	360	1.2029	2.3427	3.2193	4.0271
34	390	520	2.1909	4.1272	5.5659	7.0658
35	380	490	1.0571	2.5330	3.4364	4.1755
37	580	790	1.6846	2.3642	2.6584	2.8263
38	620		0.6755	1.3636	2.1500	
39	450	590	0.3684	0.7063	1.0804	1.4280
40	340	500	0.4818	0.8046	1.5432	2.5145
41	350	460	0.7476	1.7127	2.5861	3.2699
42	340	450	0.3574	0.6136	1.1379	1.7682
29	1110	1510	0.7204	1.2297	1.9743	2.5307
30	510		0.9599	2.1845	3.6035	
31	560	730	0.8023	1.9704	3.2410	4.3338
32	530	670	0.7550	2.1578	2.7037	3.3364
28	340	440	1.2350	2.0423	2.7338	3.4008
27	450	580	1.9504	3.1570	4.3917	5.7478
79	1200		2.6564	4.5145	7.4087	
80	430	600	1.9346	3.8830	6.4642	8.2812
81	510	680	3.4791	5.4800	7.8685	9.2191
82	560	840	2.7988	5.6571	6.9280	8.3929
83	650	860	1.3901	2.9870	4.4738	5.3407

INDEX	TIME 3	TIME 4		WEIGHT 2		
0.4	(sec)	(sec)	(g)	(g)	(g)	(g)
84	310	430	3.6238	7.4719		
85	880	1140	1.9127		4.3487	5.6163
86	1780	500	4.3459	7.7621	10.7830	E 0256
87	430	580	1.2391	2.5553	3.8205	5.0256
88	410	540	2.7738	5.6772	8.7847	11.1096
89 90	500 470	650 650	3.2400 5.1001	5.2175	6.8123	8.2284 13.3455
90	470	650	5.1001	8.7066	11.3287	13.3455
91	150		5.7183	7.9376	11.5999	
92	810	1070	1.3450	2.5149	3.5798	4.7070
93	160		2.3524	3.2521	4.3727	
94	240	340	1.5027	2.2484	3.9586	4.7602
95	190	260	2.5784	2.9198	4.1316	5.3891
96	410	580	0.8359	2.1243	3.3192	3.8626
97			0.2512			
98	180	230	10.4936	16.3872	20.0362	21.4659
99	230		8.8711	13.7238		
100	120		7.3181	10.9631	11.3673	
111	120		6.6903	11.3783	14.751	
112	90	120	4.4195	9.384	14.2601	18.7374
113			5.6786	9.4992		
114	100	130	6.9667	11.8729	15.102	17.3411
115	80	110	2.312	8.4968	14.9852	19.6369
116	90	120	4.7945	9.1669	13.6618	
117	90	120	2.8368	5.4309	7.8674	9.5669
118	90	120	2.8843	5.6893	8.5112	11.2514
119	90	120	4.2068	8.0527	11.8157	15.2366
101	450	610	0.1781	0.3485	0.4666	0.6710
102	270	360	1.7443	3.4967	5.0668	6.6456
103	330	430	2.1303	4.0350	5.8404	7.4388
104	420	570	2.1175	3.8701	5.0825	6.2315
105	340	450	1.5388	3.9788	6.3068	7.9996
106	530	680	0.4166	0.5788	0.7757	0.9437
107	440	560	3.2148	4.9510	6.3738	7.5296
108	380	500	1.2717	2.2216	3.3287	
109	400	530	2.3108	4.3307	5.8159	
110	340	460	2.1431	4.1028	5.9303	8.9431
43	540	770	2.3610	5.9660	8.6028	10.9867
44	640		2.2185	3.8167	5.3041	
45	380	510	2.1815	4.4194	6.9447	8.7896
46	450	_	1.9546	3.8765	6.2152	
47	340	450	2.3328	4.2022	6.1241	7.4637
48	500	650	2.5304	3.7664	5.4209	6.4776
49	6107		6.3390	8.0299	8.7877	
50	400	560	1.0421	2.3954	3.1763	4.4443
51	420	550	1.8062	3.5075	5.4753	7.1881

INDEX	TIME 3	TIME 4	WEIGHT 1	WEIGHT 2	WEIGHT 3	WEIGHT 4
	(sec)	(sec)	(g)	(g)	(g)	(g)
52	360	490	1.5862	2.9734	4.3726	5.5122
53	360	480	1.1033	1.9960	2.7209	3.3753
54	660	840	0.9012	1.4980	3.2057	5.2732
55			0.8769	1.4645		
56	430		1.3772	3.3113	5.1701	
57	450	560	0.9032	1.6191	2.3471	2.8067
58	390	560	1.5902	2.9278	3.8372	6.1386
59	380	500	2.0991	3.9654	5.5694	7.1331
60	440	570	1.9839	3.5463	4.9413	6.2558
61	380	520	2.3649	4.3533	6.3090	8.2492
62	1170	1440	1.6749	3.9593	5.9150	6.9347
64	580	780	1.2902	2.2914	3.7501	4.9382
65	430	600	1.4685	2.9607	4.2223	5.7282
66	410	570	1.6303	3.1330	4.3556	5.8971
67	460	610	2.0513	3.7273	5.1687	6.5212
68	1460		1.2726	2.4446	5.0568	
69	550	700	2.9362	4.8731	6.3731	8.0186
70	470	650	2.0806	3.6754	5.2225	6.8452
71	370	490	1.6664	2.9850	4.2541	5.4699
72	420	540	2.0222	3.5064	4.9241	6.1216
73	450	660	2.6252	4.3650	5.9370	7.7117
74	540	700	2.7414	4.5044	5.5023	6.3676
75	570	790	1.6589	3.2513	4.0263	4.9451
76	510	690	1.3886	2.2815	3.4982	4.5703
77	560	730	2.4575	4.7812	6.6248	7.8679
78	450	560	2.4219	3.1464	4.1112	4.7510
120	180	240	5.6851	11.8991	17.4057	22.339
121	150		14.1648	28.7388	40.7531	
122	130	180	11.7241	23.4514	33.059	47.3648
123	100		12.4783	22.2388	31.1906	
124	100	140	7.9491	16.2162	26.7777	37.4136
125	140	190	9.2767	20.5831	32.1648	43.9293
126	120	160	8.9111	17.5988	26.1549	34.5082
127	150	200	9.3506	19.6624	29.7869	40.181
128	170	220	7.6955	14.8704	20.8918	25.5498
129	150	220	9.1371	18.1905	27.5016	40.5842
130	120	160	9.3038	19.1766	29.0648	39.1312
131	210	270	4.9891	9.8923	17.4462	22.2746
132	210	290	3.6206	7.4822	11.215	15.4953
133	180	260	6.8254	13.6863	20.207	29.6019
134	180	240	8.8273	17.3115	25.5164	31.9465

INDEX		SUM 2	SUM 3		SUM 5	SLOPE
	sum(x)		sum(xy)		$sum(y^2)$	(g/sec)
4	780	63.5949	20185.79		1641.903	0.0801
1		104.9947			3261.722	0.0498
3	720		15714.76		1225.895	0.0818
2	1440	85.6191	37500.39	631800	2226.02	0.0589
8		136.9608	37681.05		5435.272	0.1259
15	330		8932.202		1834.453	0.2058
9	910	132.1407	35291.85	244900	5095.021	0.1381
14	460	61.8333	10609.9		1425.923	0.1333
6	900		15972.72		812.1433	0.0513
5	1740		47191.96		2504.931	0.0532
7	1200	97.6281	35069.3		2847.305	0.0803
17	920		17592.4		1214.461	0.0607
13	1100		8585.738	497800	148.1203	0.0167
11	2330	47.1407	35214.44	1693500	734.8853	0.0231
10	910	34.4659	12205.86	324100	459.7685	0.0364
16	700	33.5795	9284.837	197400	437.7466	0.0426
12	1710	31.1304	21063.67	1138500	390.9651	0.0203
20	2200	5.7549	5135.035	2048600	13.04263	0.0021
21	1360		7569.799		98.18256	0.0106
23	1360		5899.279		63.97801	0.0090
22	1320		7042.313		89.60336	0.0111
24	1930		10463.02		100.3068	0.0111
25	1430		3342.076		19.2175	0.0068
36	1440		5846.302		59.76353	0.0063
26	1420		7487.944		96.17591	0.0137
19	440		1145.566		11.70251	0.0080
33	900		2848.914		33.51664	0.0104
34	1330		7307.259		102.7386	0.0129
35	1230		4116.117		36.77719	0.0080
37	1990		5118.125		23.48238	0.0019
38	1240		2027.05		6.938205	0.0037
39	1470		1585.103		3.841026	0.0024
40	1160	5.3441			9.583689	0.0052
41	1170		2910.049		20.87241	0.0075
42	1100	3.87708	1347.17		4.925573	0.0040
29	3610		7051.978		12.33344	0.0016
30	1050		2772.495		18.67866	0.0071
31	1870		5876.165		33.81206	0.0068
32	1730		4629.619		23.66768	0.0048
28	1160	9.4119	3088.896		24.73532	0.0072
27	1610	15.2469	6851.465	712100		0.0112
70	2200	14 5706	12772 10	1001200	02 22601	0.0055
79	2200		12773.19		82.32601	
80	1370		8873.706	612500		0.0128
81	1680	26.0467			189.0396	0.0115
82	1990		13667.16	1207700	158.274	0.0084
83	2010	14.1916	8770.906	1311300	59.39251	0.0054

INDEX	SUM 1		SUM 3	SUM 4	SUM 5	SLOPE
	sum(x)		sum(xy)		$sum(y^2)$	(g/sec)
84	1040		10527.75	333200	334.7438	0.0269
85	3040	15.0084	12947.73	2623000	63.91372	0.0049
86	3770	22.891	32180.66	5299700	195.4101	0.0061
87	1430	12.6405		619300	47.9178	0.0086
88	1340	28.3453	11437.58		240.5187	0.0204
89	1720	23.4982			151.8339	0.0113
90	1650					0.0113
90	1630	38.4809	17928.33	795100	408.2577	0.0180
91	330	25.2558	3035.595	40500	230.2621	0.0613
92	2730	12.1467	9734.522	2198700	43.10456	0.0043
93	290	9.9772	1095.414	36500	35.23045	0.0155
94	780	12.4699	2973.47		45.64343	0.0122
95	620		2665.466	120600	61.2859	0.0138
96	1370	10.142			31.14815	0.0066
97	350	0.2512	87.92		0.063101	ERR
98	630		11677.37		1240.89	0.0751
99	500		6682.372		500.0319	0.0513
100	240		2533.848	22400	302.9597	0.0506
111	270		3195.585	26100	391.8178	0.1343
112	300	46.801	4227.522	27000	662.032	0.1594
113	90	15.1778	740.31	4500	122.4813	0.1274
114	340	51.2827	4874.314	33400	718.2848	0.1145
115	260	45.4309	3829.955	21400	687.705	0.1949
116	300	45.5058		27000		0.1459
117	300	25.702		27000	190.9637	0.0754
118	300		2544.063	27000	239.7218	0.0931
119	300		3501.171		454.3079	0.1228
119	300	39.3116	3501.171	27000	454.50/9	0.1226
101	1540	1.6642	759.296	702600	0.821128	0.0011
102	900	16.9534	4546.845	243000	85.10595	0.0181
103	1090	19.4445	6248.049	354300	110.2654	0.0166
104	1440	17.3016	7165.26	613800	84.12488	0.0098
105	1100	19.824	6733.56	372200	121.9681	0.0184
106	1880	2.7148			2.000845	0.0013
107	1470		9070.226		132.1675	0.0108
108	1250		4038.711		34.86045	0.0078
109	1350	19.6353			109.4417	0.0125
110	1130	21.1193	7268.485	387700	136.5733	0.0190
43	1810		15583.57		235.8832	0.0137
44	1200		5228.318		47.62242	0.0068
45	1220		8333.915	465000	149.776	0.0164
46	980		4447.786		57.47642	0.0178
47	1150		6710.629		116.3119	0.0162
48	1720		8783.458		91.93415	0.0095
49	16831	23.1566	131295.9	95035587	181.8859	0.0023
50	1330	11.0581	4496.763	553300	36.6646	0.0074
51	1330		7311.625	550900	97.21261	0.0123

INDEX	SUM 1	SUM 2	SUM 3	SUM 4	SUM 5	SLOPE
	sum(x)	sum(y)	sum(xy)	$sum(x^2)$	$sum(y^2)$	(g/sec)
52	1210	14.4444	5179.074	441700	60.86112	0.0107
53	1200	9.1955	3211.104	432000	23.99723	0.0063
54	1960	10.8781	7138.842	1256800	41.13932	0.0061
55	1040	2.3414	1282.164	565000	2.913714	0.0027
56	900	9.8586	3450.657	303800	39.59132	0.0146
57	1440	7.6761	3223.934	619800	16.8237	0.0045
58	1330	14.4938	5872.8	545100	63.50726	0.0102
59	1270	18.767	6986.809	478900	102.0299	0.0136
60	1470	16.7273	7121.292	634100	80.06358	0.0104
61	1280	21.2764	8082.766	494200	132.3968	0.0151
62	3580	18.4839	20153.1	4014200	101.5586	0.0045
64	1900	12.2699	7073.982	1103400	45.3642	0.0062
65	1470	14.3797	6346.309	654500	61.56233	0.0093
66	1400	15.016	6252.625	591000	66.22061	0.0099
67	1560	17.4685	7896.991	715000	87.34211	0.0102
68	2260	8.774	9033.888	2490800	33.16681	0.0031
69	1920	22.201	11898.98	1031400	137.2827	0.0113
70	1600	17.8237	8397.031	768400	91.96873	0.0099
71	1240	14.3754	5217.15	456400	59.70429	0.0106
72	1410	16.5743	6714.194	577700	78.10488	0.0108
73	1600	20.6389	9587.058	766600	120.6632	0.0105
74	1850	19.1157	9806.016	985700	98.62653	0.0074
75	1940	13.8816	7816.666	1146000	53.98801	0.0053
76	1780	11.7386	6055.492	911600	40.2585	0.0070
77	1840	21.7314	11664.85	1015800	134.691	0.0098
78	1540	14.4305	6018.802	660600	55.2394	0.0068
120	600	57.3289	10263.38	108000	975.8983	0.0924
121	300	83.6567	9695.085	35000	2687.375	0.2659
122	430	115.5993	15168.41	57300	4023.744	0.2475
123	210		5174.908	16500	1623.126	0.3119
124	330		9127.119	34100	2442.976	0.2673
125	460	105.9539	15073.19	65400	3474.079	0.2311
126	400	87.173	10424.25	48000	2264.02	0.2134
127	500	98.9809	14938.01	75000	2975.816	0.2052
128	570	69.0075	11418.74	95300	1369.609	0.1126
129	520	95.4134	15329.67	83400	2817.796	0.1852
130	400	96.6764	11655.05	48000	2830.316	0.2484
131	660	54.6022	11164.27	135000	923.2764	0.0826
132	710	37.8131	8149.737	152700	434.9726	0.0539
133	620	70.3206	13385.63	118000	1518.496	0.1135
134	600	83.6017	14867.13	108000	2049.275	0.1293

INDEX	+ or -	INTERCEPT
4	0.004764	(g) 0.381
1	0.000474	-0.258
3	0.006122	-1.069
2	0.000752	0.206
8	0.00253	4.908
15 9	0.030817 0.003053	-0.061 1.622
14	0.003033	0.168
6	0.000657	-0.190
5	0.00063	-0.082
7	0.001288	0.320
17	0.001241	2.258
13	0.00069	0.255
11 10	0.000171 0.002111	-1.648 0.437
16	0.002911	1.264
12	0.000636	-1.174
20	4.05E-05	0.377
21	0.000128	0.957
23 22	0.000133 0.000138	0.716 0.639
24	0.000138	-0.916
25	0.000107	-0.424
36	0.000106	1.525
26	0.000209	-0.342
19		0.557
33 34	0.000222	0.361
34 35	0.000198 0.000119	0.462 0.339
37	1.85E-05	1.433
38	0.000165	
39	3E-05	
40	7.59E-05	
41	0.000127	-0.108
42	6.57E-05	-0.139
29 30	7.57E-06 8.22E-05	
31	7.45E-05	
32	5.17E-05	
28	0.000138	0.268
27	0.00019	-0.677
79	0.000114	0.820
80	0.000145	0.764
81	0.000129	1.695
82	7.79E-05	
83	4.27E-05	0.813

INDEX	+ or -	
84 85 86 87 88	0.000461 3.79E-05 0.000103 0.000112 0.000284 0.000149	0.092 0.260 0.997
90	0.000228	2.215
91 92 93 94 95	0.012018 3.2E-05 0.002136 0.00025 0.000379 8.18E-05	1.619 0.277
97 98 99 100 111 112	0.002942 0.007641 0.011369 0.040234 0.030198	ERR 5.264 4.075 5.834 -1.151 -0.257
113 114 115 116 117 118	0.07628 0.021689 0.036912 0.027628 0.014286 0.01763	1.858 3.088 -1.309 0.437 0.769 0.103
119	0.023267	0.103
101 102 103 104 105 106 107 108 109	1.4E-05 0.000387 0.000298 0.000137 0.0003 1.89E-05 0.000156 0.00012	0.057 1.540 0.309 0.695
43 44 45 46 47 48 49 50	0.000128 0.000268 0.000231 0.001328 0.00029 0.000128 3.7E-05 9.53E-05 0.00016	0.758 1.080 0.588 -1.786 0.386 0.480 -5.010 0.310 0.412

INDEX	+ or -	
		(g)
52	0.000167	0.375
53	0.000101	0.414
54	4.82E-05	-0.270
55		-0.218
56	0.001008	-1.090
57	6.14E-05	0.284
58	0.000137	0.218
59 60	0.000213	0.377
61	0.000146 0.000223	0.369 0.499
62	2.13E-05	0.499
64	5.95E-05	0.122
65	0.000118	0.122
66	0.000118	0.299
67	0.000134	0.400
68	4.4E-05	0.608
69	0.000147	0.119
70	0.000119	0.507
71	0.000169	0.318
72	0.000164	0.335
73	0.000127	0.953
74	8.85E-05	1.348
75	5.02E-05	0.907
76	8.66E-05	-0.163
77	0.000103	0.902
78	0.000113	0.974
120	0.002965	0.465
121	0.01618	1.297
122	0.010121	2.289
123	0.031631	0.138
124	0.013872	0.037
125	0.008894	-0.086
126	0.010265	0.456
127	0.007899	-0.909
128	0.004085	1.203
129	0.006339	-0.221
130	0.011952	-0.674
131	0.002199	0.028
132	0.00142	-0.115
133	0.003301	-0.014
134	0.004146	1.510

LIST OF REFERENCES
.

LIST OF REFERENCES

- Beavers, G.S.; and D.D. Joseph, (1975), "The rotating rod viscometer", Journal of Fluid Mechanics, vol. 69, part 3, pp. 475-511.
- Bird, R. Byron; R.C. Armstrong, and O. Hassager, 1987,

 Dynamics of Polymeric Liquids. vol 1., John Wiley

 & Sons, New York.
- Bird, R. Byron; W.E. Stewart, and E.L. Lightfoot, 1960, Transport Phenomena, John Wiley & Sons, New York.
- Blyler, L. L., Jr., 1966, "Analysis of Normal Stress Extrusion of Polymer Melts", Ph.D. thesis, Princeton University, N.J..
- Cattanach, J.B.; G. Guff, and F.N. Cogswell, 1986, "The Processing of Thermoplastics Containing High Loadings of Long and Continuous Reinforcing Fibers", Journal of Polymer Engineering, vol. 6, no. 1-4, pp. 345-362.
- Chmielewski, C.; C.A. Petty and K. Jayaraman, (1990), "Crossflow of Elastic Liquids Through Arrays of Cylinders", Journal of Non-Newtonian Fluid Mechanics, vol. 35, pp. 309-325.
- Choplin, L.; P.J. Carreau and A. Ait Kadi, 1983, "Highly Elastic-Constant Viscosity Fluids", Polymer Engineering and Science, Vol. 23, No. 8, pp. 459-464.
- Custom Scientific Instruments, Inc., Cedar Knolls, New Jersey, Bulletin: Plastics CS-194.
- D'Amato, Dominic A., 1975, "Processing Versatility With a New Mixing Extruder", Proceedings of 33rd. Technical Conference of the Society of Plastics Engineers, pp. 506-9, May 1975.
- Davidson, R.L., ed., Handbook of Water Soluble Gums and Resins, McGraw-Hill Book Co., New York, NY, pp. 16-1 -- 16-26.
- Good, Paul A.; Arthur J. Schwartz, and Christopher W. Macosko, 1974, "Analysis of the Normal Stress Extruder", AIChE Journal, vol. 20, no. 1, pp. 67-73, January 1974.

- Goppel, J.M., 1969, "New Concepts in Processing", Plastics and Polymers, pp. 449-61, October 1969.
- Hull, Derek, 1987, An Introduction to Composite Materials, Cambridge University Press, 1987.
- Kataoka, T., S. Ohnishi, T. Kitano, K. Nakama, and H. Takayama, 1976, "Mixing effect of filler and polymer by an elastic melt extruder", Rheological Acta, vol. 15, pp. 268-270.
- Kocherov, V.L., and Yu. L. Lukach, 1973, "Flow of Polymer Melts in a Disc-Type Extruder and in Rotational Devices of the "Cone-Plate" and "Plate-Plate" Type", Polymer Engineering and Science, vol. 13, no. 3, pp. 194-201, May 1973.
- Lee, Walter J., and J.C. Seferis, 1987, "Hot-melt prepreg processing of advanced composites: A Comparison of Methods", Society of Plastics Engineers ANTEC '88 Proceedings, 1987.
- Maxwell, Bryce and Anthony J. Scalora, 1959, "The Elastic Melt Extruder--Works Without Screw, Modern Plastics, vol. 37, no. 9, October 1959, pp. 107-210.
- Maxwell, Bryce, 1962, U.S. Patent #3,046,603. July 31, 1962.
- Maxwell, Bryce, 1970, "Scaling Up the Elastic Melt Extruder", Society of Plastics Engineers Journal, vol. 26, pp. 48-50, June 1970.
- Maxwell, Bryce, 1973, "The Application of Melt Elasticity to Polymer Processing", Polymer Engineering and Science, vol. 13, no. 3, pp. 227-230, May 1973.
- Maxwell, Bryce, 1974, "A New Twist in Mixing Extruders", Plastics Engineering, pp. 40-45, May 1974.
- Middleman, Stanley, 1977, Fundamentals of Polymer Processing, McGraw-Hill Book Co., 1977.
- Prilutski, G., R.K. Gupta, T. Sridhar, and M.E. Ryan, 1983, "Model Viscoelastic Liquids", Journal of Non-Newtonian Fluid Mechanics, Vol. 12, pp. 233-241.

- Raghava, R.S.; (1988), "Development and Characterization of Thermosetting-Thermoplastic Polymer Blends for Applications in damage-tolerant Composites", Journal of Polymer Science, part b, vol. 26, pp. 65-81.
- Remnev, V.P.; and N.V. Tyabin, 1971, "Velocity and Pressure Distribution in the Gap of a Disk Extruder" Polymer Mechanics, vol. 7, no. 3, May-June 1971, pp. 451-456.
- Rheometrics Mechanical Spectrometer manual.
- Starita, Joseph M., 1972, "Microstructure of Melt Blended Polymer Systems", Trans. Society of Rheology, vol. 16, no. 2, pp. 339-367.
- Tanner, Roger I.; 1973, "A Correlation of Normal Strss Data for Polyisobutylene Solutions", Transactions of the Society of Rheology, vol. 17, no. 2, pp. 365-373.
- Tanner, Roger I.; 1988, Engineering Rheology, Clarendon Press, Oxford, revised edition.
- Tomita, Yukio; and Hiroshi Kato, 1967, "A Study on the Elastodynamic Pump" Bulletin of JSME, vol. 10, no. 39, pp. 507-515.

			•
			i i
		e ^r	